Supplementary Information

Bioactive O^N^O^ Schiff base appended homoleptic titanium(IV) complexes: DFT, BSA/CT-DNA interactions, molecular docking and antitumor activity against HeLa and A549 cell lines

Sathish Thanigachalam and Madhvesh Pathak*

Department of Chemistry, School of Advanced Sciences, Vellore Institute of Technology, Vellore - 632014, Tamil Nadu, India

*Email of corresponding author: madhveshpathak@vit.ac.in

Fig. S17	UV-Visible studies of titanium(IV) complexes: **(a)** TiH_2L^1, **(b)** TiH_2L^2, **(c)** TiH_2L^3, **(d)** TiH_2L^4 and **(e)** TiH_2L^5 in water and octanol
	DFT
Fig. S18	Optimized molecular geometry of free ligands (H_2L^1-H_2L^5) by using the DFT/B3LYP method
Fig. S19	Optimized molecular geometry of **TiH_2L^1-TiH_2L^5** by DFT/B3LYP method
Fig. S20	Electrostatic potential mapped on the surface of optimized molecular geometries of free ligands by DFT/B3LYP method
Fig. S21	FMOs of free ligand (H_2L^1-TiH_2L^5) by using DFT/B3LYP method
Fig. S22	TD-DFT spectra: **(a)** H_2L^1 -H_2L^5 for ligands and **(b)** TiH_2L^1-TiH_2L^5 in aqueous phase
	CT-DNA interaction
Fig. S23	DNA binding plots of all the five titanium(IV) derivatives: **(a)** TiH_2L^1, **(b)** TiH_2L^2, **(c)** TiH_2L^3, **(d)** TiH_2L^4 and **(e)** TiH_2L^5
Fig. S24	$\{[DNA]/(\varepsilon_a-\varepsilon_f)\}$ *vs* [DNA] linear plots of all the five complexes: **(a)** TiH_2L^1, **(b)** TiH_2L^2, **(c)** TiH_2L^3, **(d)** TiH_2L^4 and **(e)** TiH_2L^5
Fig. S25	Fluorescence quenching of EtBr-DNA with titanium(IV) complexes: **(a)** TiH_2L^1, **(b)** TiH_2L^2, **(c)** TiH_2L^3, **(d)** TiH_2L^4 and **(e)** TiH_2L^5
Fig. S26	CT-DNA intercalation Stern-Volmer plot of I_0/I *vs* concentration of titanium(IV) complexes: **(a)** TiH_2L^1, **(b)** TiH_2L^2, **(c)** TiH_2L^3, **(d)** TiH_2L^4 and **(e)** TiH_2L^5
Fig. S27	Scatchard plot of $\log([I_0-I]/I)$ *vs* log[complex] for CT-DNA with presence of titanium(IV) derivatives: **(a)** TiH_2L^1, **(b)** TiH_2L^2, **(c)** TiH_2L^3, **(d)** TiH_2L^4 and **(e)** TiH_2L^5
Fig. S28	Relative viscosity of CT-DNA interaction with EtBr and titanium(IV) derivatives **(TiH_2L^1-TiH_2L^5)**
	BSA interaction
Fig. S29	BSA binding plots of all the five titanium(IV) derivatives: **(a)** TiH_2L^1, **(b)** TiH_2L^2, **(c)** TiH_2L^3, **(d)** TiH_2L^4 and **(e)** TiH_2L^5
Fig. S30	Fluorescence quenching plot for BSA of all the five titanium(IV) derivatives: **(a)** TiH_2L^1, **(b)** TiH_2L^2, **(c)** TiH_2L^3, **(d)** TiH_2L^4 and **(e)** TiH_2L^5
Fig. S31	Stern-Volmer plot of I_0/I *vs* concentration of complexes: **(a)** TiH_2L^1, **(b)** TiH_2L^2, **(c)** TiH_2L^3, **(d)** TiH_2L^4 and **(e)** TiH_2L^5 for BSA binding
Fig. S32	Scatchard plot of $\log[I_0-I/I]$ *vs* log[Complex] for BSA in the presence of titanium(IV) derivatives: **(a)** TiH_2L^1, **(b)** TiH_2L^2, **(c)** TiH_2L^3, **(d)** TiH_2L^4 and **(e)** TiH_2L^5
Fig. S33	Anti-inflammatory activity of **TiH_2L^1-TiH_2L^5**
Fig. S34	Microscopic images (a-h) of HeLa and A549 cells treated with titanium(IV) derivatives **(TiH_2L^2-TiH_2L^4)** in 100 µg/mL concentration (dead cells are revealed as red circles and live cells are demonstrated as blue circles)
	Table
Table S1	FTIR spectral data (cm^{-1}) of **TiH_2L^1-TiH_2L^5**
Table S2	Calculated molecular electronic parameters of ligands (H_2L^1-H_2L^5) and titanium(IV) derivatives **(TiH_2L^1-TiH_2L^5)**
Table S3	Optimized bond length of Ti(IV) complexes
Table S4	Optimized bond angle of the Ti(IV) derivatives
Table S5	Chemical shifts (ppm): protons of the **TiH_2L^3** and CT-DNA bound with TiH_2L^3 in the system

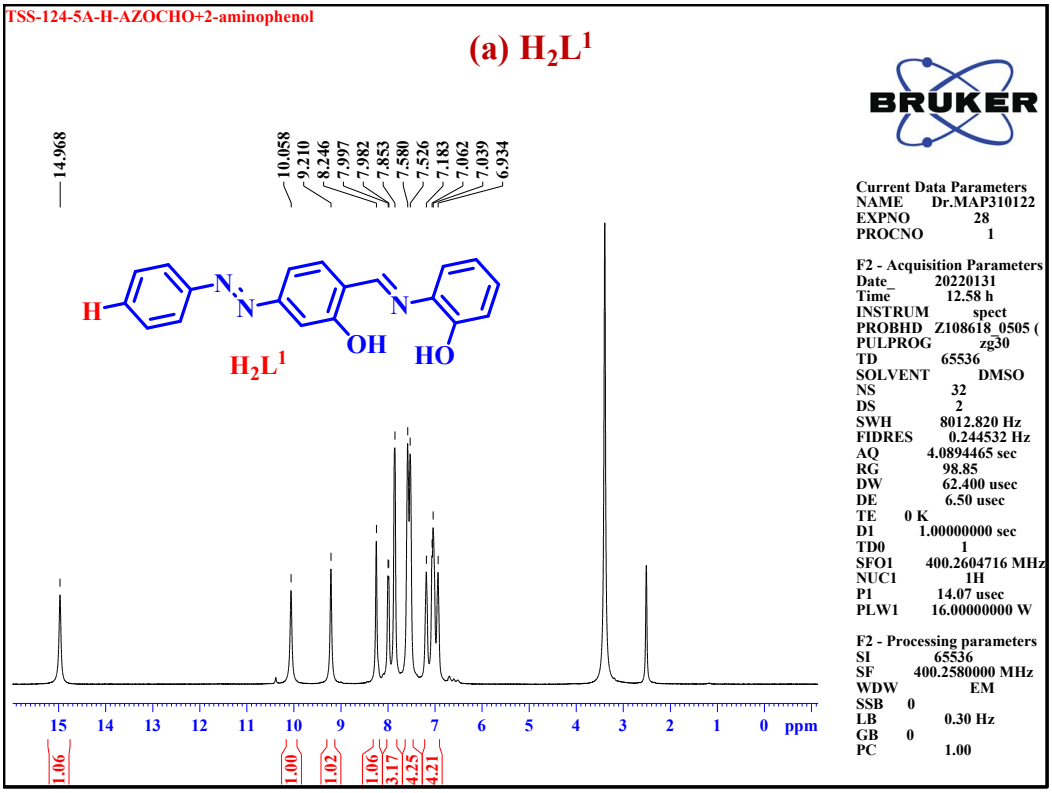

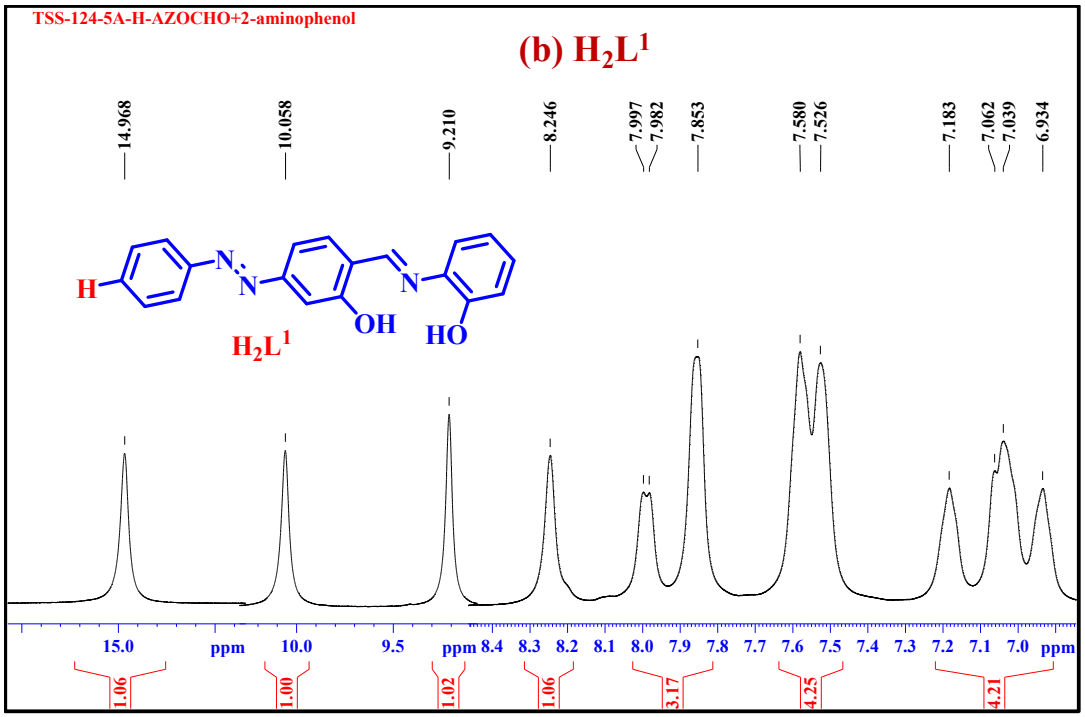

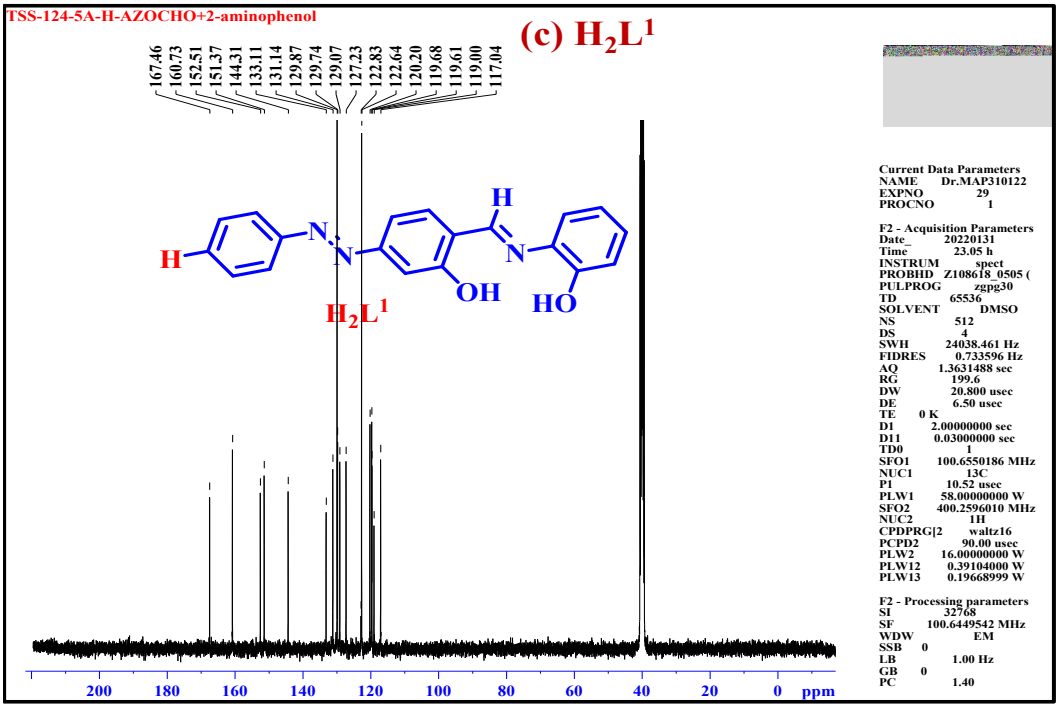

Fig. S1 NMR Spectrum of ligand H_2L^1: **(a)** ^1H NMR spectrum, **(b)** ^1H NMR expansion spectrum and **(c)** ^{13}C NMR spectrum

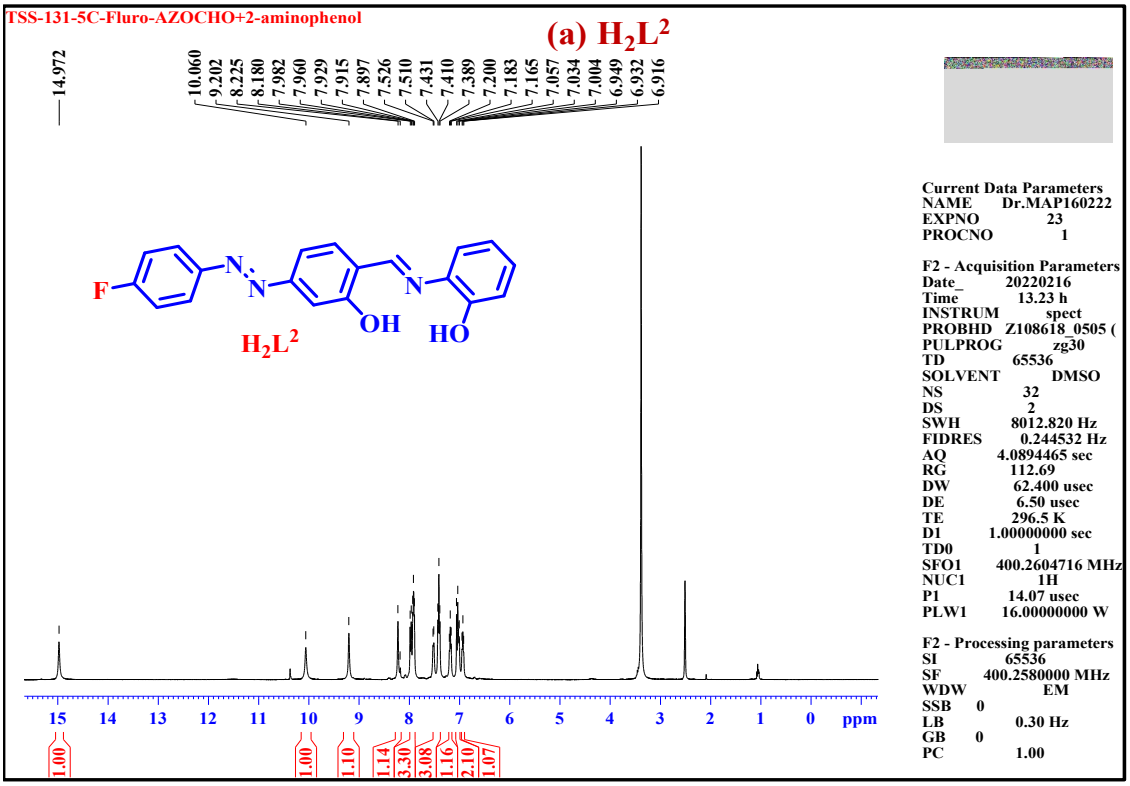
TSS-131-5C-Fluro-AZOCHO+2-aminophenol
(a) H2L2
14.972
10.060
9.202
8.225
8.180
7.982
7.960
7.929
7.915
7.897
7.526
7.510
7.431
7.410
7.389
7.200
7.183
7.165
7.057
7.034
7.004
6.949
6.932
6.916
F
N
N
OH
N
HO
H2L2
15 14 13 12 11 10 9 8 7 6 5 4 3 2 1 0 ppm
1.00 1.00 1.10 1.14 3.30 3.08 1.16 2.10 1.07
Current Data Parameters
NAME Dr.MAP160222
EXPNO 23
PROCNO 1
F2 - Acquisition Parameters
Date_ 20220216
Time 13.23 h
INSTRUM spect
PROBHD Z108618_0505 (
PULPROG zg30
TD 65536
SOLVENT DMSO
NS 32
DS 2
SWH 8012.820 Hz
FIDRES 0.244532 Hz
AQ 4.0894465 sec
RG 112.69
DW 62.400 usec
DE 6.50 usec
TE 296.5 K
D1 1.00000000 sec
TD0 1
SFO1 400.2604716 MHz
NUC1 1H
P1 14.07 usec
PLW1 16.00000000 W
F2 - Processing parameters
SI 65536
SF 400.2580000 MHz
WDW EM
SSB 0
LB 0.30 Hz
GB 0
PC 1.00

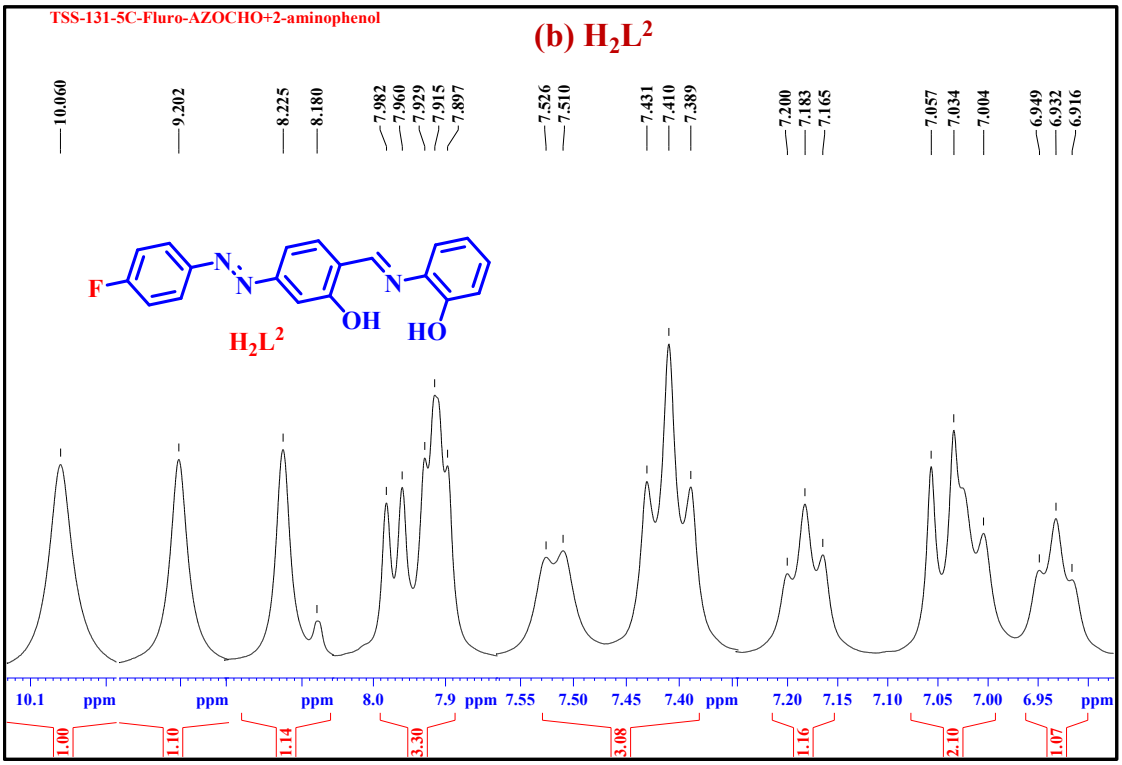
TSS-131-5C-Fluro-AZOCHO+2-aminophenol
(b) H2L2
10.060
9.202
8.225
8.180
7.982
7.960
7.929
7.915
7.897
7.526
7.510
7.431
7.410
7.389
7.200
7.183
7.165
7.057
7.034
7.004
6.949
6.932
6.916
F
N
N
OH
N
HO
H2L2
10.1 ppm ppm ppm 8.0 7.9 ppm 7.55 7.50 7.45 7.40 ppm 7.20 7.15 7.10 7.05 7.00 6.95 ppm
1.00 1.10 1.14 3.30 3.08 1.16 2.10 1.07

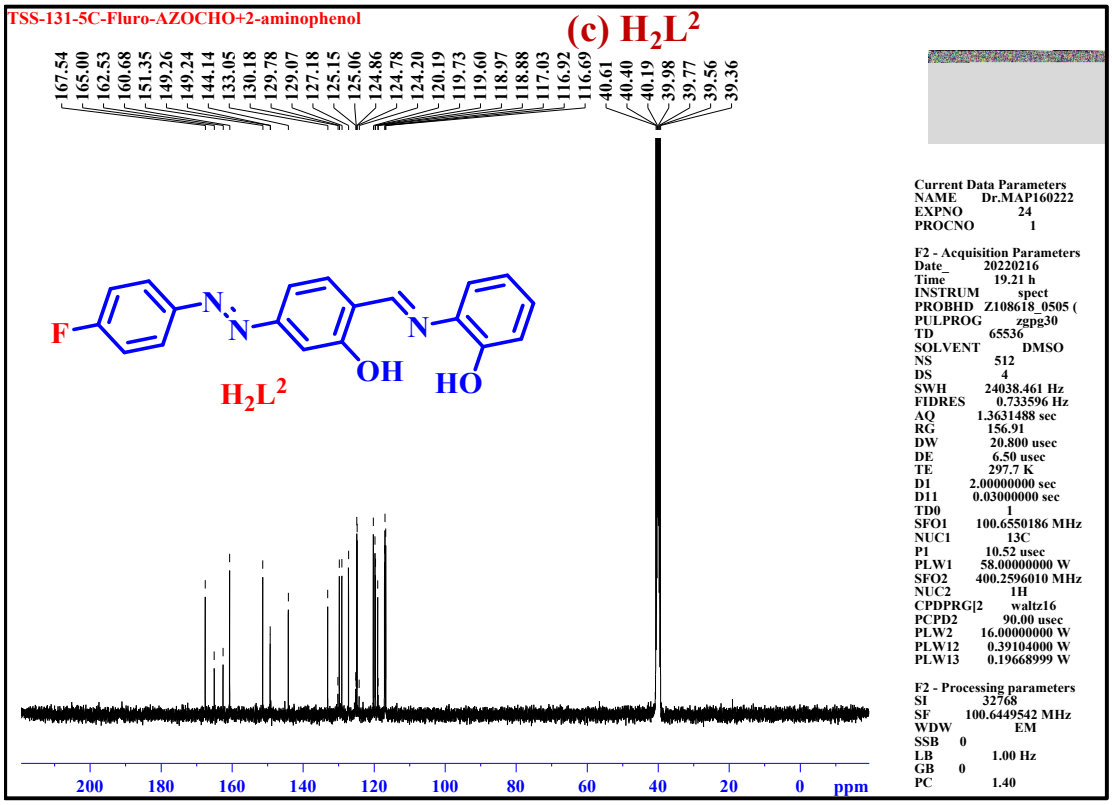

Fig. S2 NMR Spectrum of ligand H_2L^2: **(a)** ^1H NMR spectrum, **(b)** ^1H NMR expansion spectrum and **(c)** ^{13}C NMR spectrum

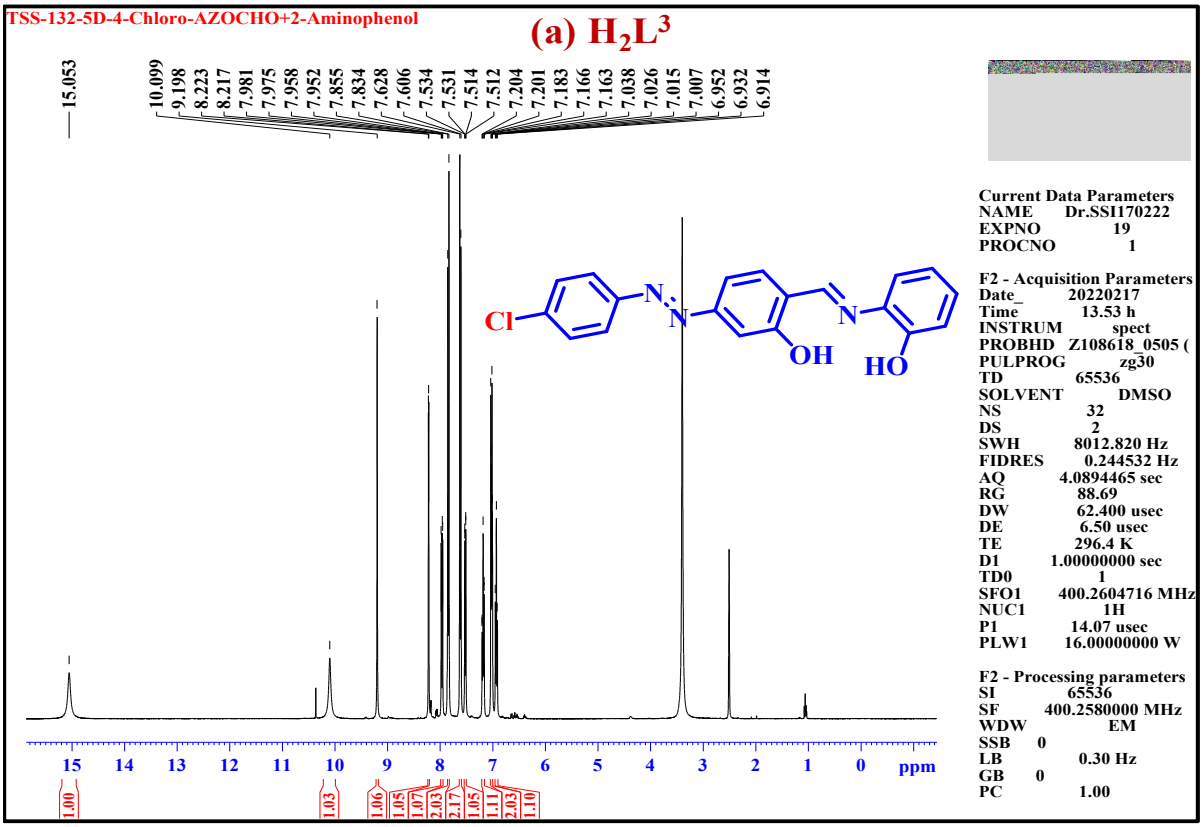

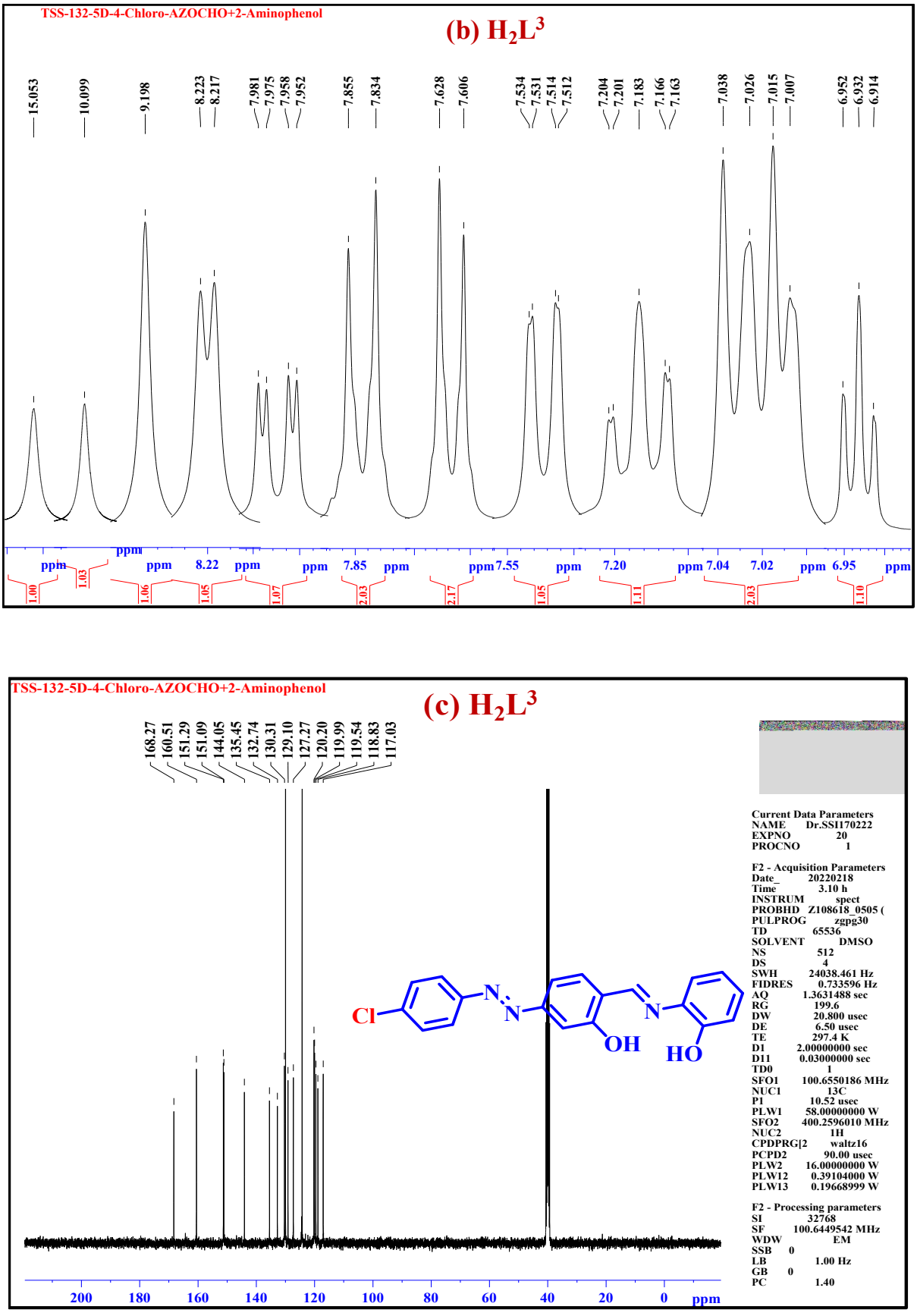

Fig. S3 NMR Spectrum of ligand H_2L^3: **(a)** ^1H NMR spectrum, **(b)** ^1H NMR expansion spectrum and **(c)** ^{13}C NMR spectrum

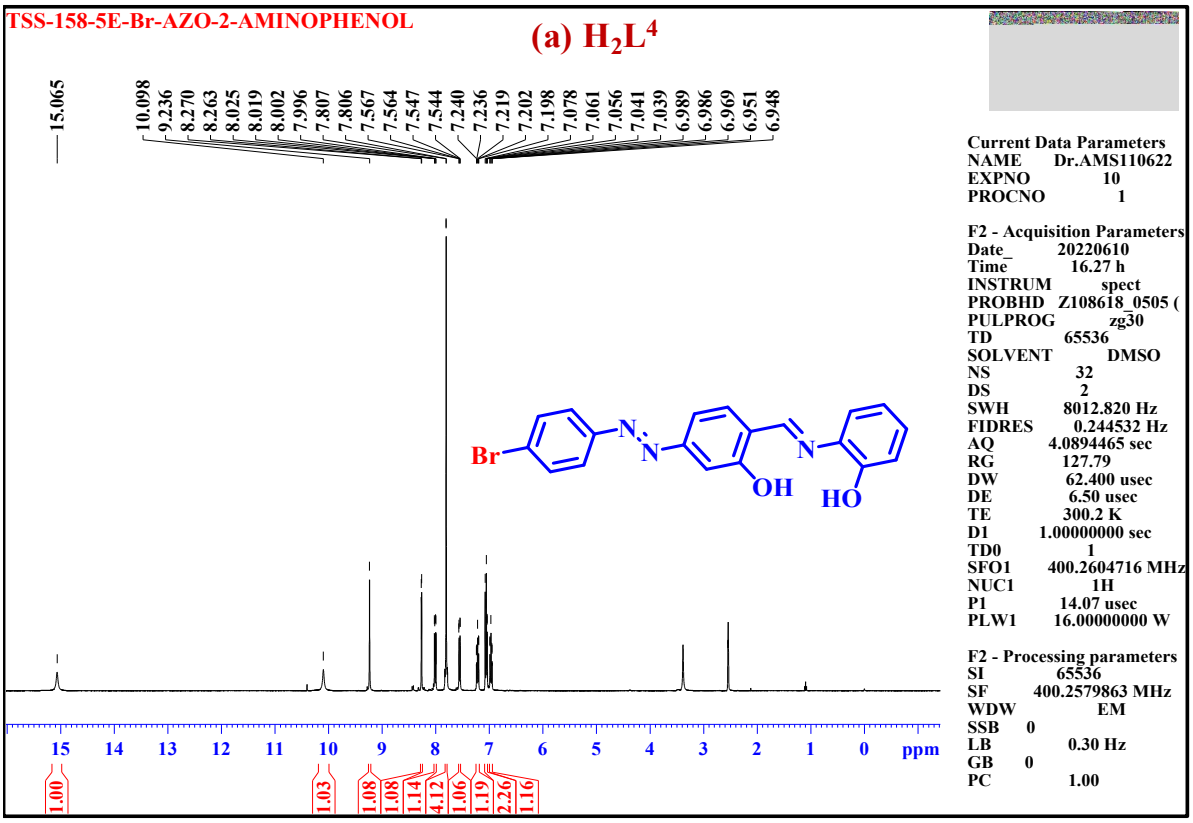
TSS-158-5E-Br-AZO-2-AMINOPHENOL
(a) H_2L^4
15.065
10.098
9.236
8.270
8.263
8.025
8.019
8.002
7.996
7.807
7.806
7.567
7.564
7.547
7.544
7.240
7.236
7.219
7.202
7.198
7.078
7.061
7.056
7.041
7.039
6.989
6.986
6.969
6.951
6.948
Br
N
N
N
OH
HO
15 14 13 12 11 10 9 8 7 6 5 4 3 2 1 0 ppm
1.00 1.03 1.08 1.08 1.14 4.12 1.06 1.19 2.26 1.16
Current Data Parameters
NAME Dr.AMS110622
EXPNO 10
PROCNO 1
F2 - Acquisition Parameters
Date_ 20220610
Time 16.27 h
INSTRUM spect
PROBHD Z108618_0505 (
PULPROG zg30
TD 65536
SOLVENT DMSO
NS 32
DS 2
SWH 8012.820 Hz
FIDRES 0.244532 Hz
AQ 4.0894465 sec
RG 127.79
DW 62.400 usec
DE 6.50 usec
TE 300.2 K
D1 1.00000000 sec
TD0 1
SFO1 400.2604716 MHz
NUC1 1H
P1 14.07 usec
PLW1 16.00000000 W
F2 - Processing parameters
SI 65536
SF 400.2579863 MHz
WDW EM
SSB 0
LB 0.30 Hz
GB 0
PC 1.00

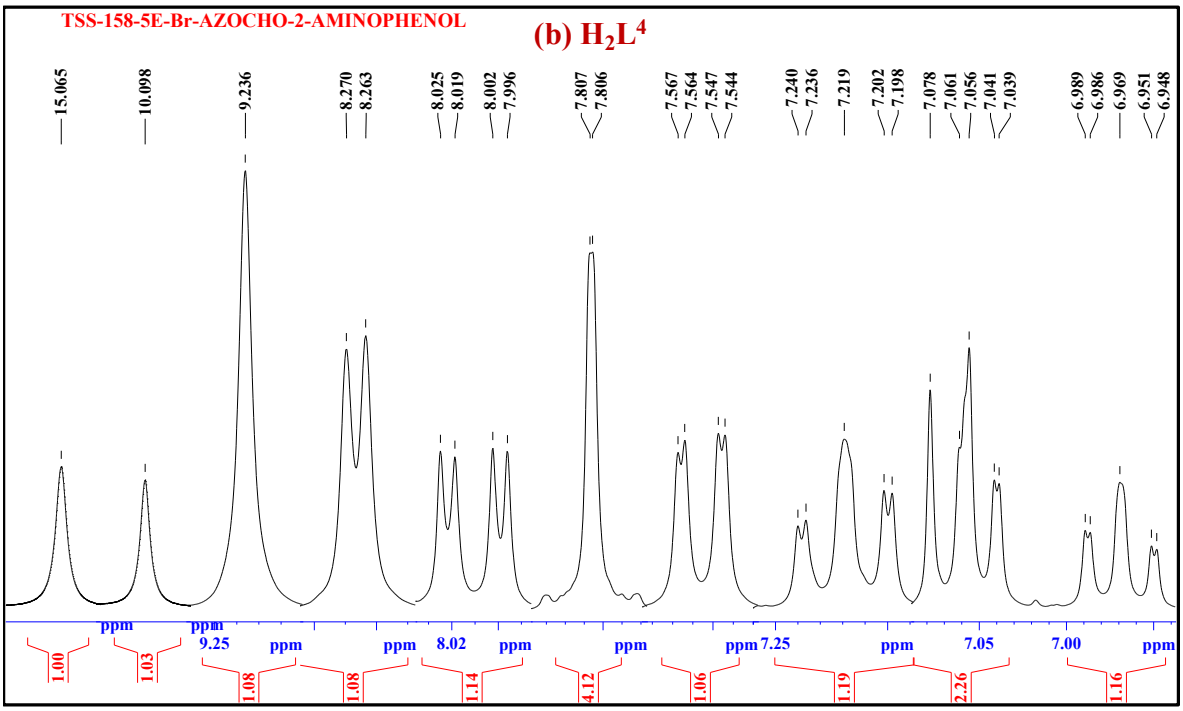
TSS-158-5E-Br-AZOCHO-2-AMINOPHENOL
(b) H_2L^4
15.065
10.098
9.236
8.270
8.263
8.025
8.019
8.002
7.996
7.807
7.806
7.567
7.564
7.547
7.544
7.240
7.236
7.219
7.202
7.198
7.078
7.061
7.056
7.041
7.039
6.989
6.986
6.969
6.951
6.948
ppm
9.25
8.02
7.25
7.05
7.00
1.00 1.03 1.08 1.08 1.14 4.12 1.06 1.19 2.26 1.16

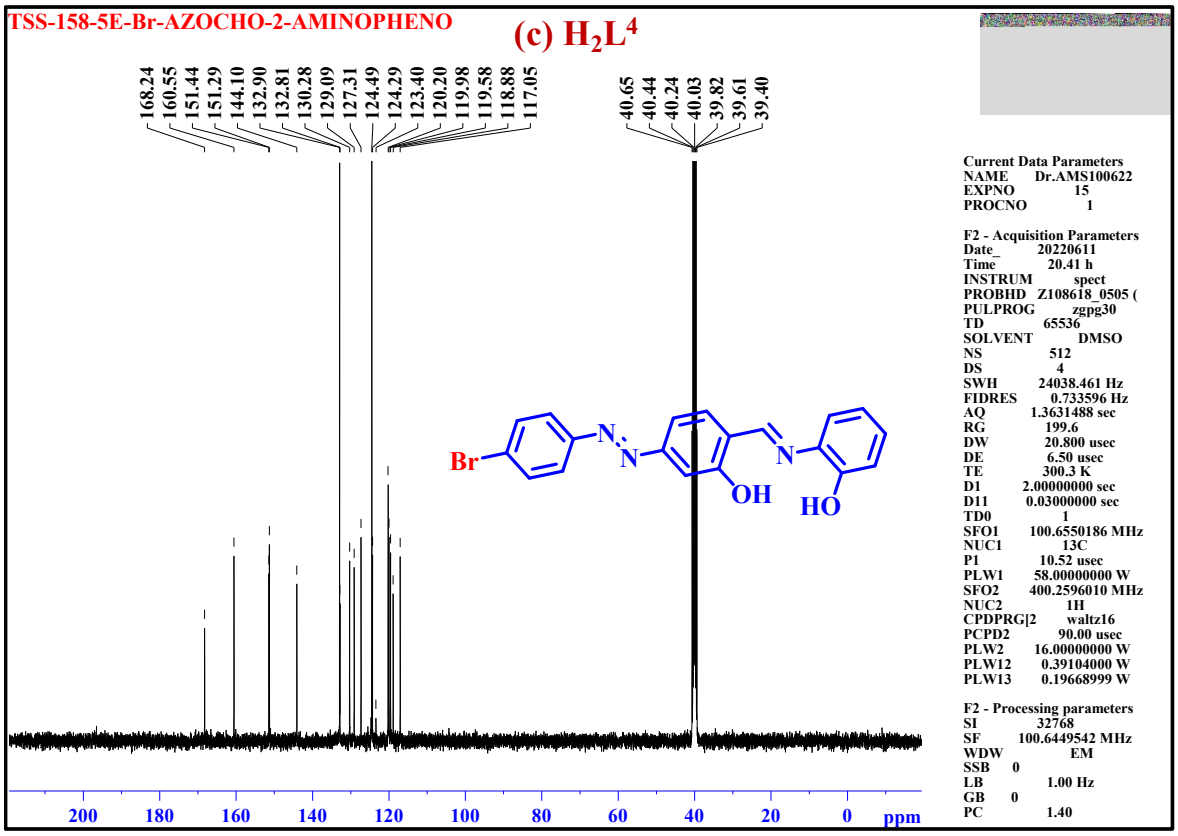

Fig. 4 NMR Spectrum of ligand H_2L^4: **(a)** ^1H NMR spectrum, **(b)** ^1H NMR expansion spectrum and **(c)** ^{13}C NMR spectrum

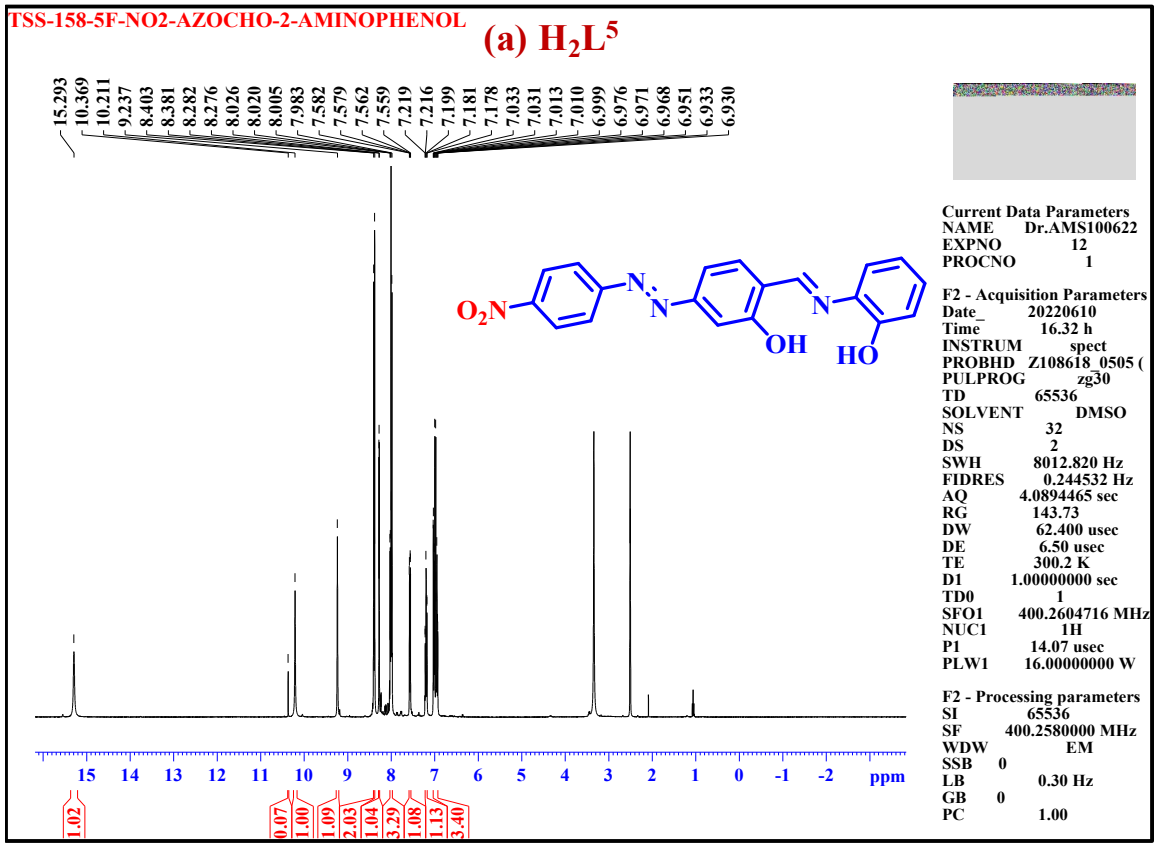
TSS-158-5F-NO2-AZOCHO-2-AMINOPHENOL
(a) H_2L^5
15.293
10.369
10.211
9.237
8.403
8.381
8.282
8.276
8.026
8.020
8.005
7.983
7.582
7.579
7.562
7.559
7.219
7.216
7.199
7.181
7.178
7.033
7.031
7.013
7.010
6.999
6.976
6.971
6.968
6.951
6.933
6.930
O_2N
N
N
OH
N
HO
15 14 13 12 11 10 9 8 7 6 5 4 3 2 1 0 -1 -2 ppm
1.02
0.07
1.00
1.09
2.03
1.04
3.29
1.08
1.13
3.40
Current Data Parameters
NAME Dr.AMS100622
EXPNO 12
PROCNO 1
F2 - Acquisition Parameters
Date_ 20220610
Time 16.32 h
INSTRUM spect
PROBHD Z108618_0505 (
PULPROG zg30
TD 65536
SOLVENT DMSO
NS 32
DS 2
SWH 8012.820 Hz
FIDRES 0.244532 Hz
AQ 4.0894465 sec
RG 143.73
DW 62.400 usec
DE 6.50 usec
TE 300.2 K
D1 1.00000000 sec
TD0 1
SFO1 400.2604716 MHz
NUC1 1H
P1 14.07 usec
PLW1 16.00000000 W
F2 - Processing parameters
SI 65536
SF 400.2580000 MHz
WDW EM
SSB 0
LB 0.30 Hz
GB 0
PC 1.00

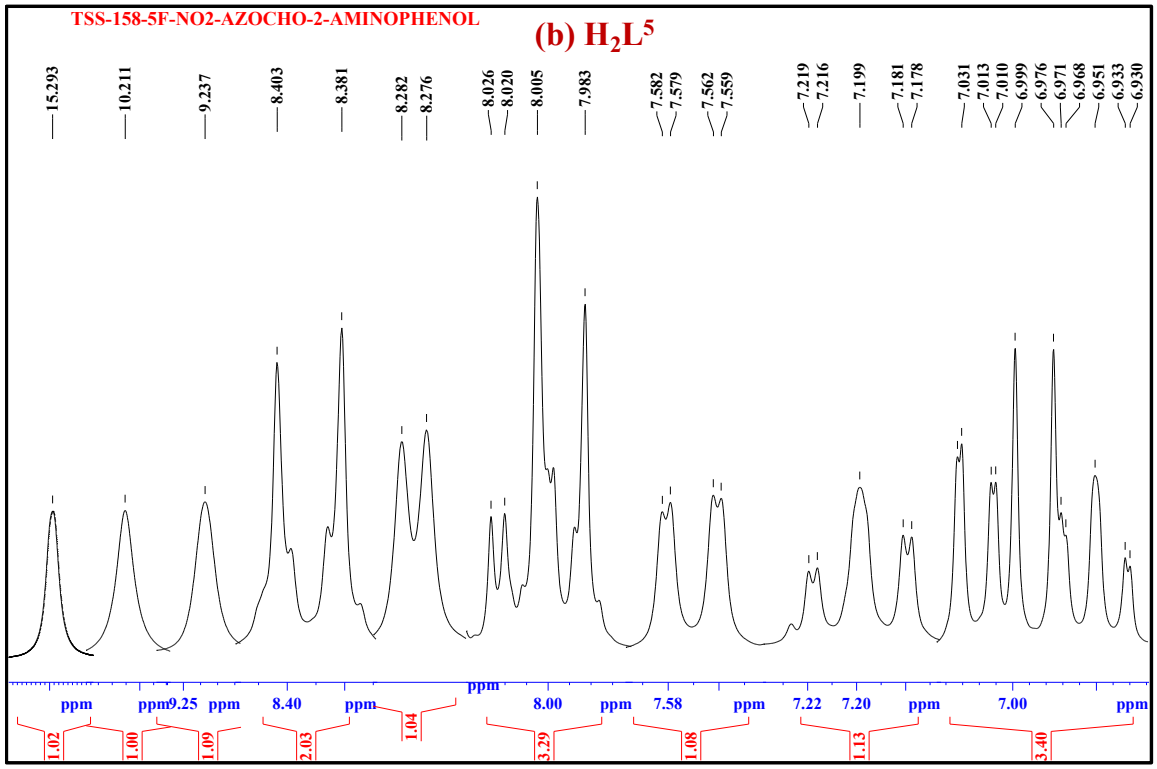
TSS-158-5F-NO2-AZOCHO-2-AMINOPHENOL
(b) H_2L^5
15.293
10.211
9.237
8.403
8.381
8.282
8.276
8.026
8.020
8.005
7.983
7.582
7.579
7.562
7.559
7.219
7.216
7.199
7.181
7.178
7.031
7.013
7.010
6.999
6.976
6.971
6.968
6.951
6.933
6.930
ppm
ppm ppm 9.25 ppm 8.40 ppm 8.00 ppm 7.58 ppm 7.22 7.20 ppm 7.00 ppm
1.02
1.00
1.09
2.03
1.04
3.29
1.08
1.13
3.40

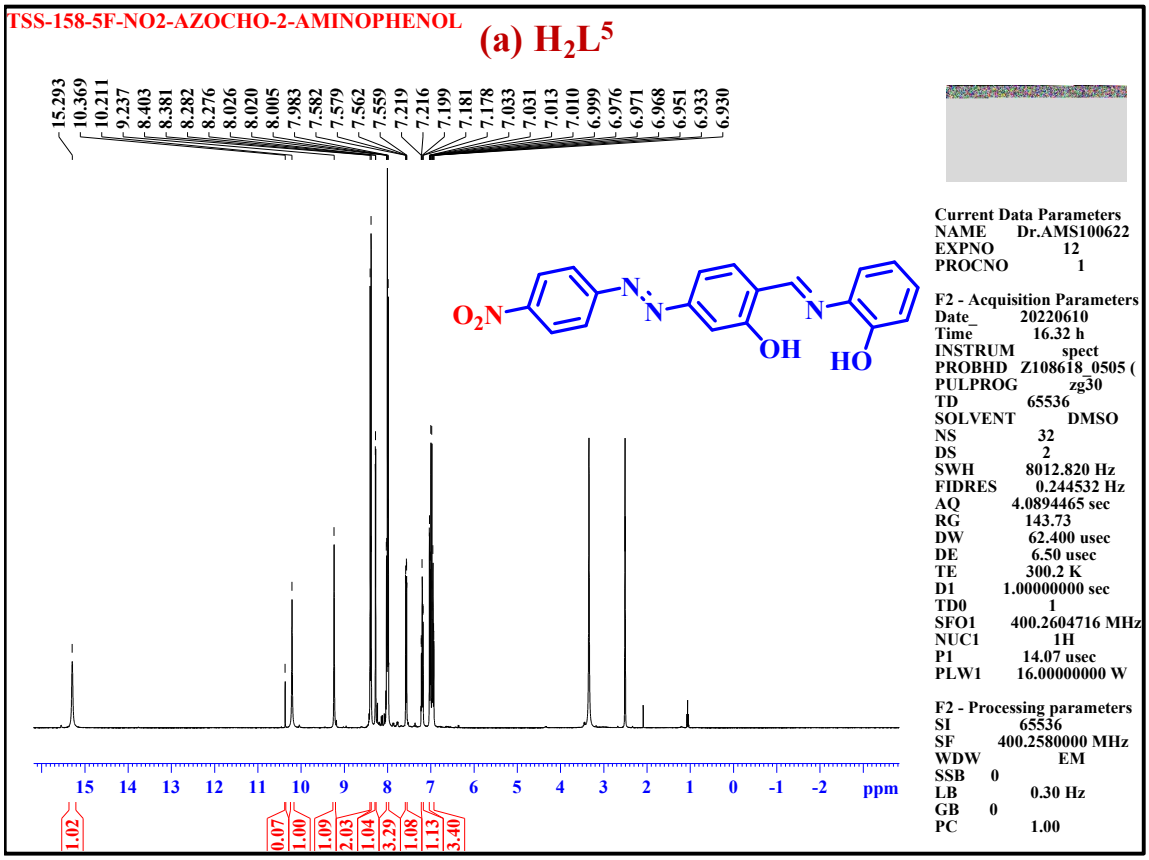

Fig. S5 NMR Spectrum of ligand H_2L^5: **(a)** ^1H NMR spectrum, **(b)** ^1H NMR expansion spectrum **(c)** ^{13}C NMR spectrum

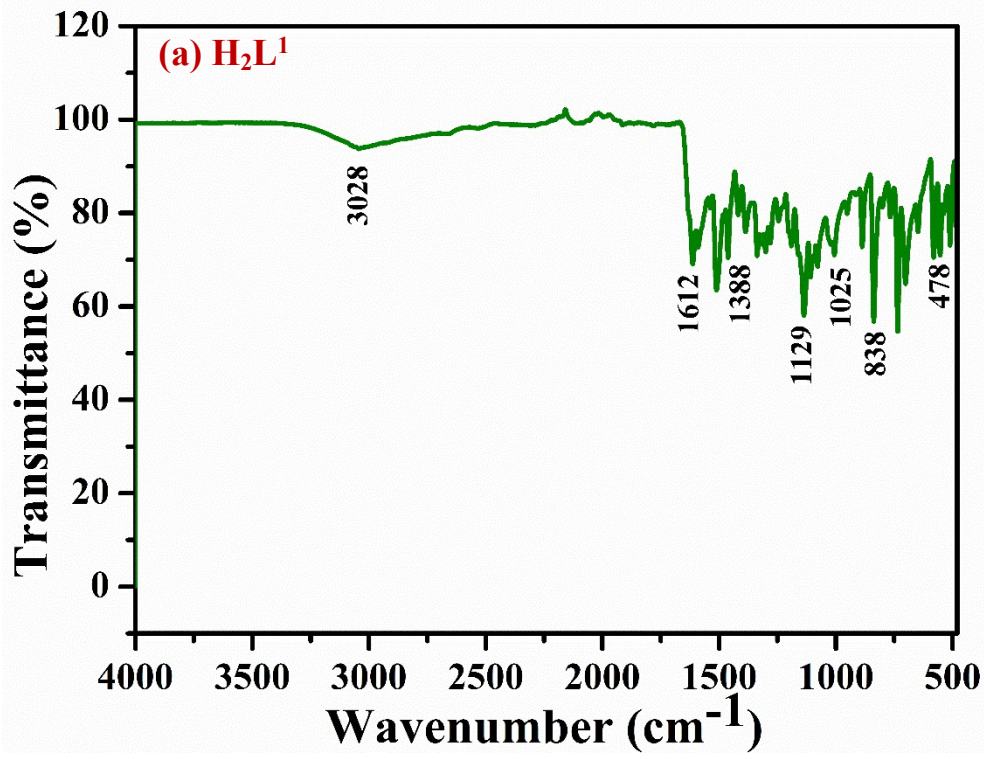

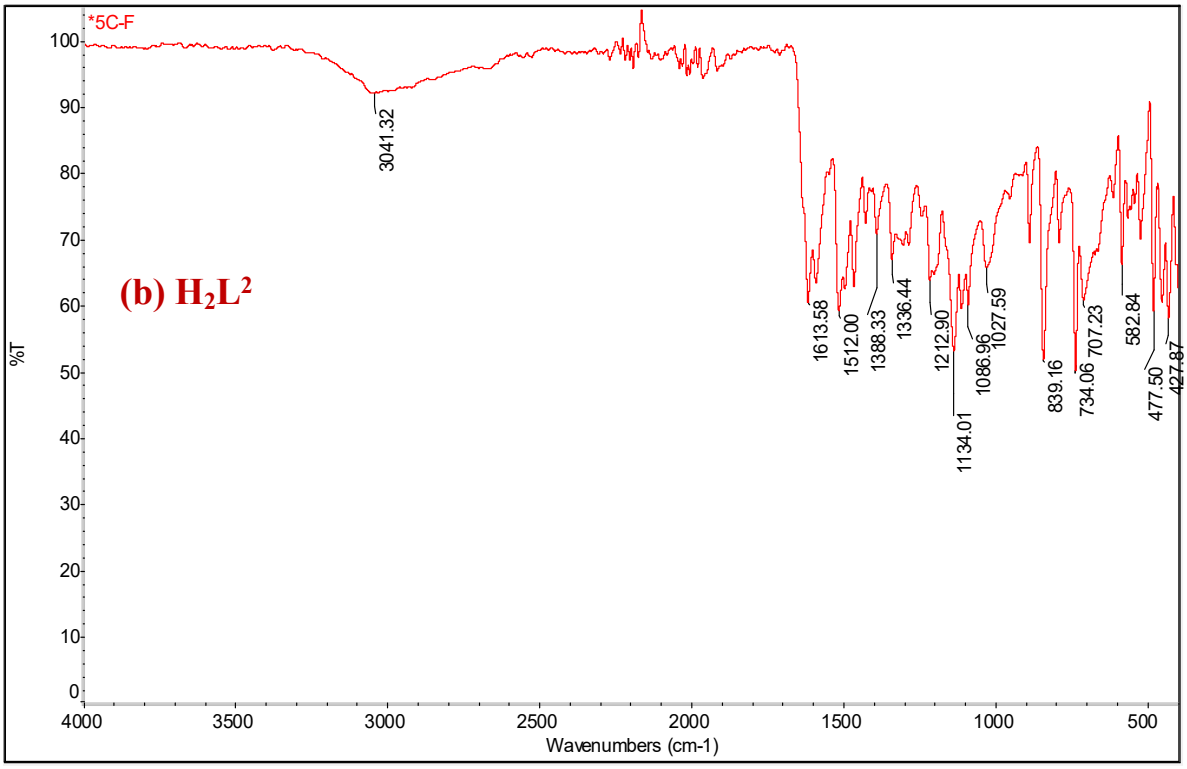
*5C-F
(b) H2L2
%T
Wavenumbers (cm-1)
3041.32
1613.58
1512.00
1388.33
1336.44
1212.90
1134.01
1086.96
1027.59
839.16
734.06
707.23
582.84
477.50
427.87

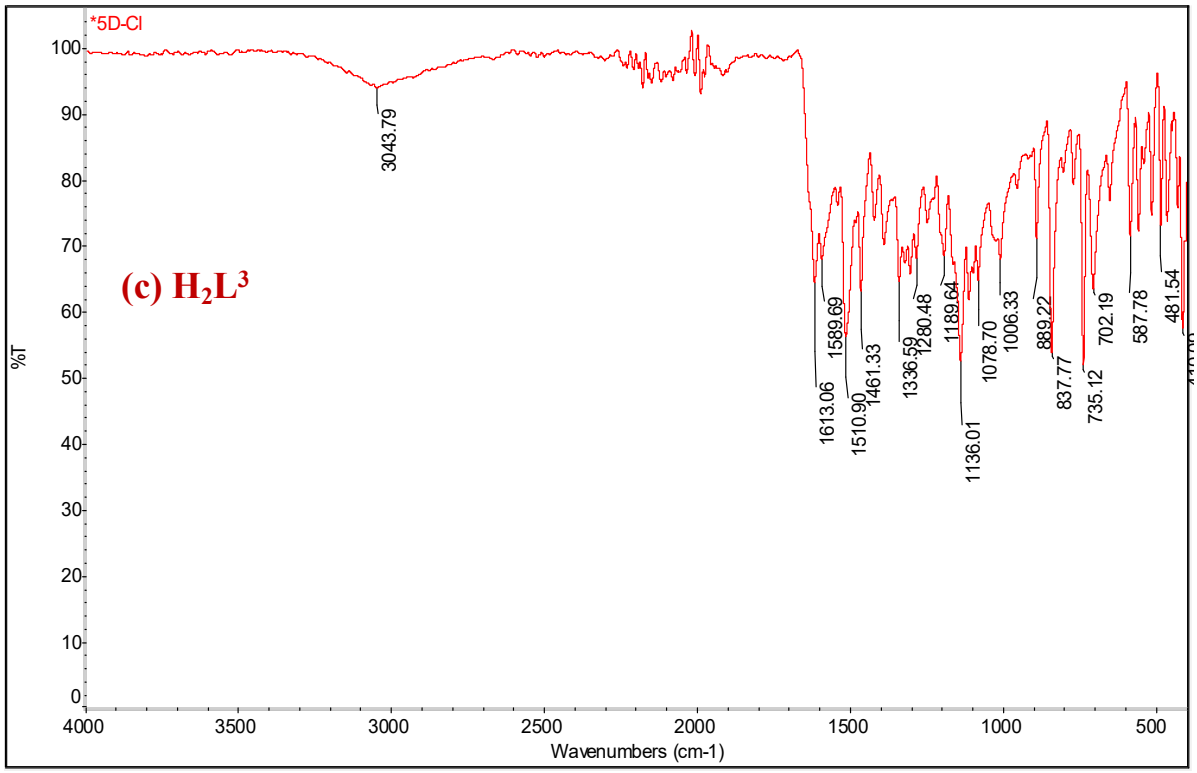
*5D-Cl
(c) H2L3
%T
Wavenumbers (cm-1)
3043.79
1613.06
1589.69
1510.90
1461.33
1336.59
1280.48
1189.64
1136.01
1078.70
1006.33
889.22
837.77
735.12
702.19
587.78
481.54

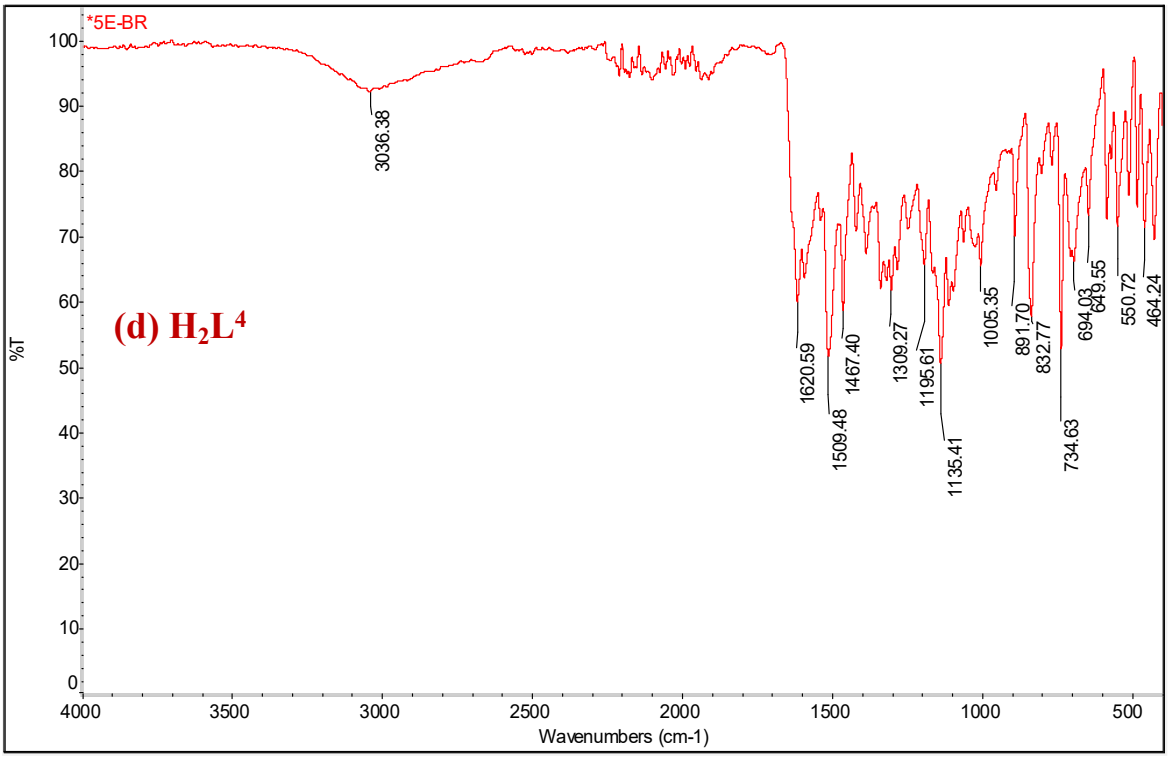

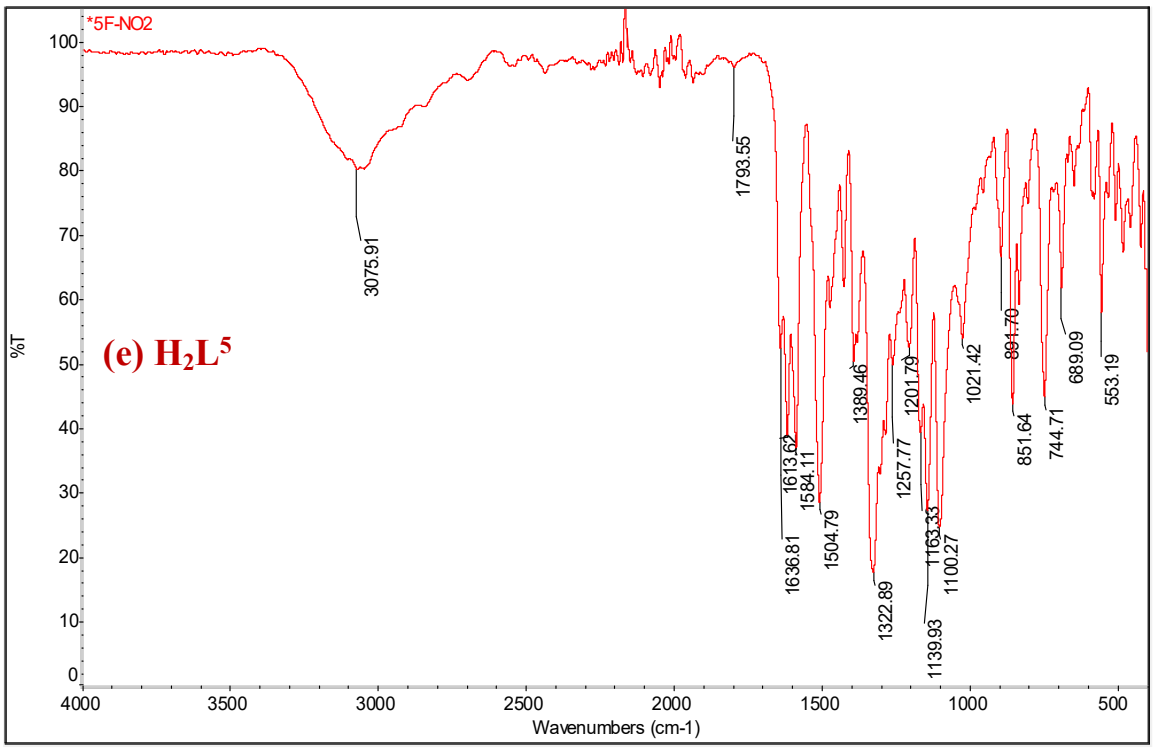

Fig. S6 FTIR Spectra of ligands **(a)** H_2L^1, **(b)** H_2L^2, **(c)** H_2L^3, **(d)** H_2L^4 and **(e)** H_2L^5

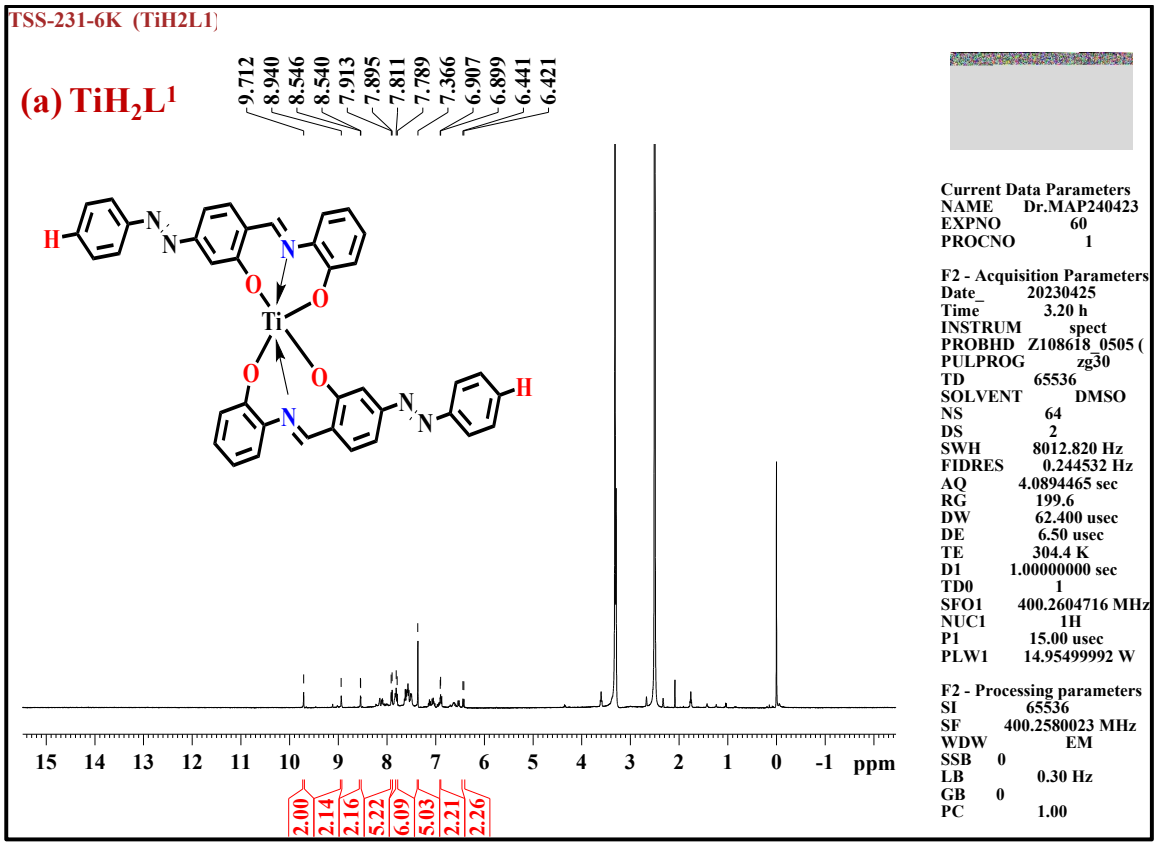
TSS-231-6K (TiH2L1)
(a) TiH2L1
9.712
8.940
8.546
8.540
7.913
7.895
7.811
7.789
7.366
6.907
6.899
6.441
6.421
Current Data Parameters
NAME Dr.MAP240423
EXPNO 60
PROCNO 1
F2 - Acquisition Parameters
Date_ 20230425
Time 3.20 h
INSTRUM spect
PROBHD Z108618_0505 (
PULPROG zg30
TD 65536
SOLVENT DMSO
NS 64
DS 2
SWH 8012.820 Hz
FIDRES 0.244532 Hz
AQ 4.0894465 sec
RG 199.6
DW 62.400 usec
DE 6.50 usec
TE 304.4 K
D1 1.00000000 sec
TD0 1
SFO1 400.2604716 MHz
NUC1 1H
P1 15.00 usec
PLW1 14.95499992 W
F2 - Processing parameters
SI 65536
SF 400.2580023 MHz
WDW EM
SSB 0
LB 0.30 Hz
GB 0
PC 1.00
15 14 13 12 11 10 9 8 7 6 5 4 3 2 1 0 -1 ppm
2.00
2.14
2.16
5.22
6.09
5.03
2.21
2.26

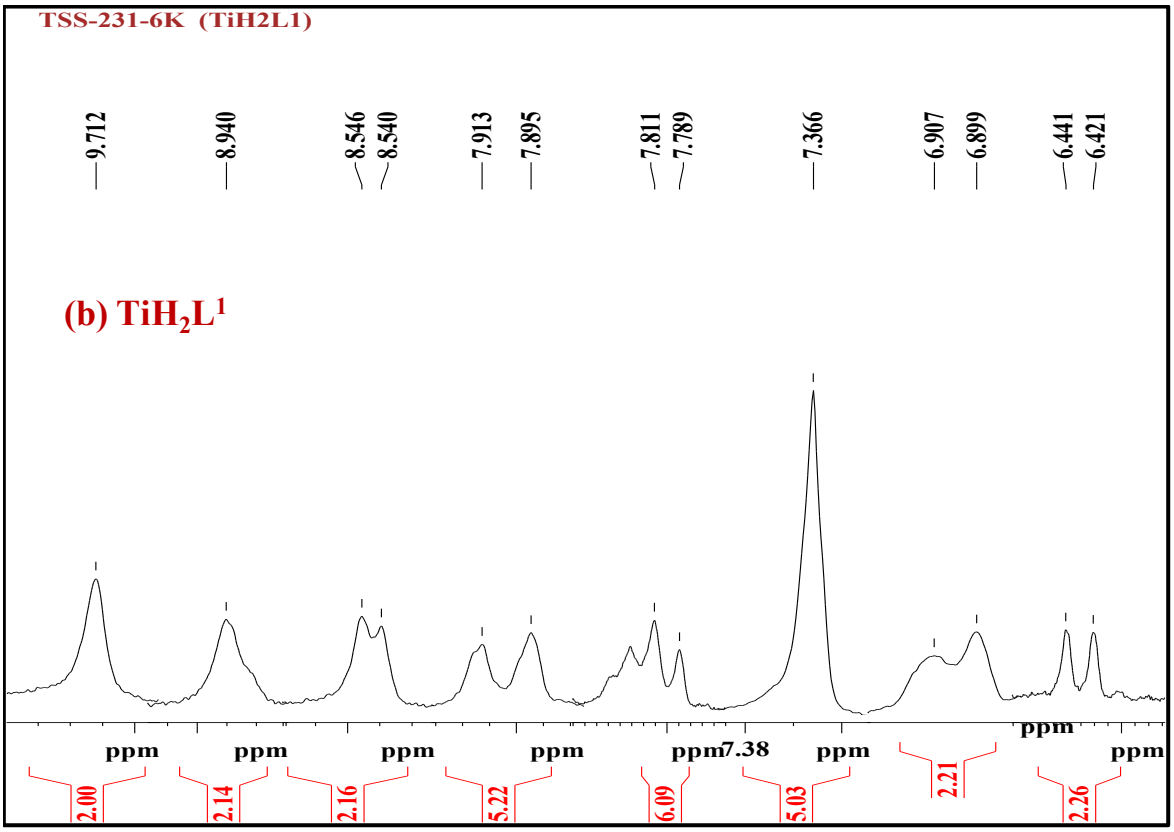
TSS-231-6K (TiH2L1)
9.712
8.940
8.546
8.540
7.913
7.895
7.811
7.789
7.366
6.907
6.899
6.441
6.421
(b) TiH2L1
ppm
7.38
2.00
2.14
2.16
5.22
6.09
5.03
2.21
2.26

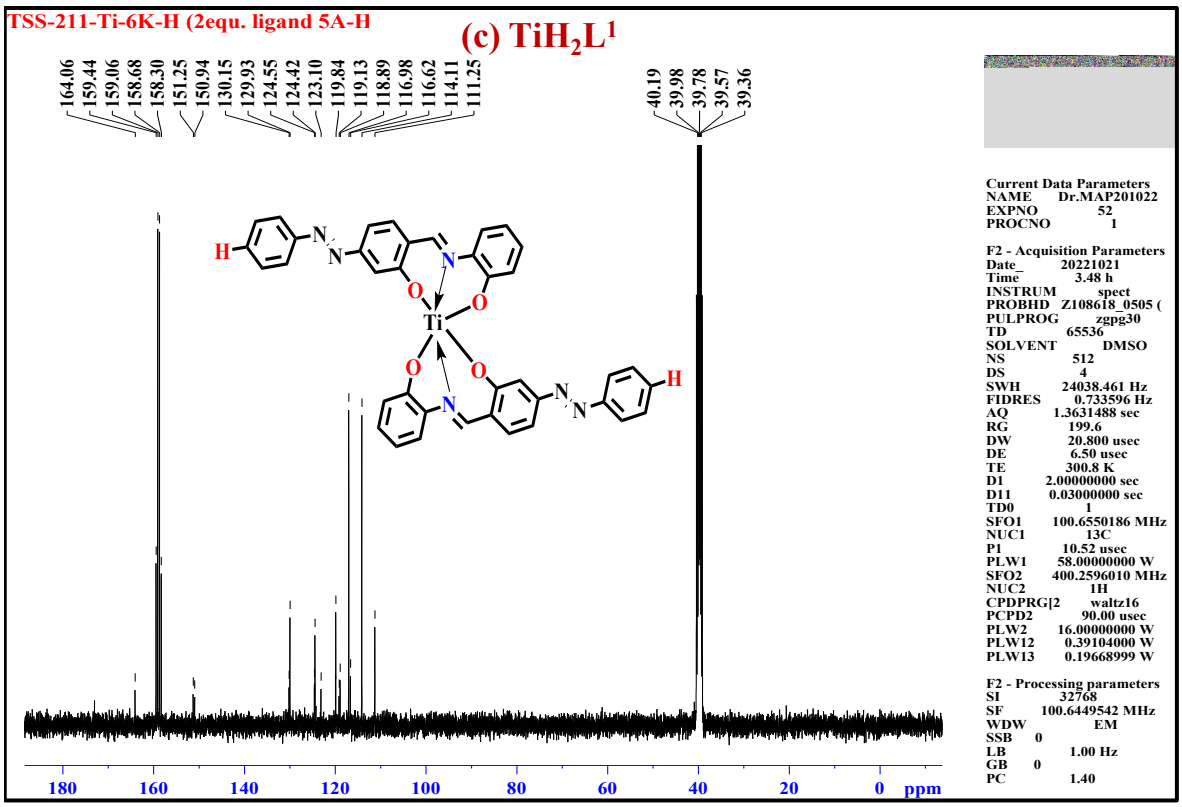

SI Fig. 7. NMR Spectrum of **TiH_2L^1**: **(a)** ^{1}H NMR spectrum, **(b)** ^{1}H NMR expansion spectrum **(c)** ^{13}C NMR spectrum

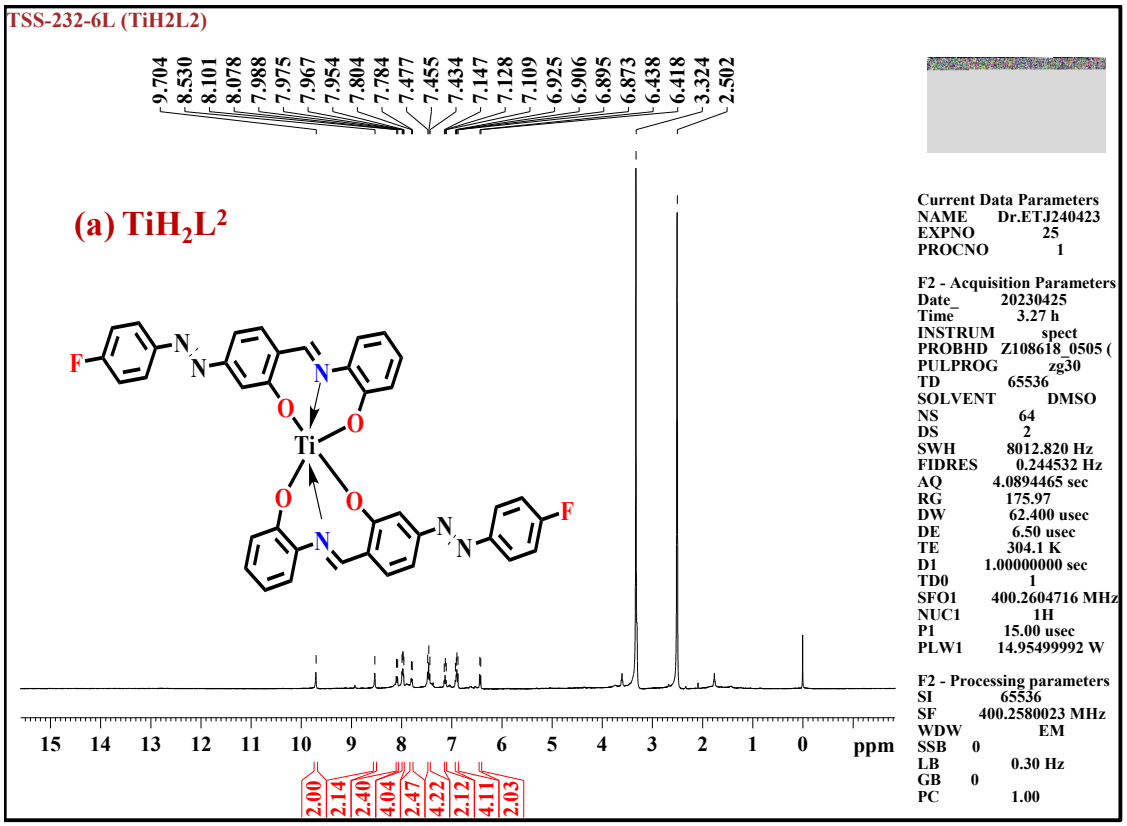

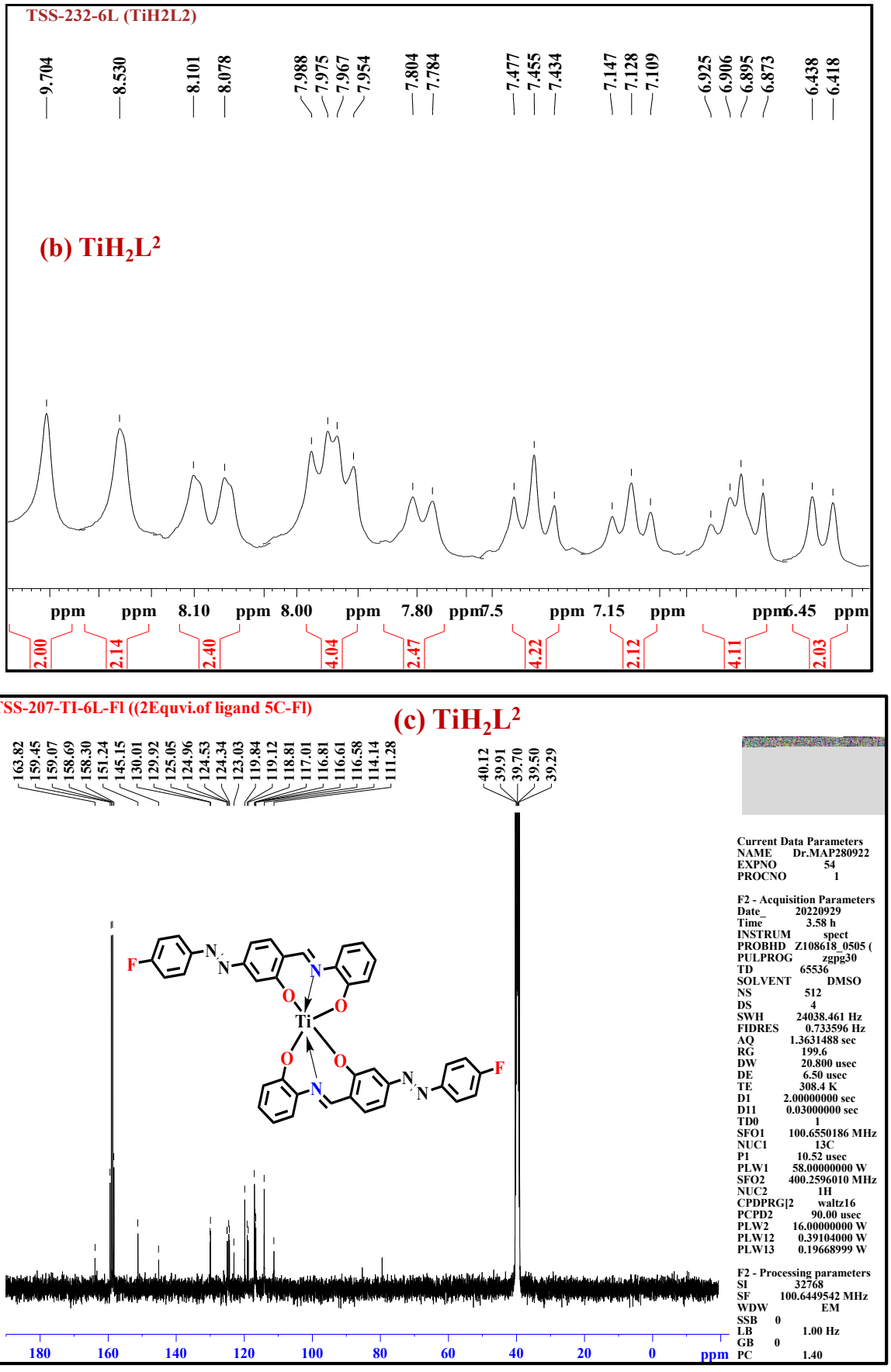

Fig. S8 NMR Spectrum of **TiH_2L^2**: **(a)** ^{1}H NMR spectrum, **(b)** ^{1}H NMR expansion spectrum **(c)** ^{13}C NMR spectrum

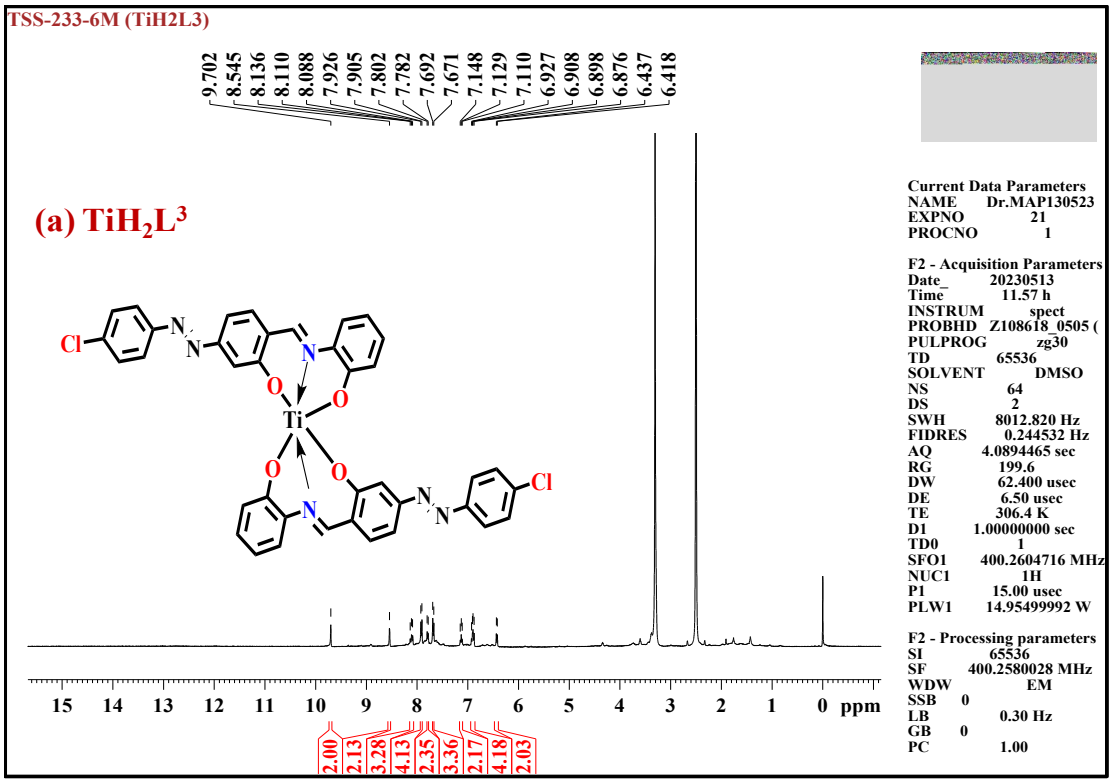
TSS-233-6M (TiH2L3)
9.702
8.545
8.136
8.110
8.088
7.926
7.905
7.802
7.782
7.692
7.671
7.148
7.129
7.110
6.927
6.908
6.898
6.876
6.437
6.418
(a) TiH2L3
Cl
N
N
O
O
Ti
O
O
N
N
Cl
15 14 13 12 11 10 9 8 7 6 5 4 3 2 1 0 ppm
2.00
2.13
3.28
4.13
2.35
3.36
2.17
4.18
2.03
Current Data Parameters
NAME Dr.MAP130523
EXPNO 21
PROCNO 1
F2 - Acquisition Parameters
Date_ 20230513
Time 11.57 h
INSTRUM spect
PROBHD Z108618_0505 (
PULPROG zg30
TD 65536
SOLVENT DMSO
NS 64
DS 2
SWH 8012.820 Hz
FIDRES 0.244532 Hz
AQ 4.0894465 sec
RG 199.6
DW 62.400 usec
DE 6.50 usec
TE 306.4 K
D1 1.00000000 sec
TD0 1
SFO1 400.2604716 MHz
NUC1 1H
P1 15.00 usec
PLW1 14.95499992 W
F2 - Processing parameters
SI 65536
SF 400.2580028 MHz
WDW EM
SSB 0
LB 0.30 Hz
GB 0
PC 1.00

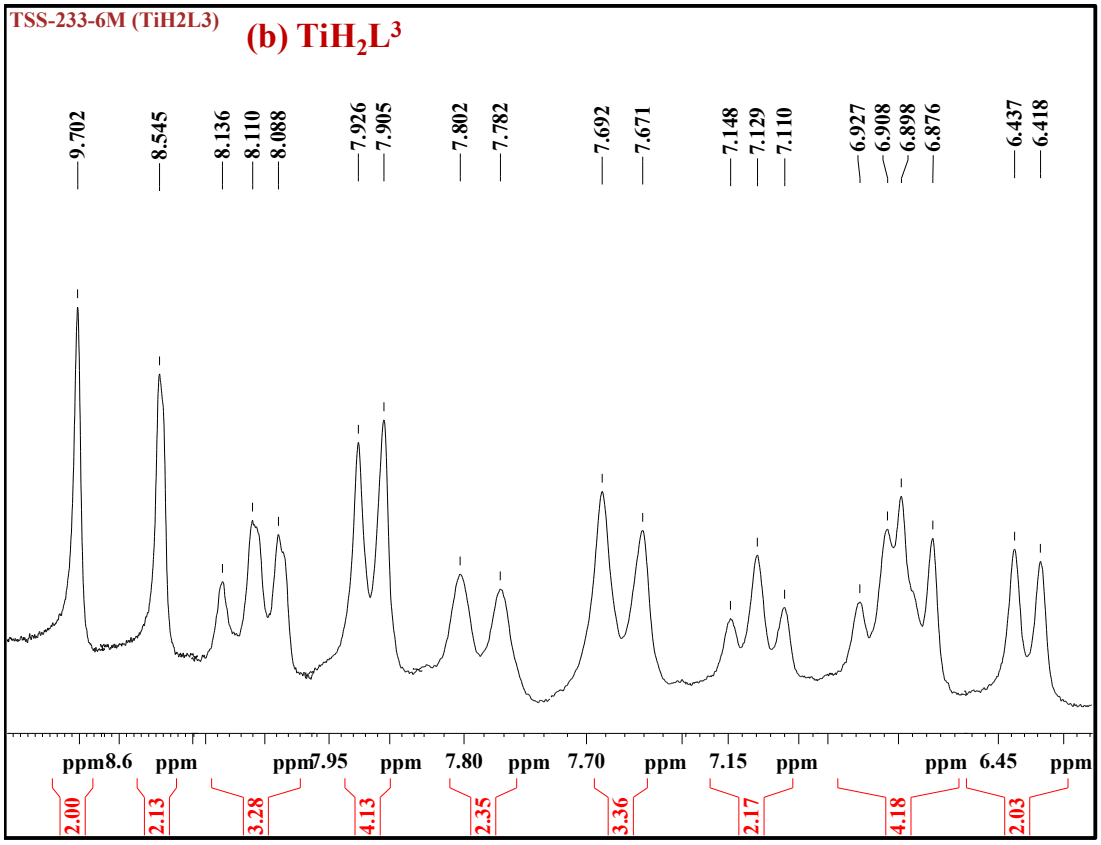
TSS-233-6M (TiH2L3)
(b) TiH2L3
9.702
8.545
8.136
8.110
8.088
7.926
7.905
7.802
7.782
7.692
7.671
7.148
7.129
7.110
6.927
6.908
6.898
6.876
6.437
6.418
ppm 8.6 ppm 7.95 ppm 7.80 ppm 7.70 ppm 7.15 ppm 6.45 ppm
2.00
2.13
3.28
4.13
2.35
3.36
2.17
4.18
2.03

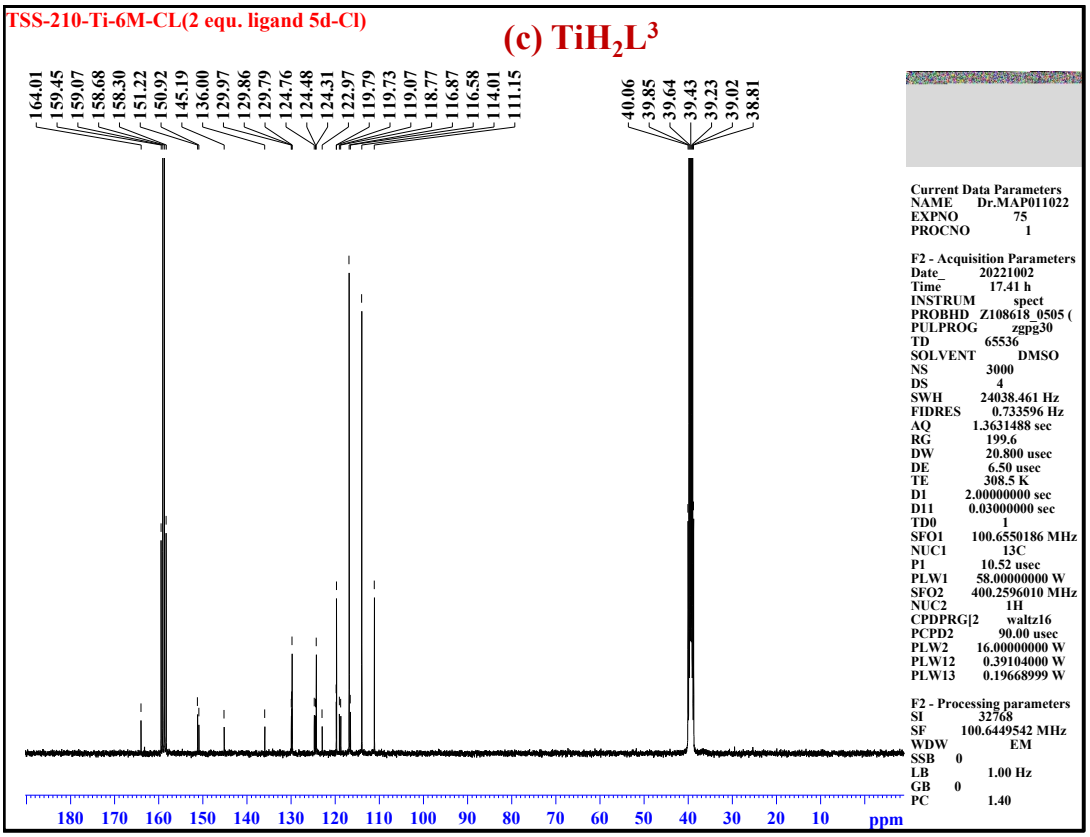

Fig. S9 NMR Spectrum of **TiH_2L^3**: **(a)** ^{1}H NMR spectrum, **(b)** ^{1}H NMR expansion spectrum **(c)** ^{13}C NMR spectrum

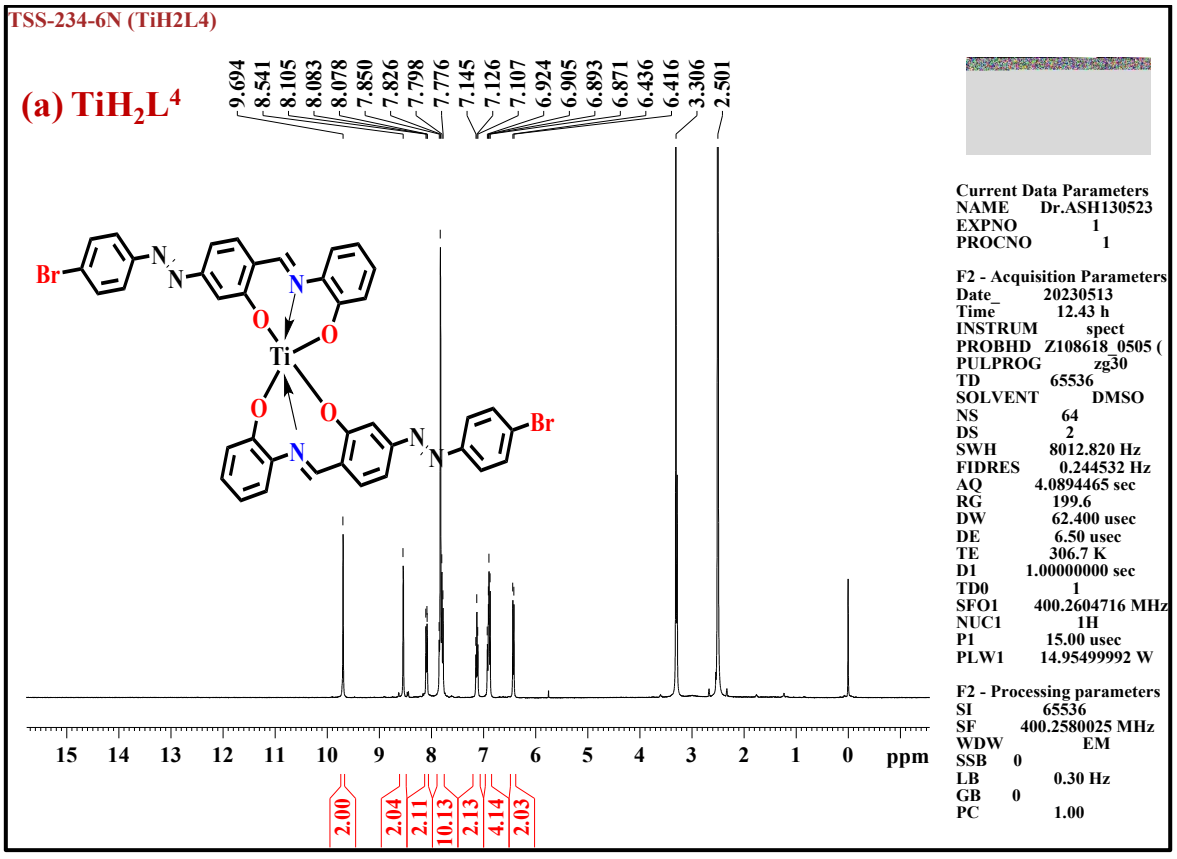

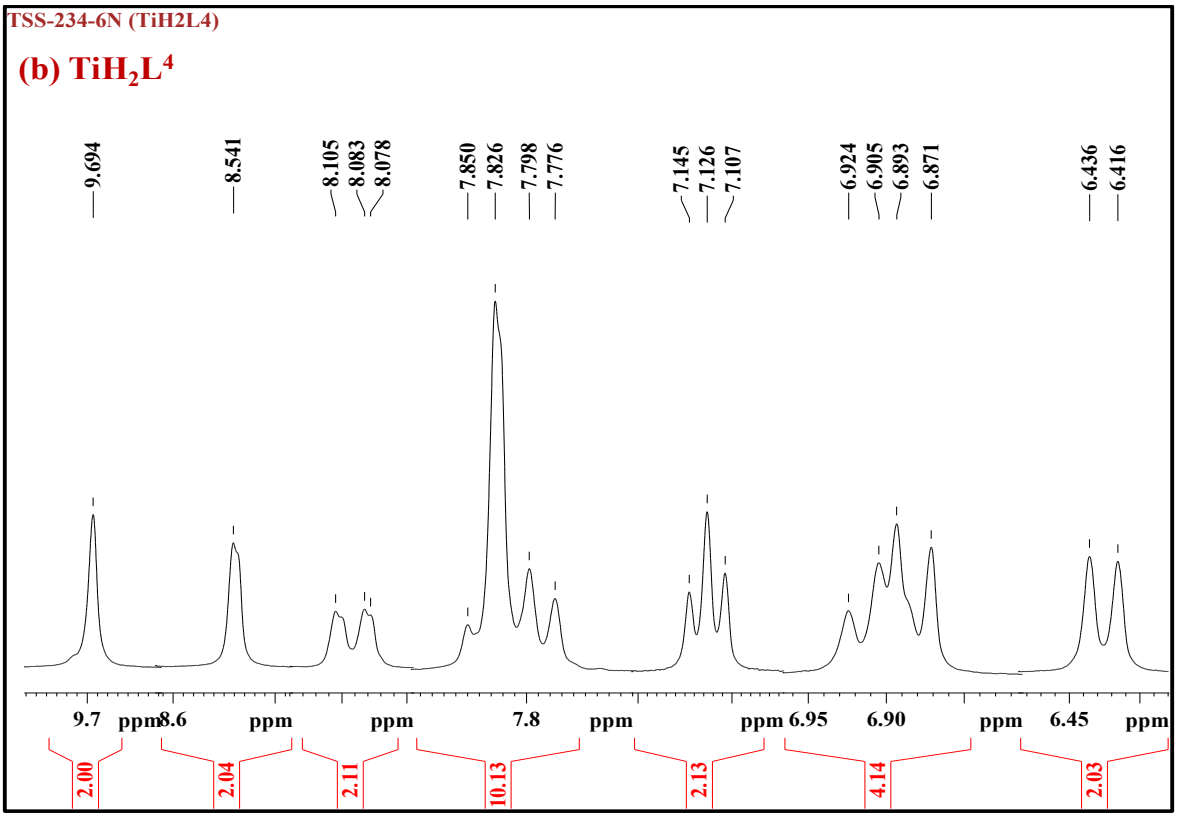

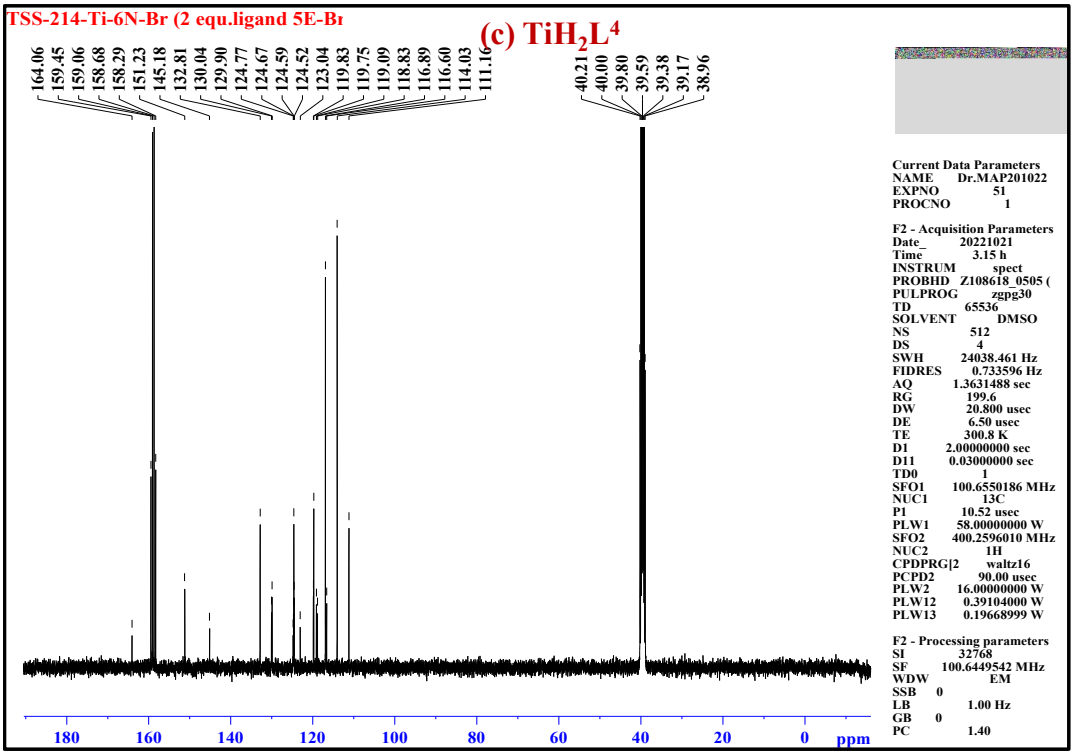

Fig. S10 NMR Spectrum of **TiH_2L^4**: **(a)** ^{1}H NMR spectrum, **(b)** ^{1}H NMR expansion spectrum **(c)** ^{13}C NMR spectrum

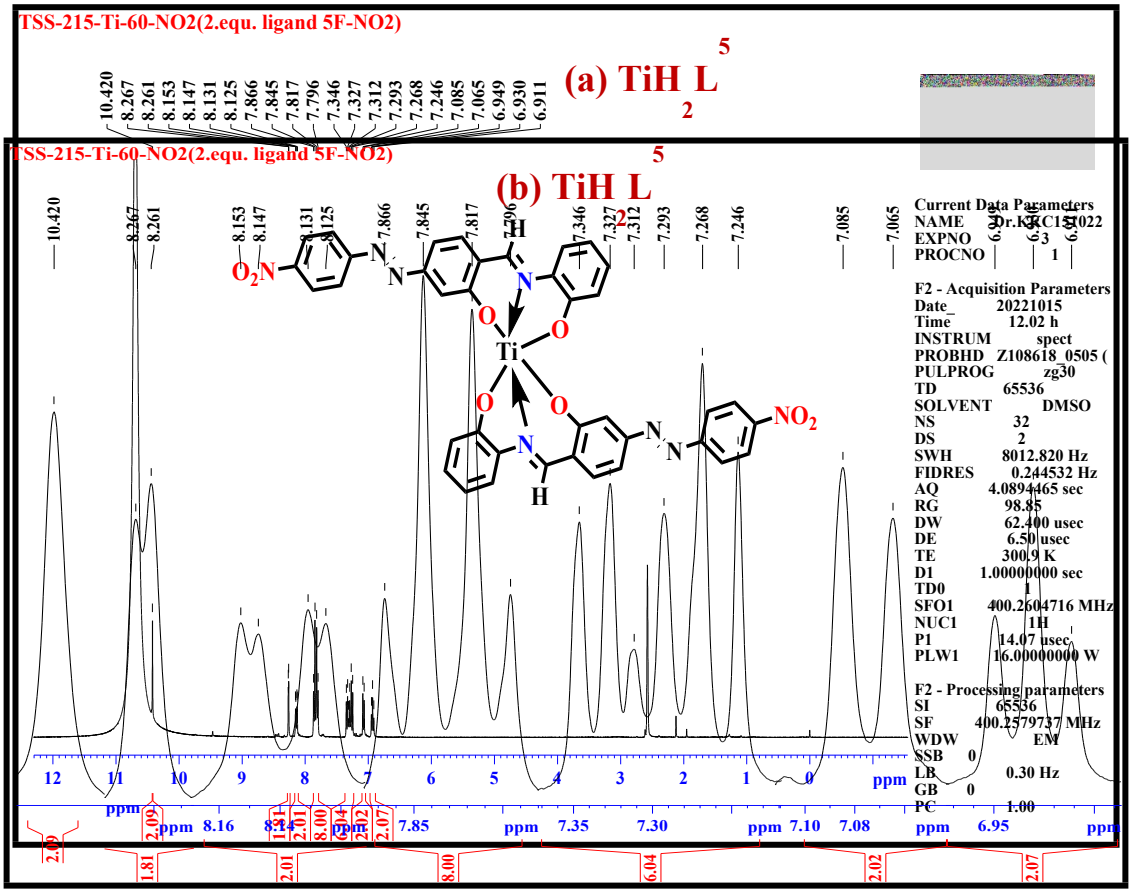

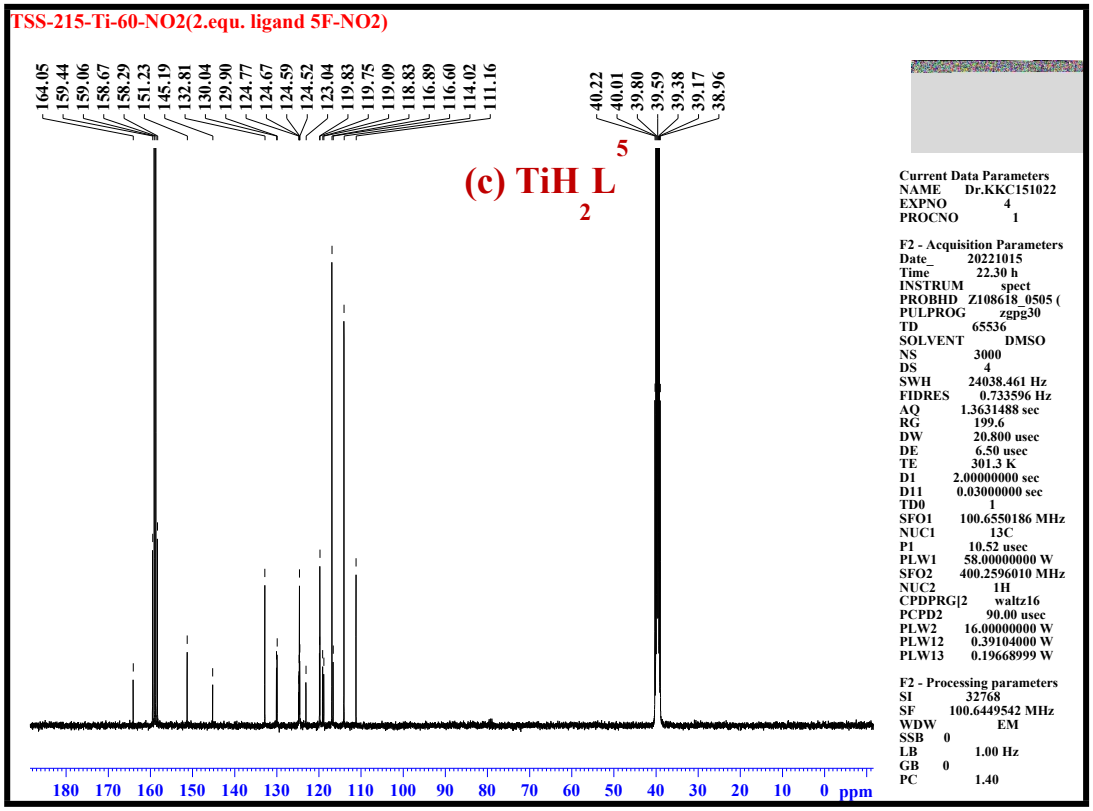

Fig. S11 NMR Spectrum of **TiH_2L^5**:

(a) ^{1}H NMR spectrum, **(b)** ^{1}H NMR expansion spectrum **(c)** ^{13}C NMR spectrum

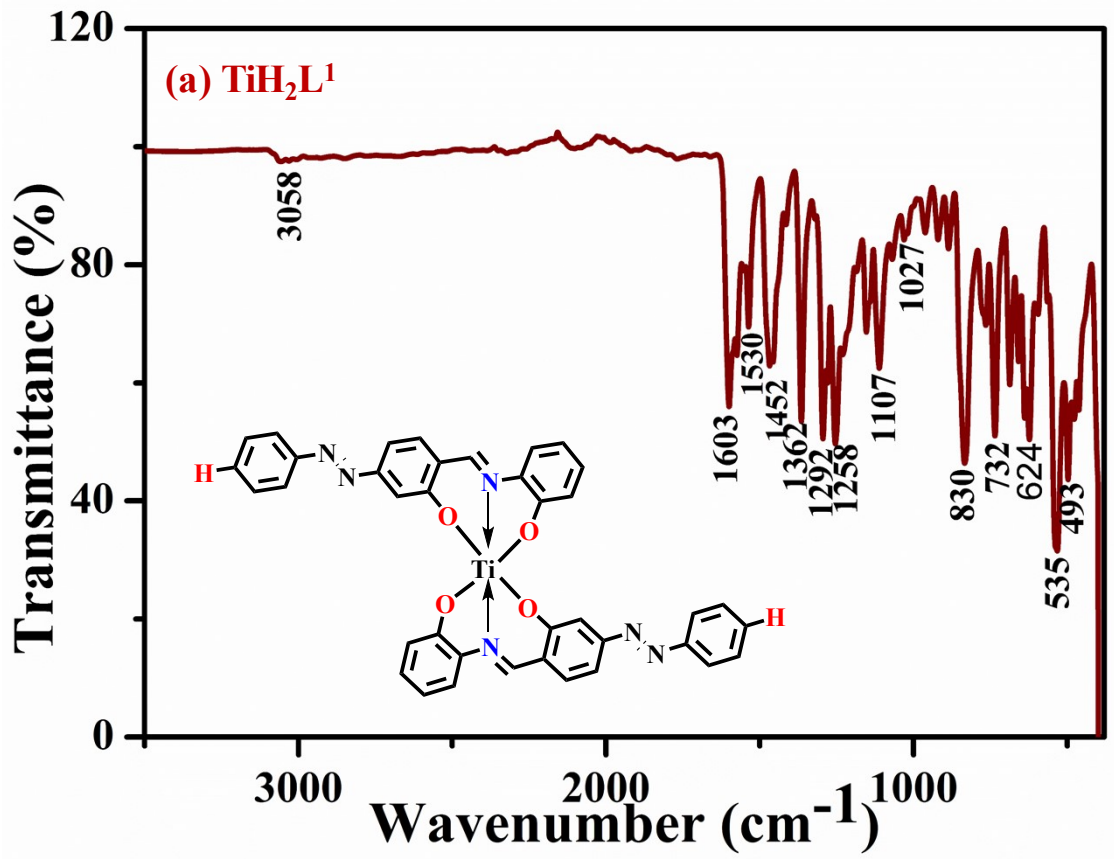

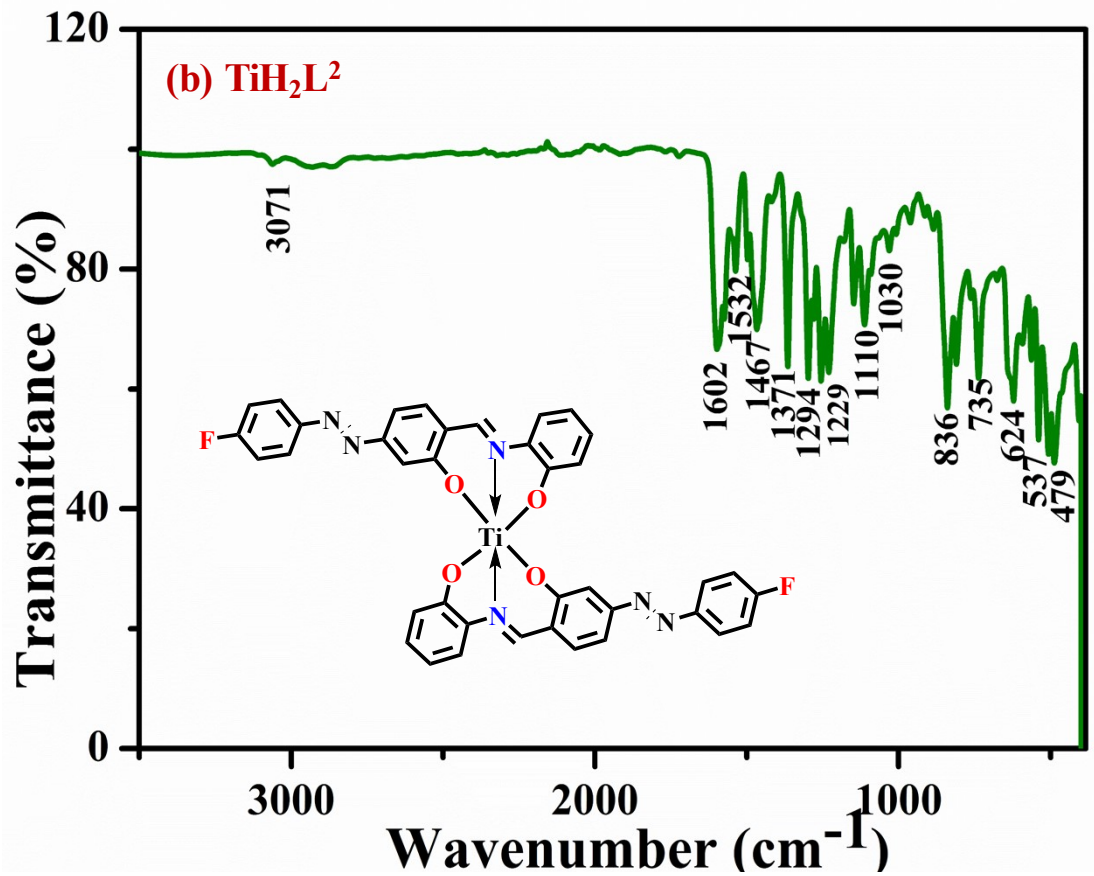

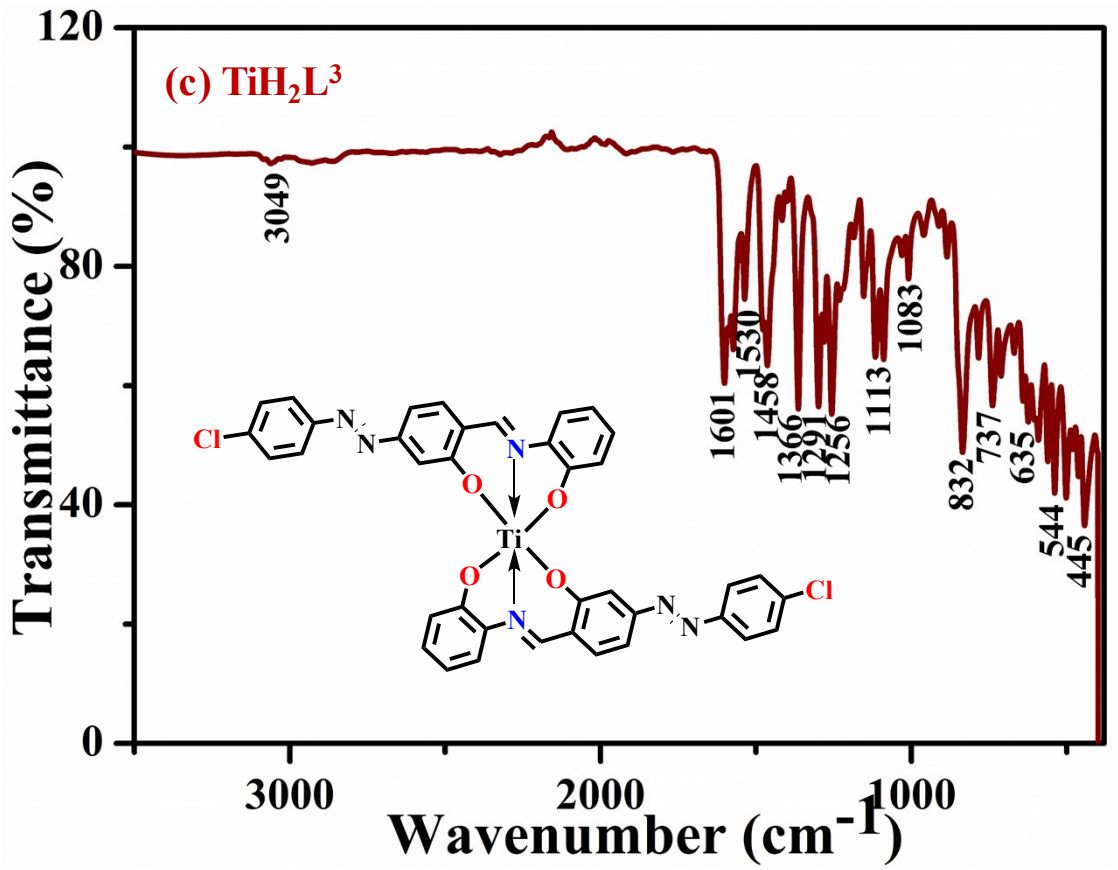
(c) TiH2L3
Transmittance (%)
Wavenumber (cm-1)
3049
1601
1530
1458
1366
1291
1256
1113
1083
832
737
635
544
445
Cl
Ti
O
N

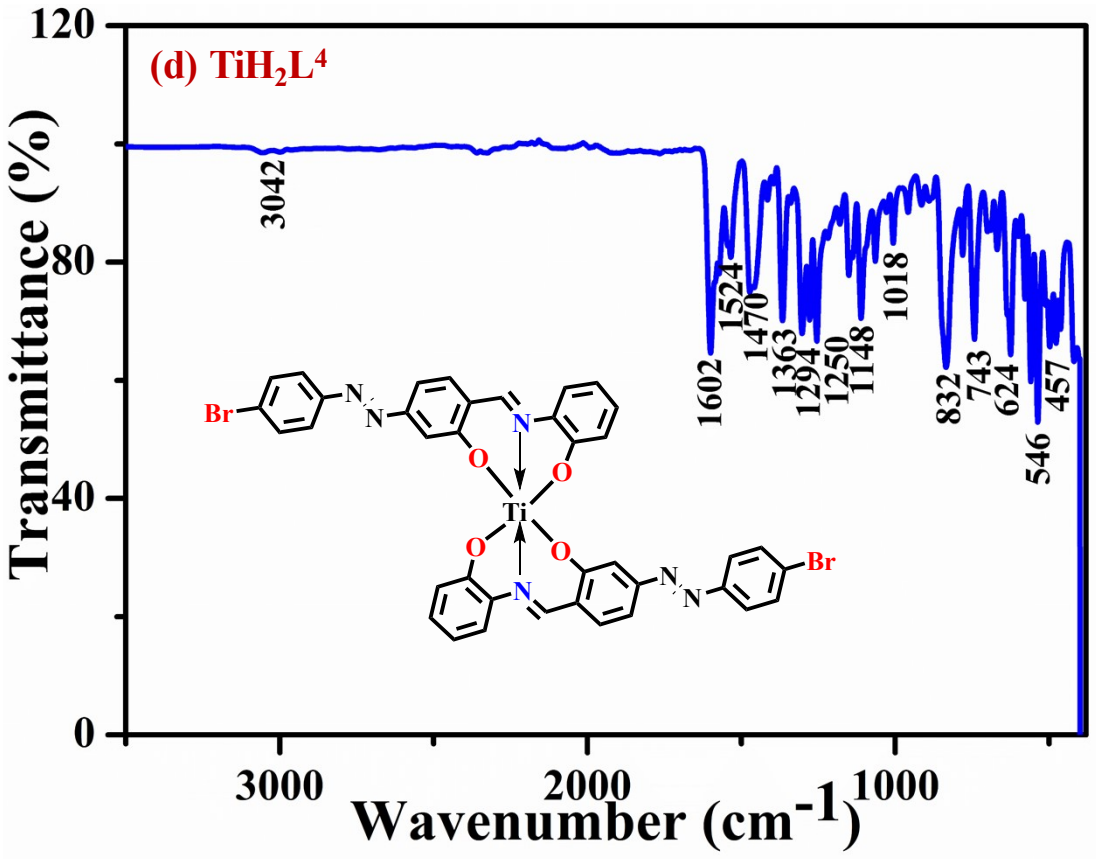
(d) TiH2L4
Transmittance (%)
Wavenumber (cm-1)
3042
1602
1524
1470
1363
1294
1250
1148
1018
832
743
624
546
457
Br
Ti
O
N

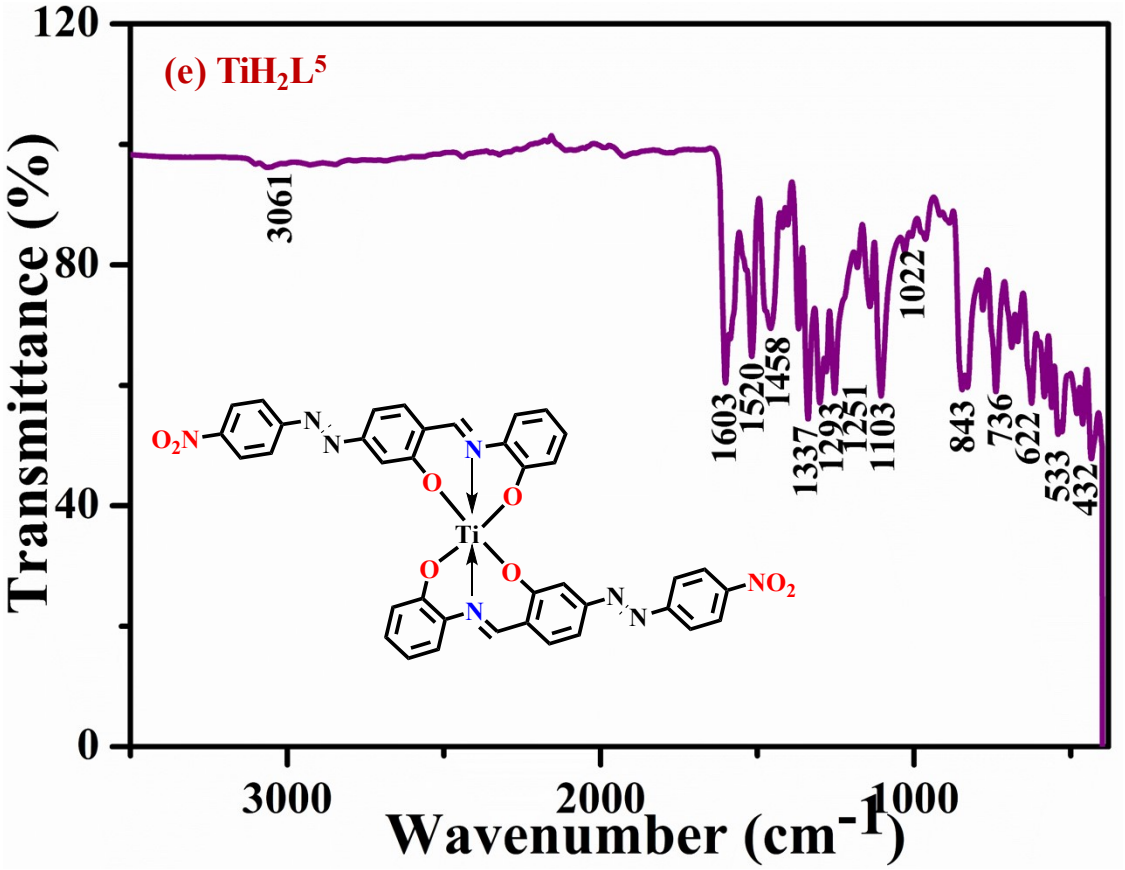

Fig. S12 FTIR Spectra of titanium(IV) complexes: **(a)** TiH_2L^1, **(b)** TiH_2L^2, **(c)** TiH_2L^3, **(d)** TiH_2L^4 and **(e)** TiH_2L^5

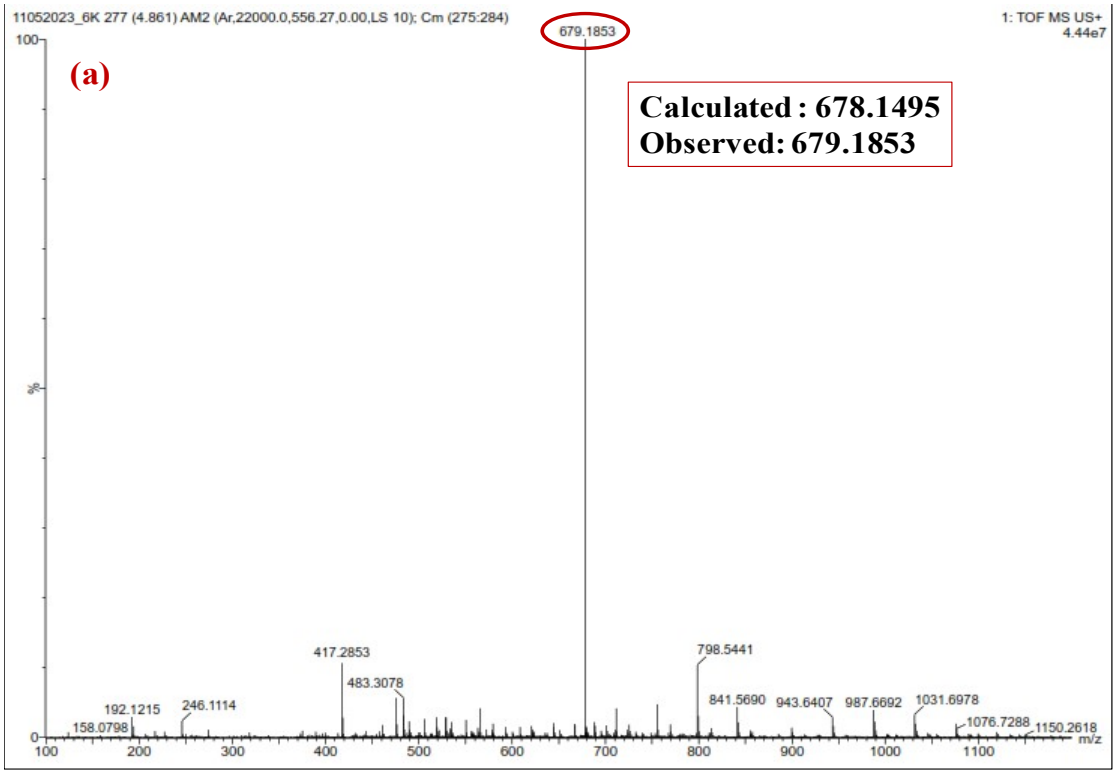

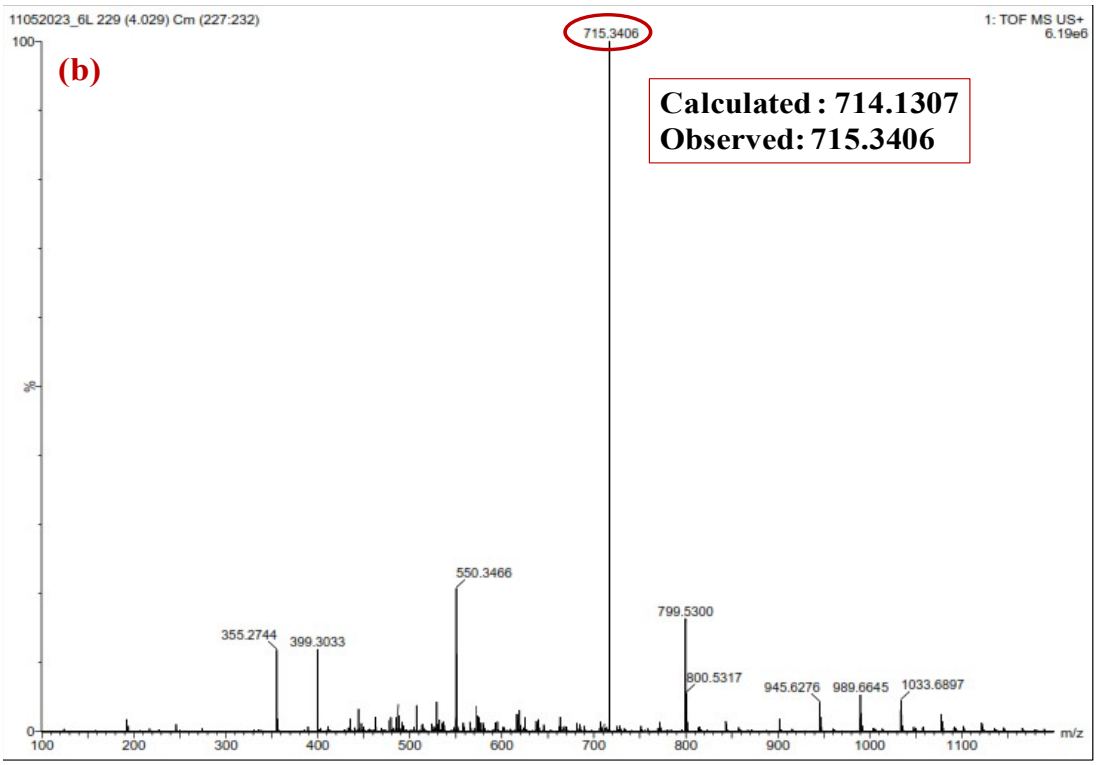
11052023_6L 229 (4.029) Cm (227:232)
1: TOF MS US+
6.19e6
(b)
715.3406
Calculated : 714.1307
Observed: 715.3406
550.3466
799.5300
355.2744
399.3033
800.5317
945.6276
989.6645
1033.6897
%
m/z

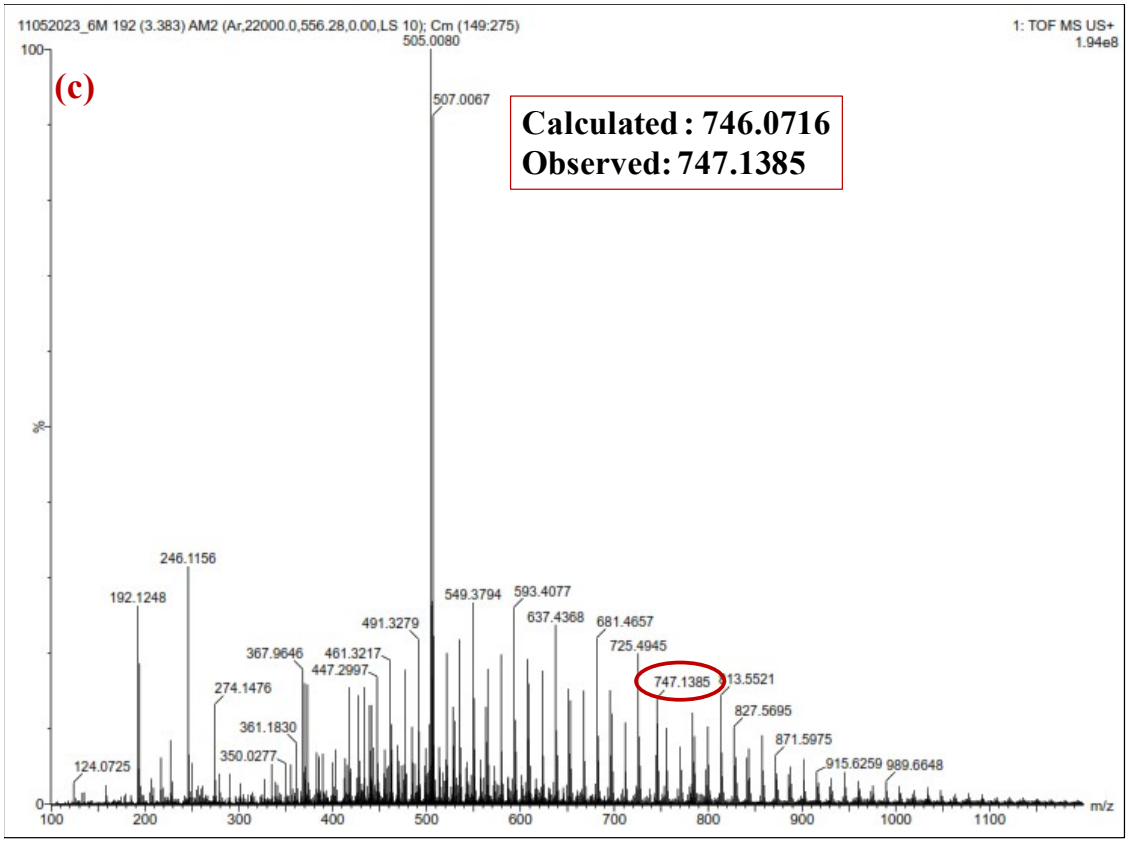
11052023_6M 192 (3.383) AM2 (Ar,22000.0,556.28,0.00,LS 10); Cm (149:275)
1: TOF MS US+
1.94e8
(c)
505.0080
507.0067
Calculated : 746.0716
Observed: 747.1385
246.1156
192.1248
549.3794
593.4077
637.4368
681.4657
491.3279
725.4945
367.9646
461.3217
447.2997
747.1385
274.1476
827.5695
361.1830
871.5975
350.0277
915.6259
989.6648
124.0725
%
m/z

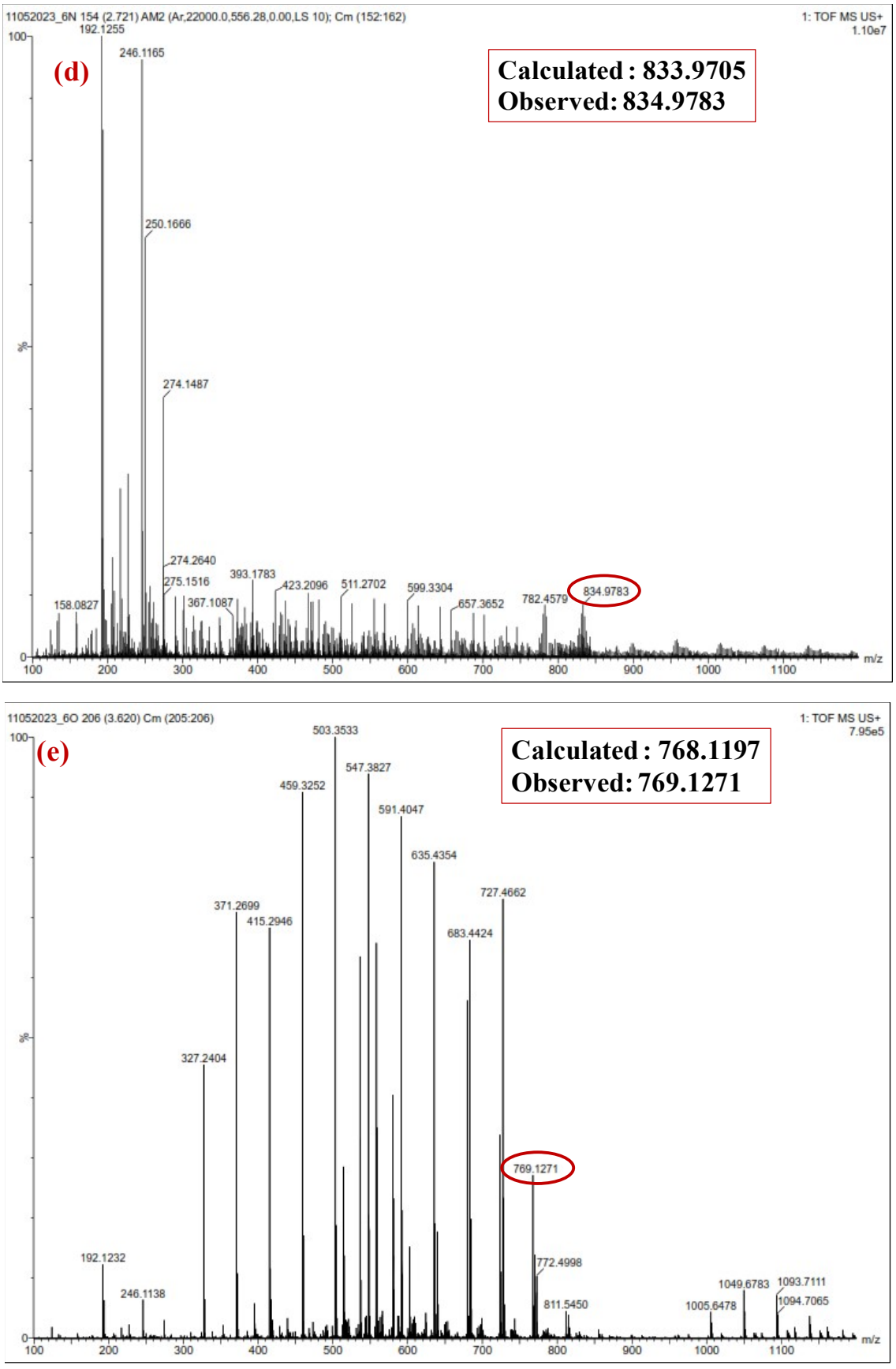

Fig. S13 HRMS of titanium(IV) complexes: **(a)** TiH_2L^1, **(b)** TiH_2L^2, **(c)** TiH_2L^3, **(d)** TiH_2L^4 and **(e)** TiH_2L^5

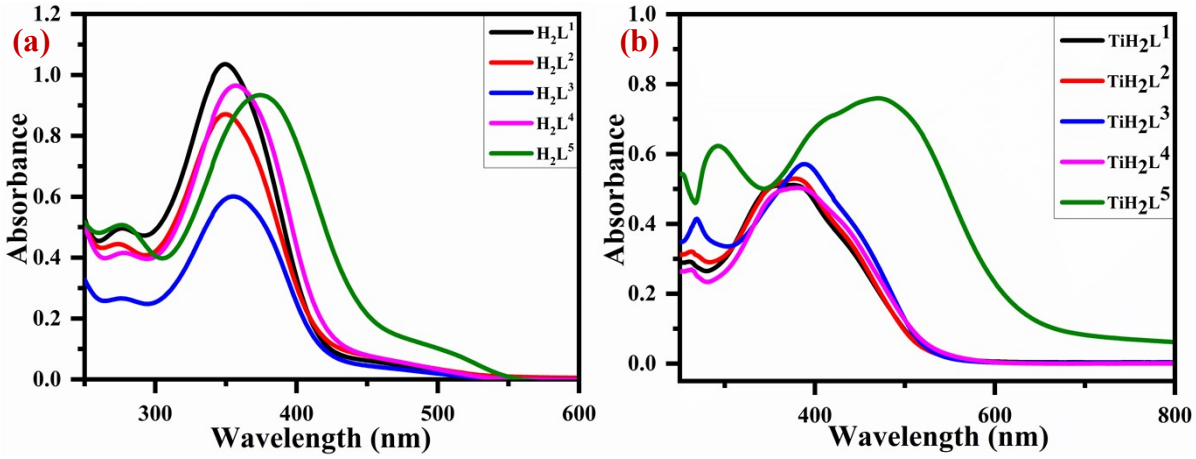

Fig. S14 UV-Visible Spectra: (a) ligands (H_2L^1-H_2L^5) and (b) complexes **(TiH_2L^1-TiH_2L^5**

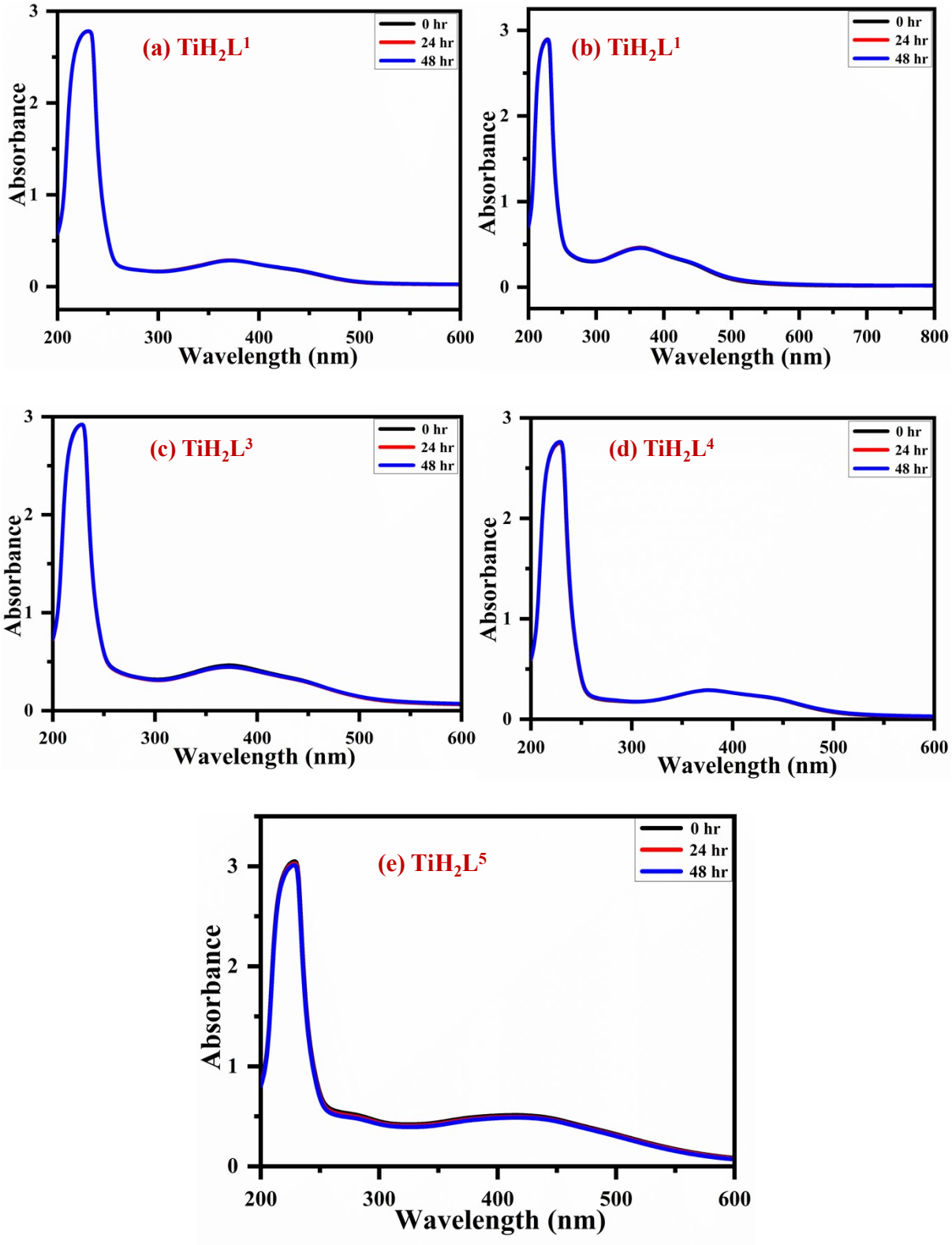

Fig. S15 UV-Visible stability spectra in 10% DMSO: **(a)** TiH_2L^1, **(b)** TiH_2L^2, **(c)** TiH_2L^3, **(d)** TiH_2L^4 and **(e)** TiH_2L^5

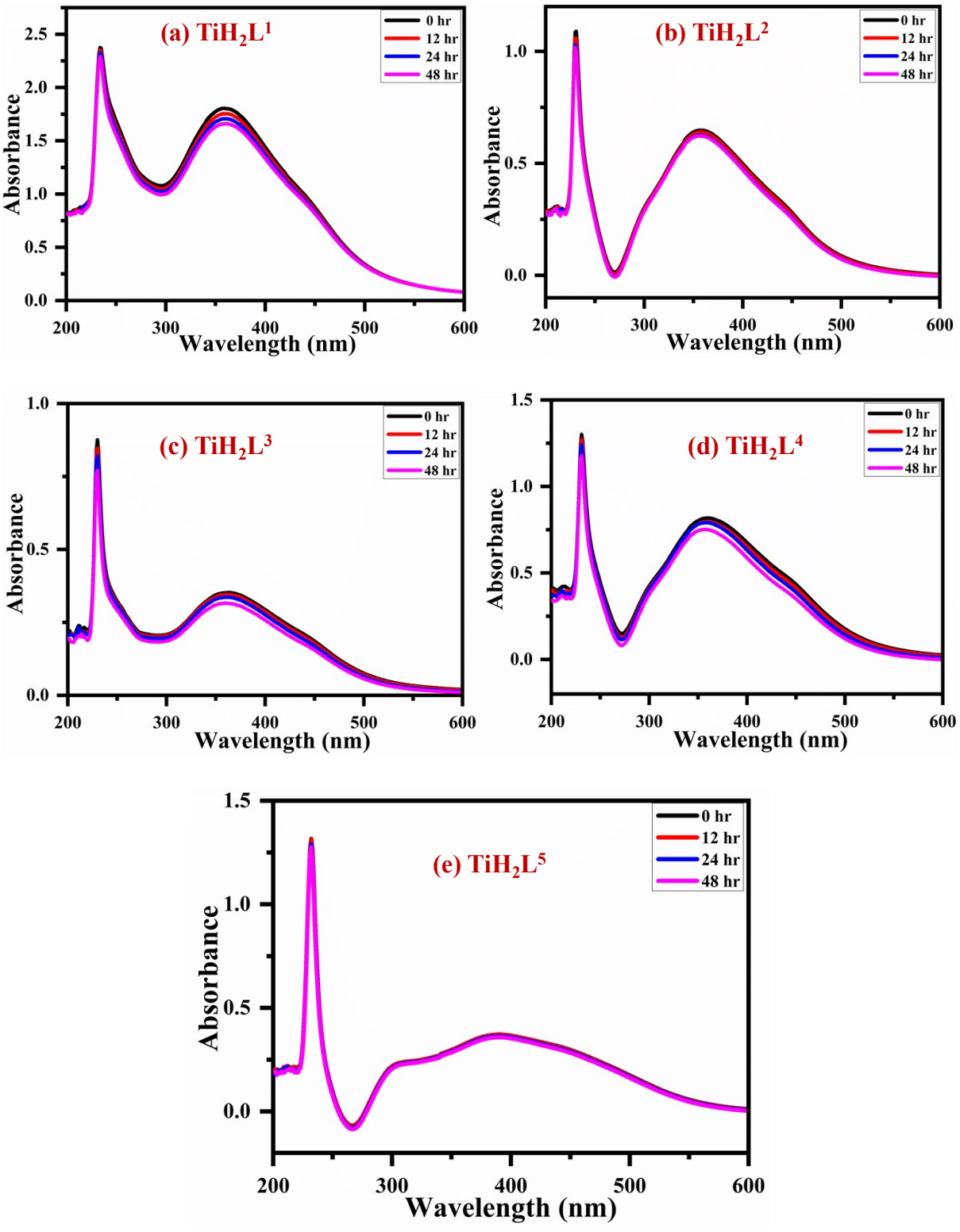

Fig. S16 Stability studies of titanium(IV) complexes: **(a)** TiH_2L^1, **(b)** TiH_2L^2, **(c)** TiH_2L^3, **(d)** TiH_2L^4 and **(e)** TiH_2L^5 in GSH medium

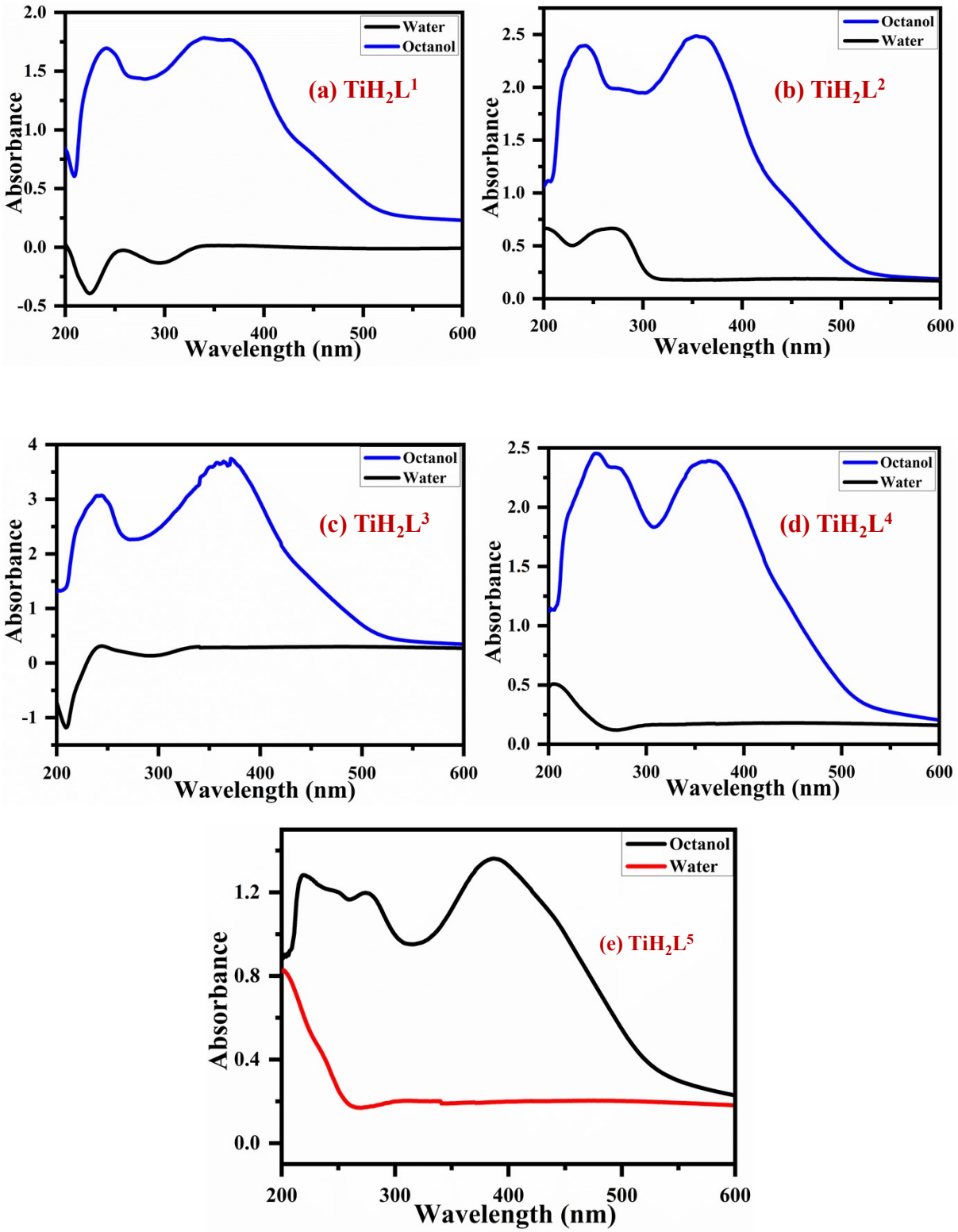

Fig. S17 UV-Visible studies of titanium(IV) complexes: **(a)** TiH_2L^1, **(b)** TiH_2L^2, **(c)** TiH_2L^3, **(d)** TiH_2L^4 and **(e)** TiH_2L^5 in water and octanol

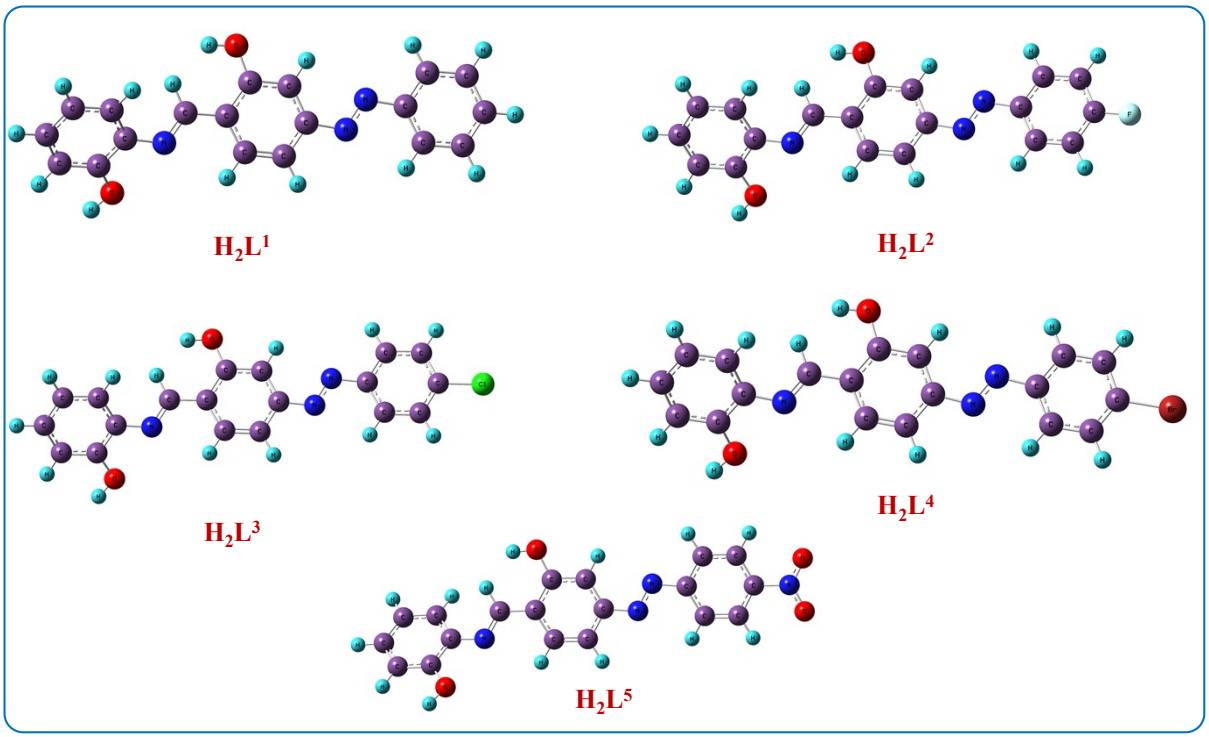

Fig. S18 Optimized molecular geometry of free ligand (H_2L^1-H_2L^5) by using the DFT/B3LYP method

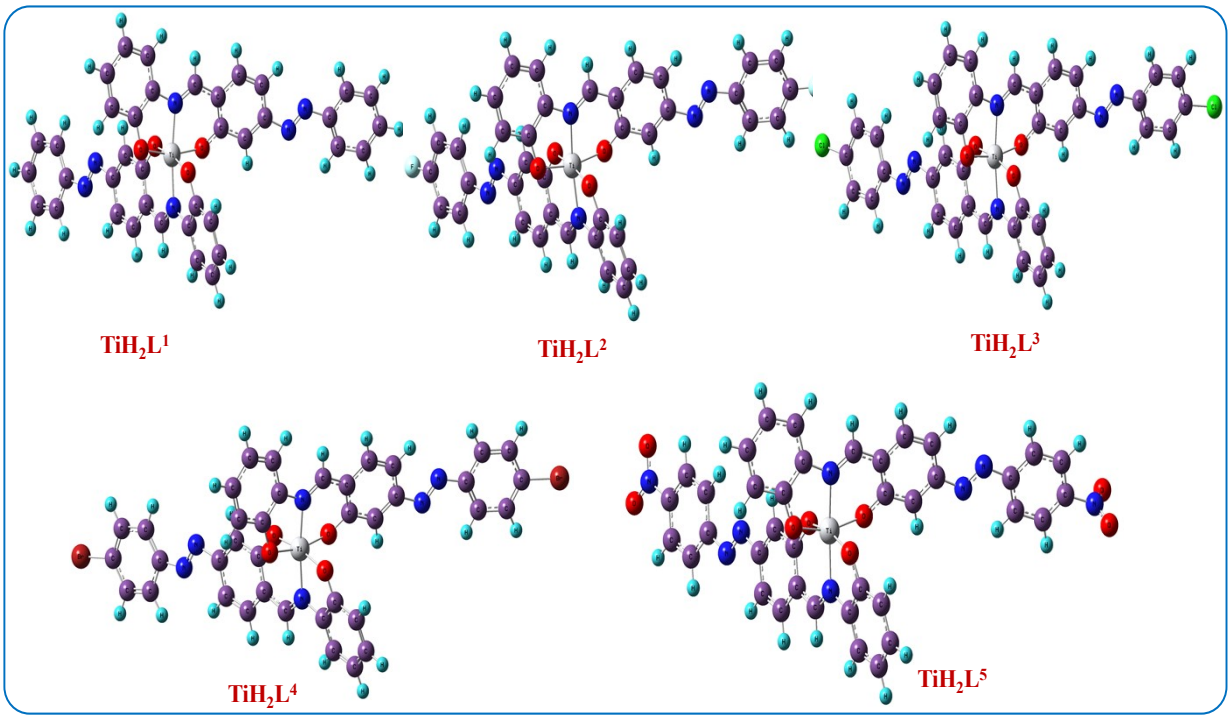

Fig. S19 Optimized molecular geometry of **TiH_2L^1-TiH_2L^5** by DFT/B3LYP method

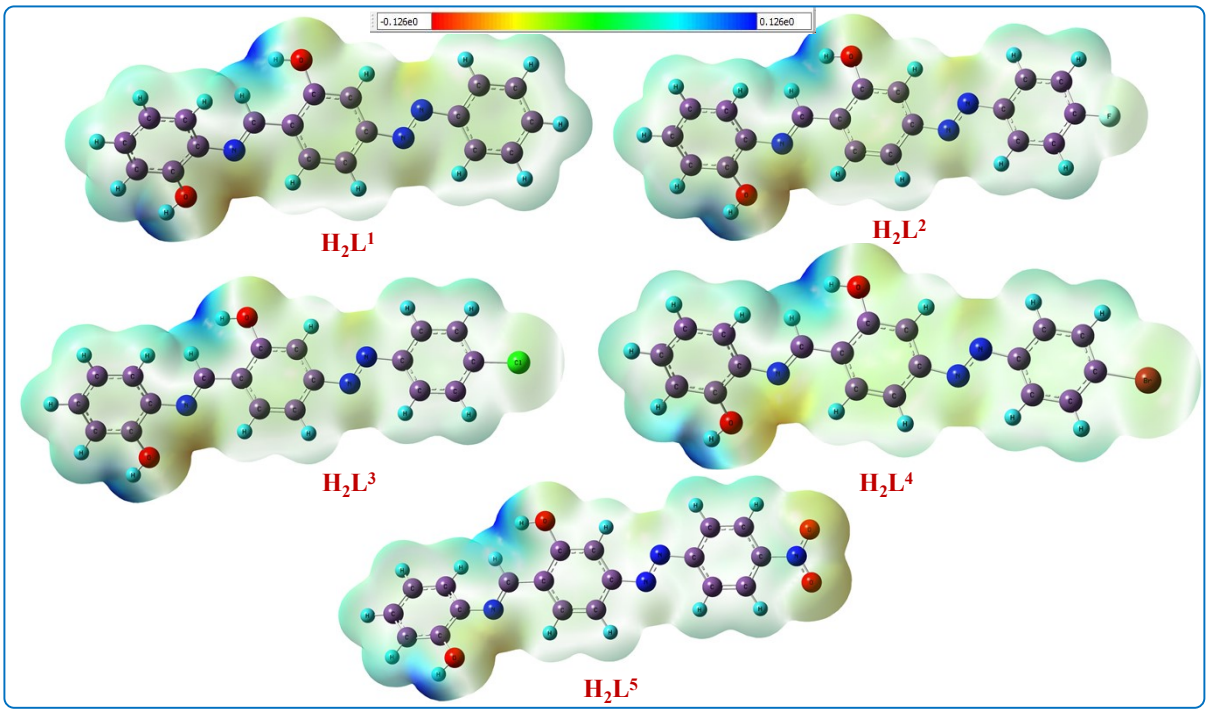

Fig. S20 Electrostatic potential mapped on the surface of optimized molecular geometries of free ligands by DFT/B3LYP method

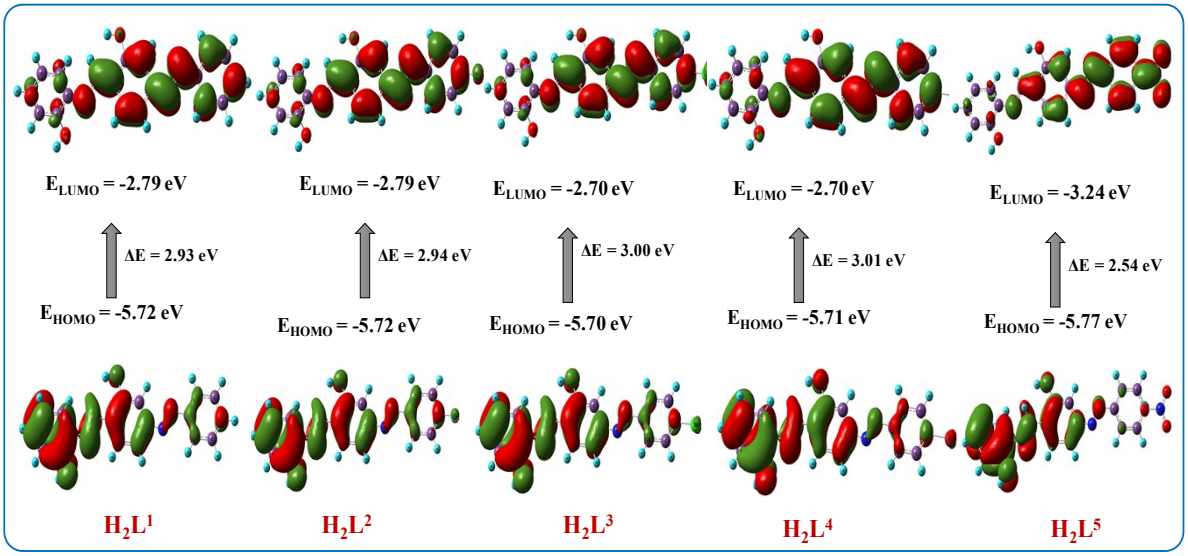

Fig. S21 FMOs of free ligand (H_2L^1-TiH_2L^5) by using DFT/B3LYP method

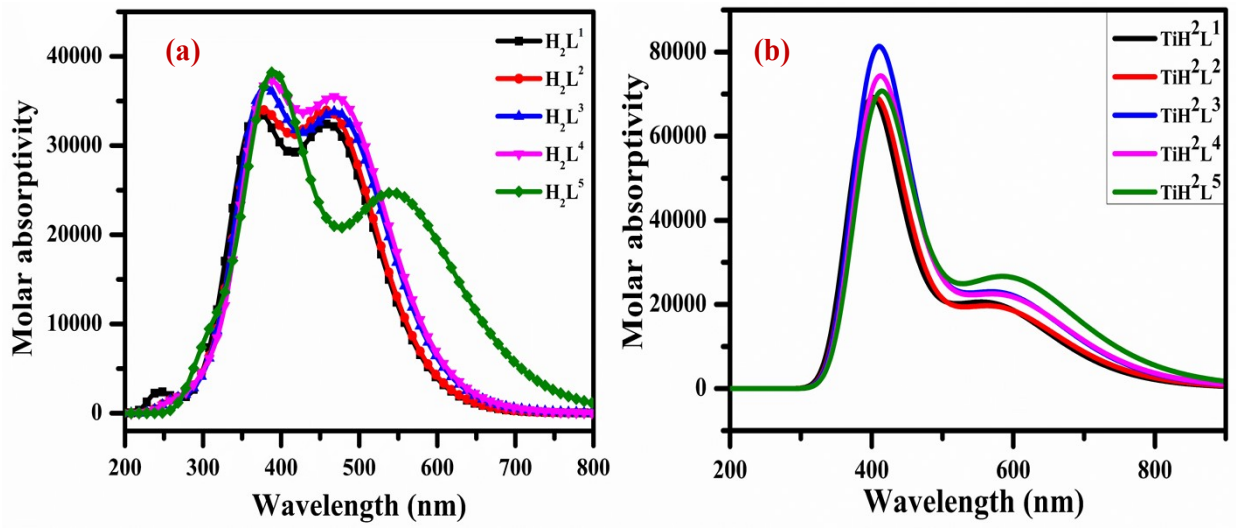

Fig. S22 TD-DFT spectra: (a) H_2L^1-H_2L^5 for ligands and (b) **TiH_2L^1-TiH_2L^5** in aqueous phase

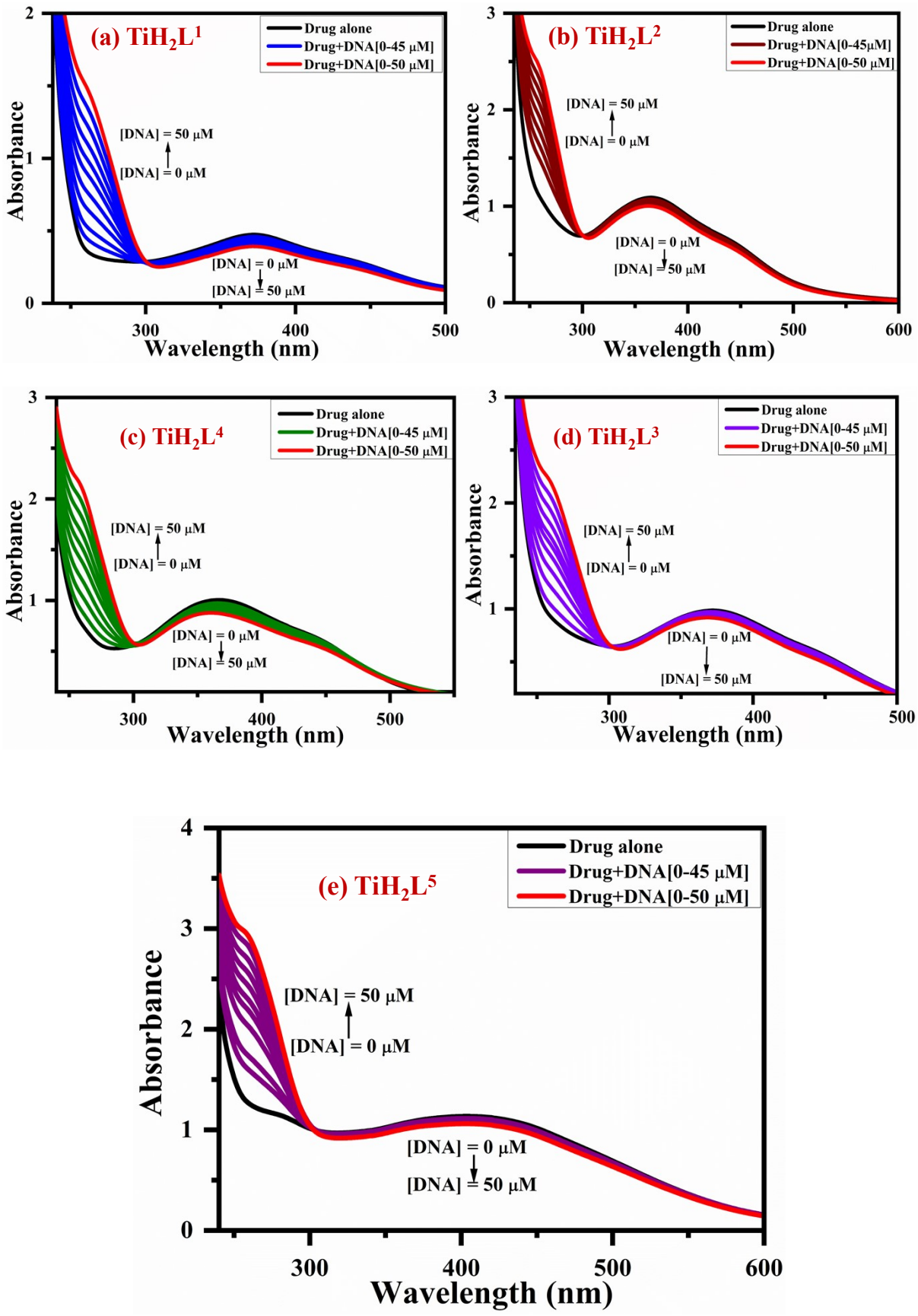

Fig. S23 DNA binding plots of all the five titanium(IV) derivatives: **(a)** TiH_2L^1, **(b)** TiH_2L^2, **(c)** TiH_2L^3, **(d)** TiH_2L^4 and **(e)** TiH_2L^5

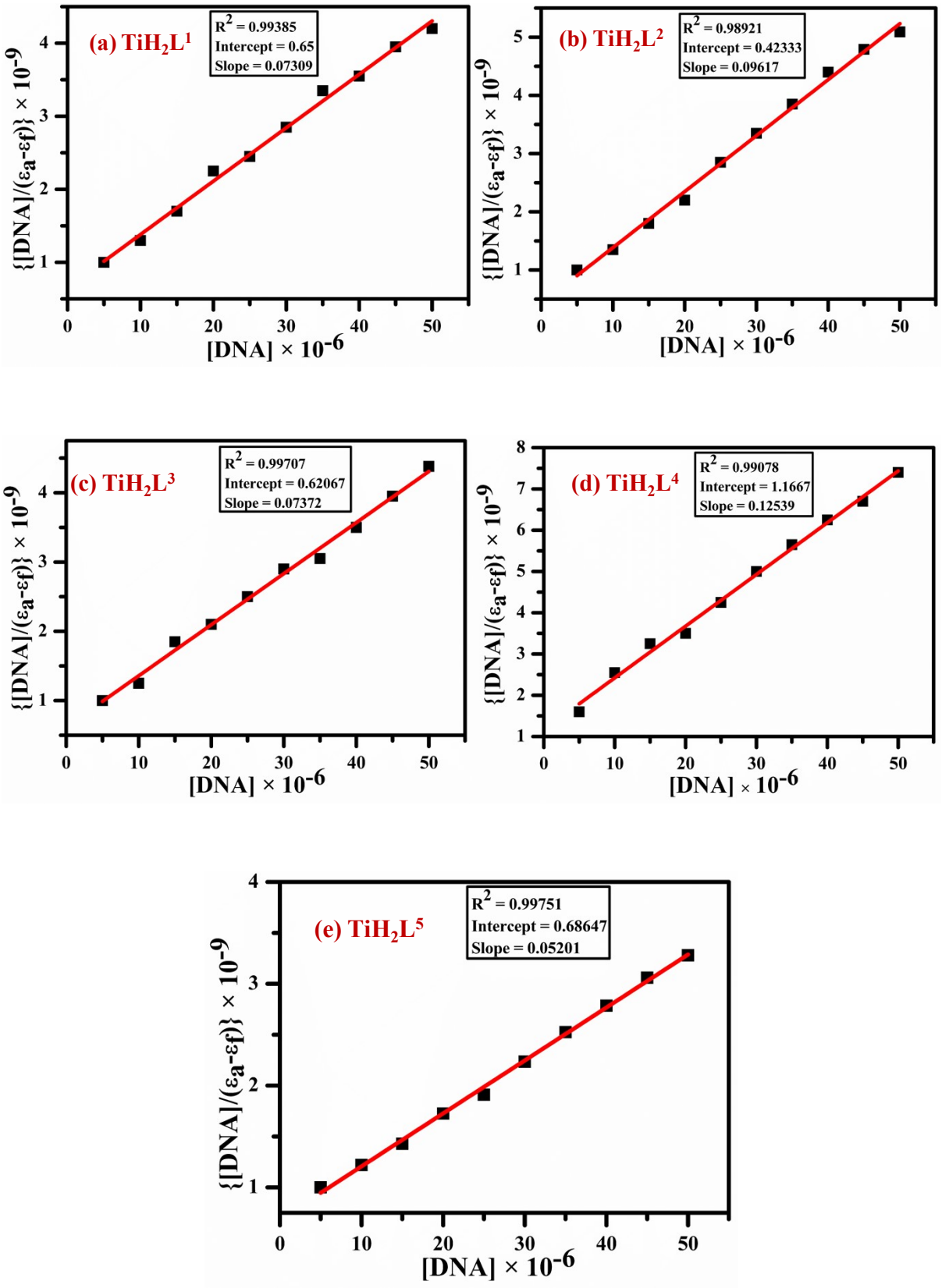

Fig. S24 {[DNA]/(ε_a-ε_f)} *vs* [DNA] linear plots of all the five complexes: **(a)** TiH_2L^1, **(b)** TiH_2L^2, **(c)** TiH_2L^3, **(d)** TiH_2L^4 and **(e)** TiH_2L^5

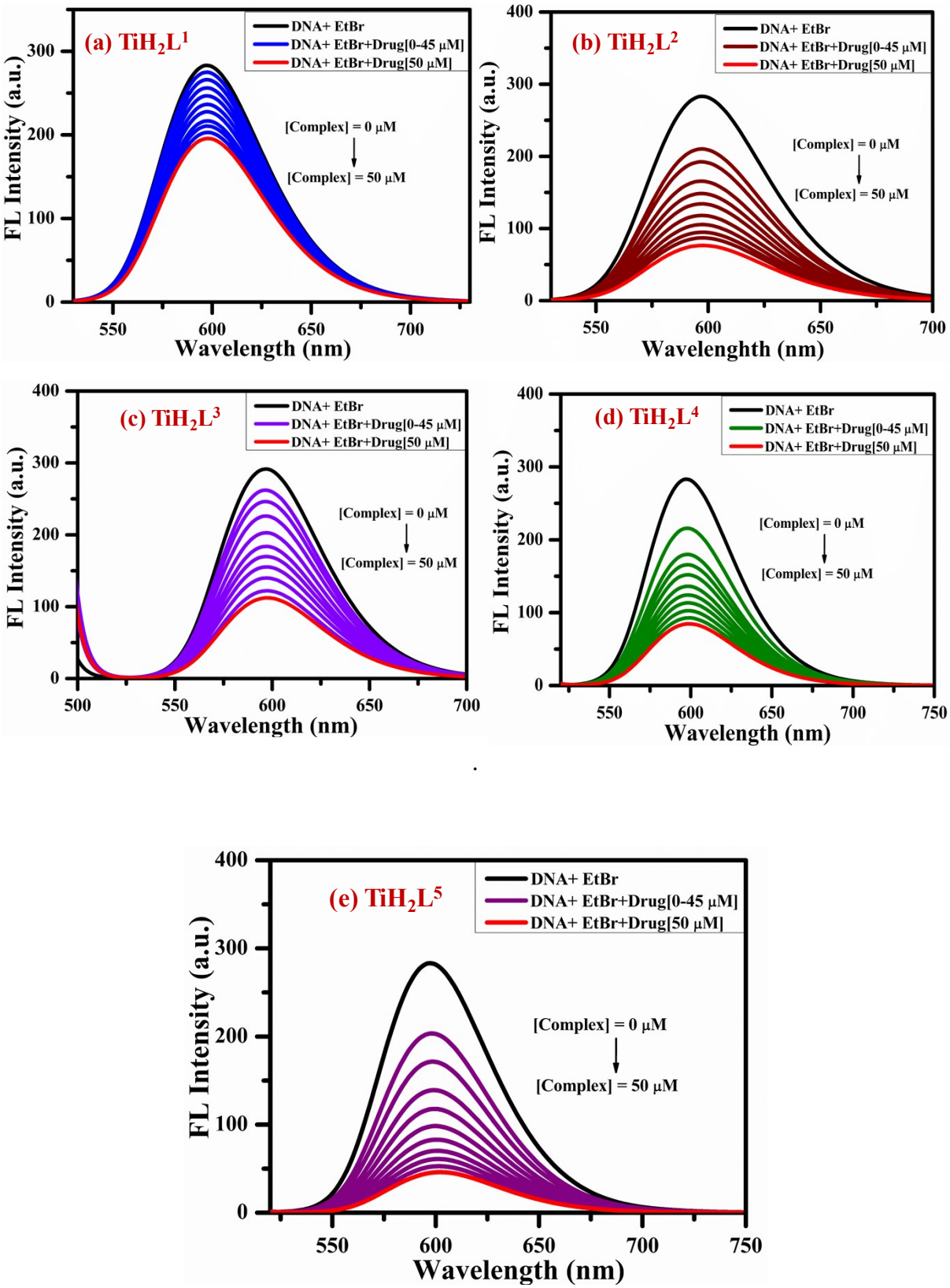

Fig. S25 Fluorescence quenching of EtBr-DNA with titanium(IV) complexes: **(a)** TiH_2L^1, **(b)** TiH_2L^2, **(c)** TiH_2L^3, **(d)** TiH_2L^4 and **(e)** TiH_2L^5

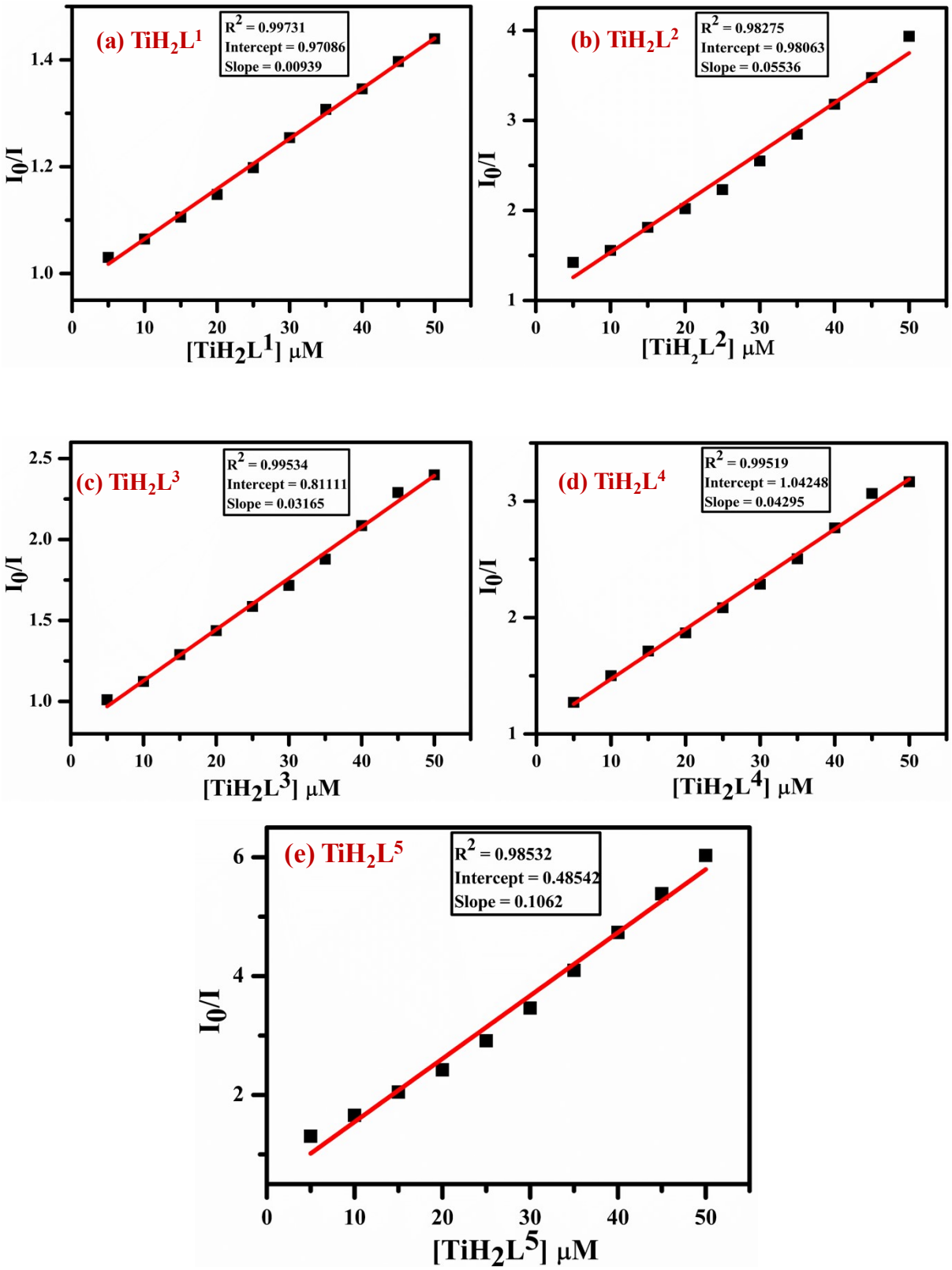

Fig. S26 CT-DNA intercalation Stern-Volmer plot of I_0/I *vs* concentration of titanium(IV) complexes: **(a)** TiH_2L^1, **(b)** TiH_2L^2, **(c)** TiH_2L^3, **(d)** TiH_2L^4 and **(e)** TiH_2L^5

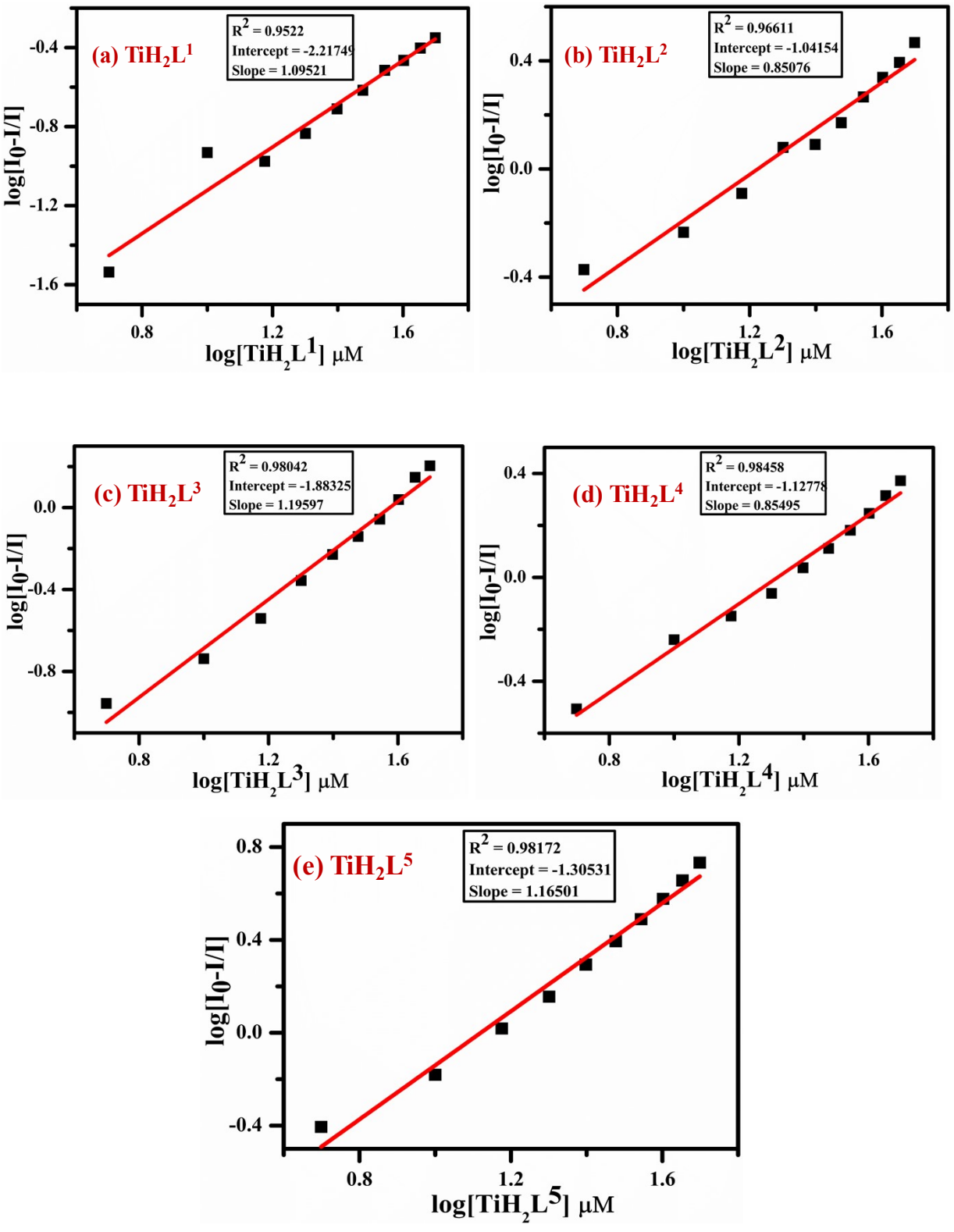

Fig. S27 Scatchard plot of log([I_0-I]/I) *vs* log[complex] for CT-DNA with presence of titanium(IV) derivatives: **(a)** TiH_2L^1, **(b)** TiH_2L^2, **(c)** TiH_2L^3, **(d)** TiH_2L^4 and **(e)** TiH_2L^5

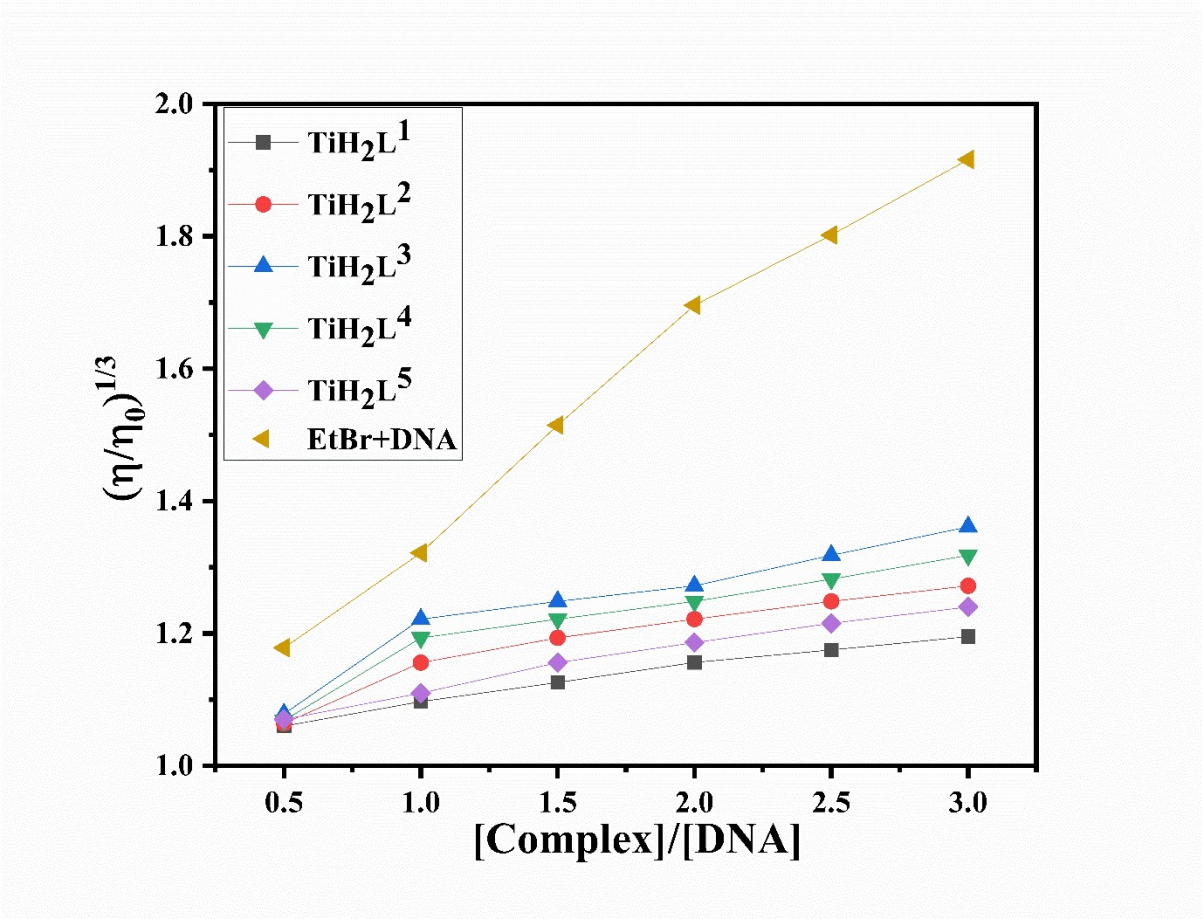

Fig. S28 Relative viscosity of CT-DNA interaction with EtBr and titanium(IV) derivatives (**TiH_2L^1-TiH_2L^5**)

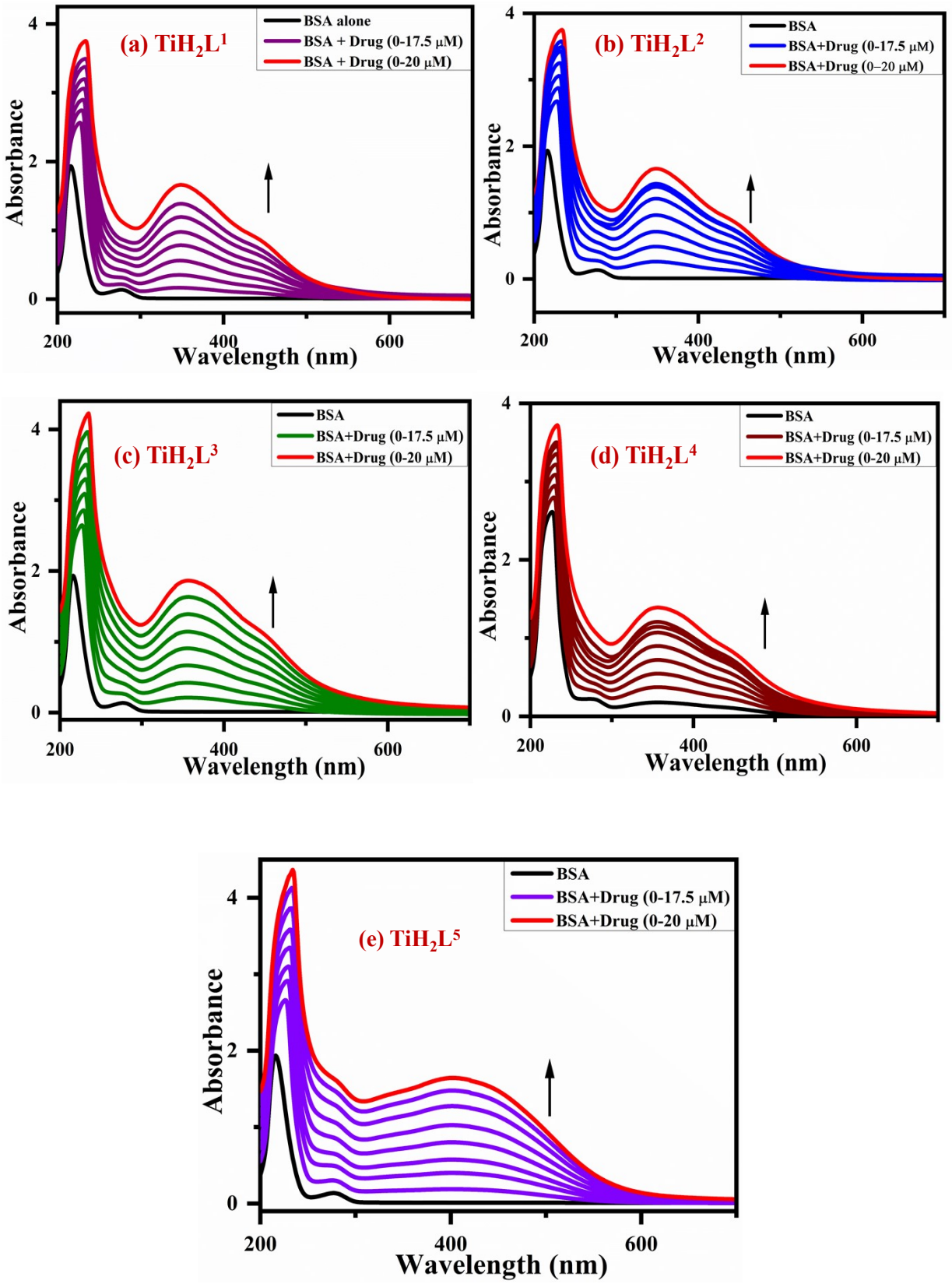

Fig. S29 BSA binding plots of all the five titanium(IV) derivatives: **(a)** TiH_2L^1, **(b)** TiH_2L^2, **(c)** TiH_2L^3, **(d)** TiH_2L^4 and **(e)** TiH_2L^5

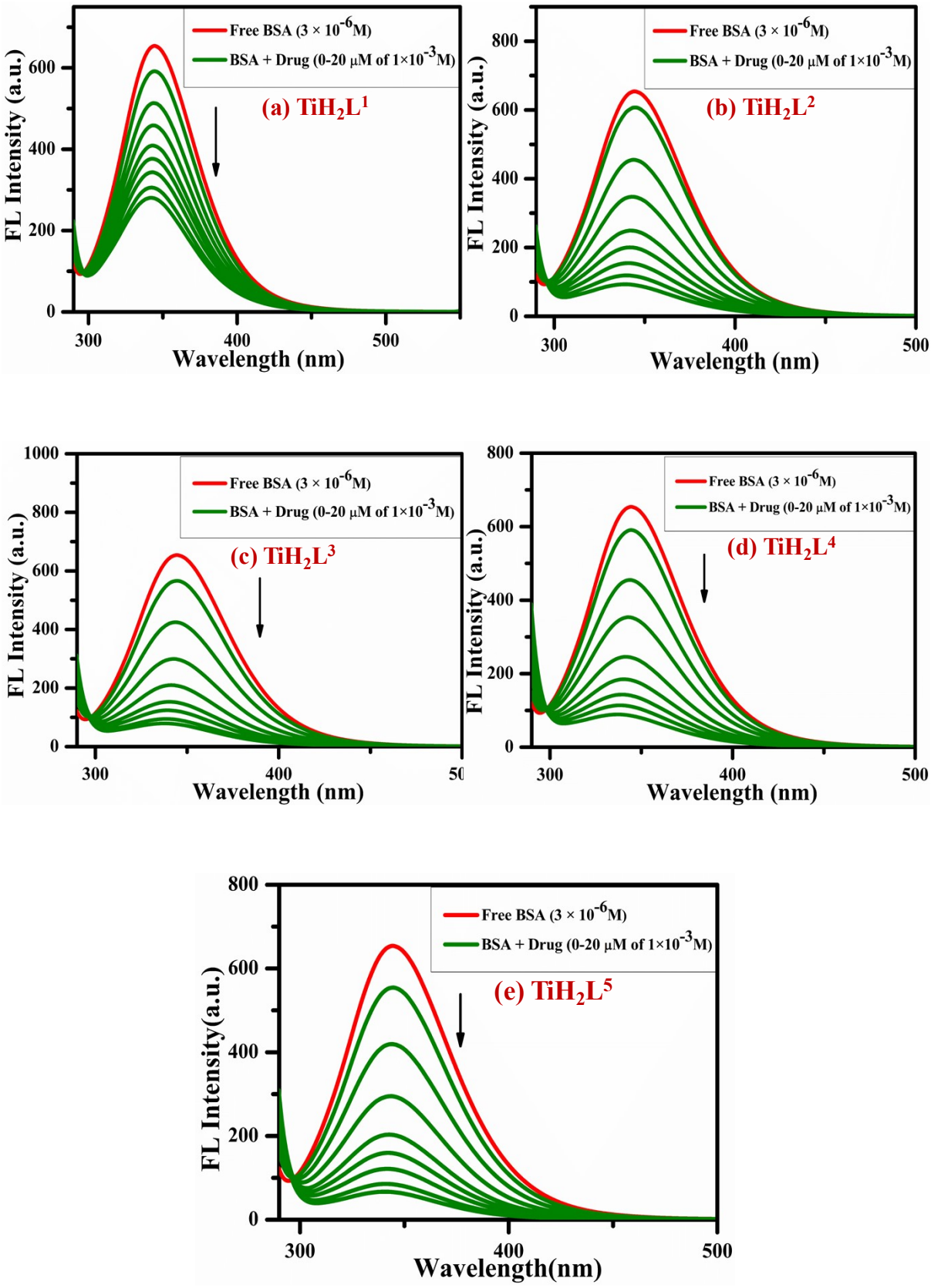

Fig. S30 Fluorescence quenching plot for BSA of all the five titanium(IV) derivatives: **(a)** TiH_2L^1, **(b)** TiH_2L^2, **(c)** TiH_2L^3, **(d)** TiH_2L^4 and **(e)** TiH_2L^5

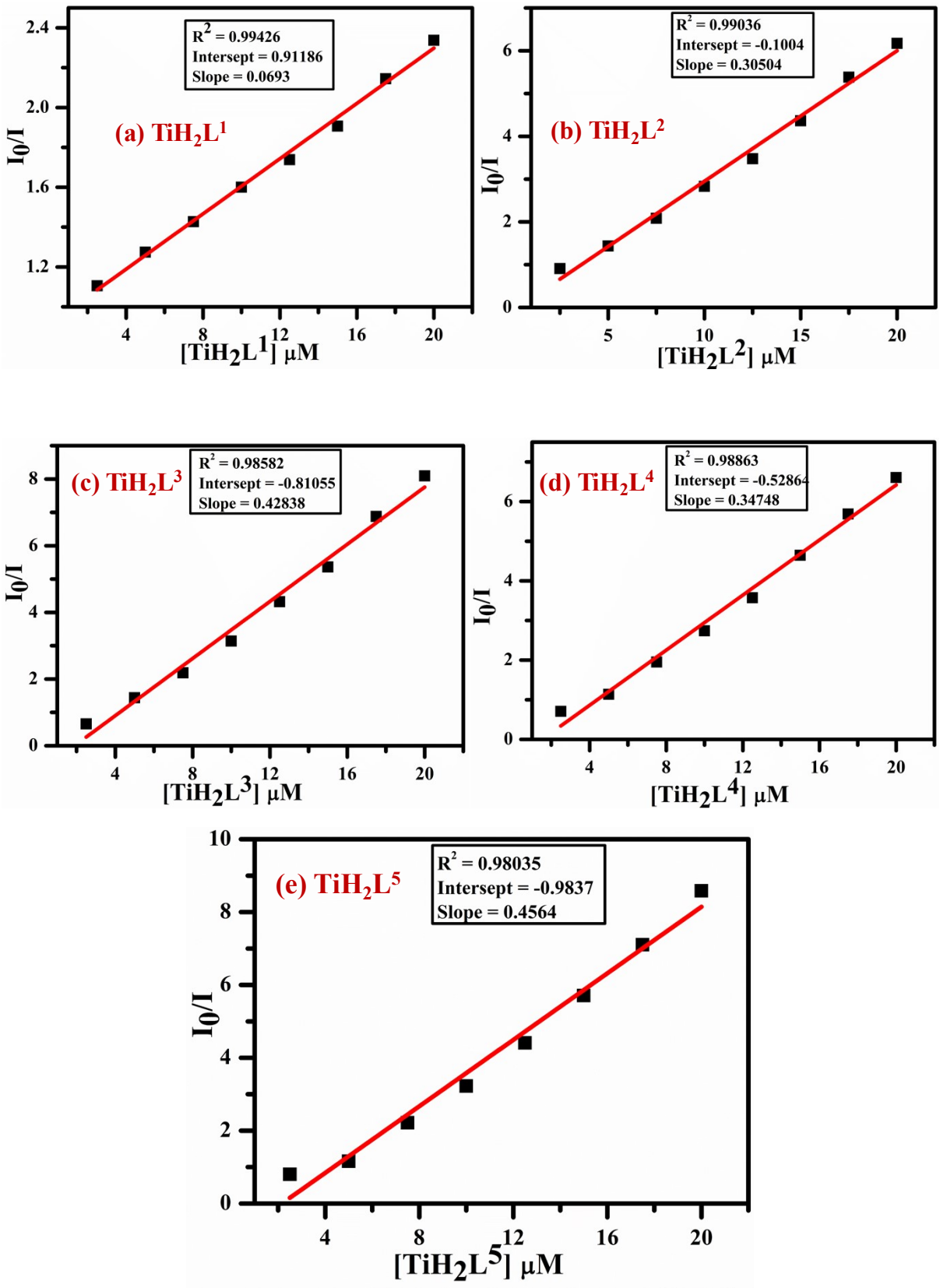

Fig. S31 Stern-Volmer plot of I_0/I *vs* concentration of complexes: **(a)** TiH_2L^1, **(b)** TiH_2L^2, **(c)** TiH_2L^3, **(d)** TiH_2L^4 and **(e)** TiH_2L^5 for BSA binding

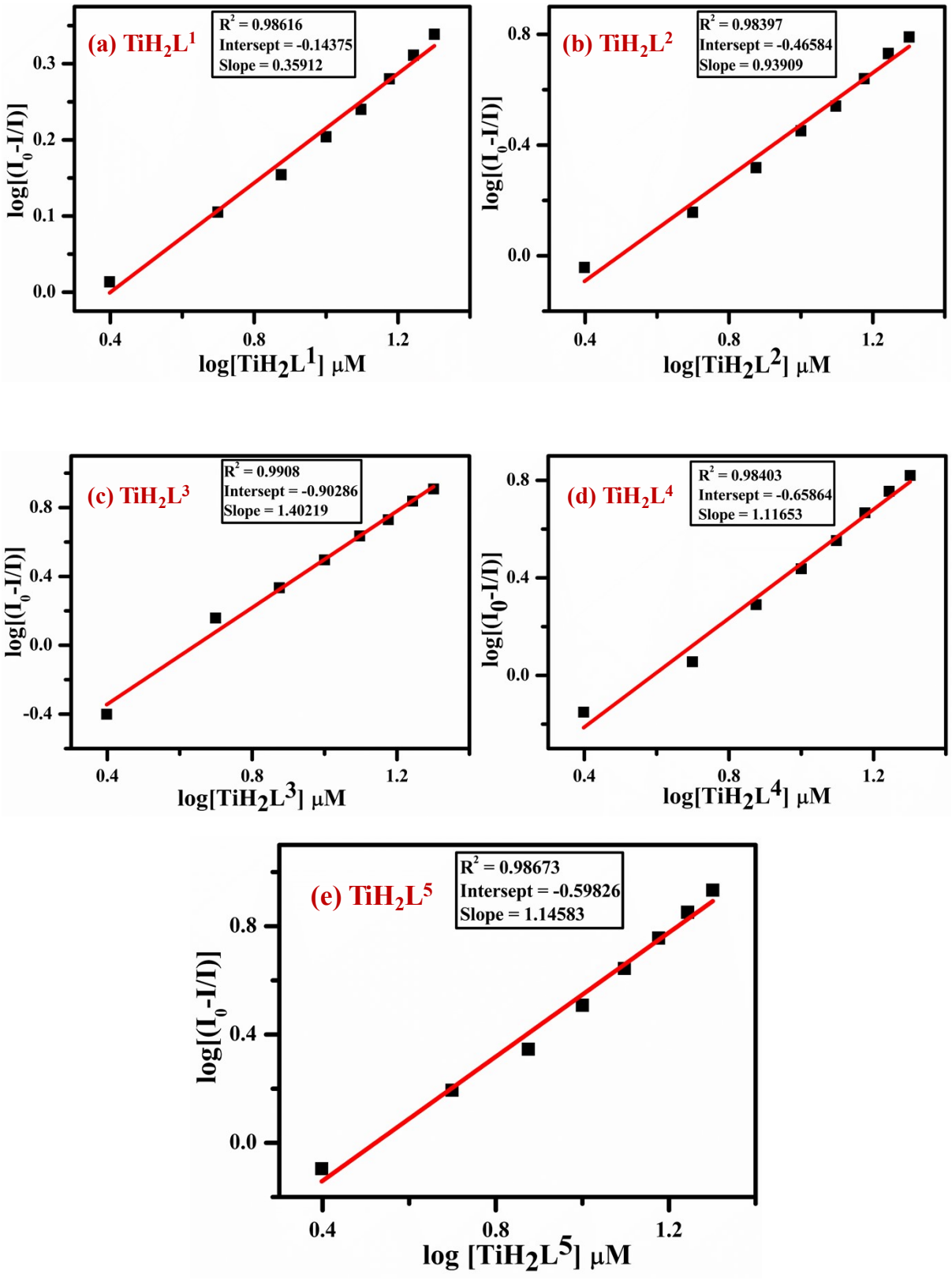

Fig. S32 Scatchard plot of log[I_0-I/I] *vs* log[Complex] for BSA in the presence of titanium(IV) derivatives: **(a)** TiH_2L^1, **(b)** TiH_2L^2, **(c)** TiH_2L^3, **(d)** TiH_2L^4 and **(e)** TiH_2L^5

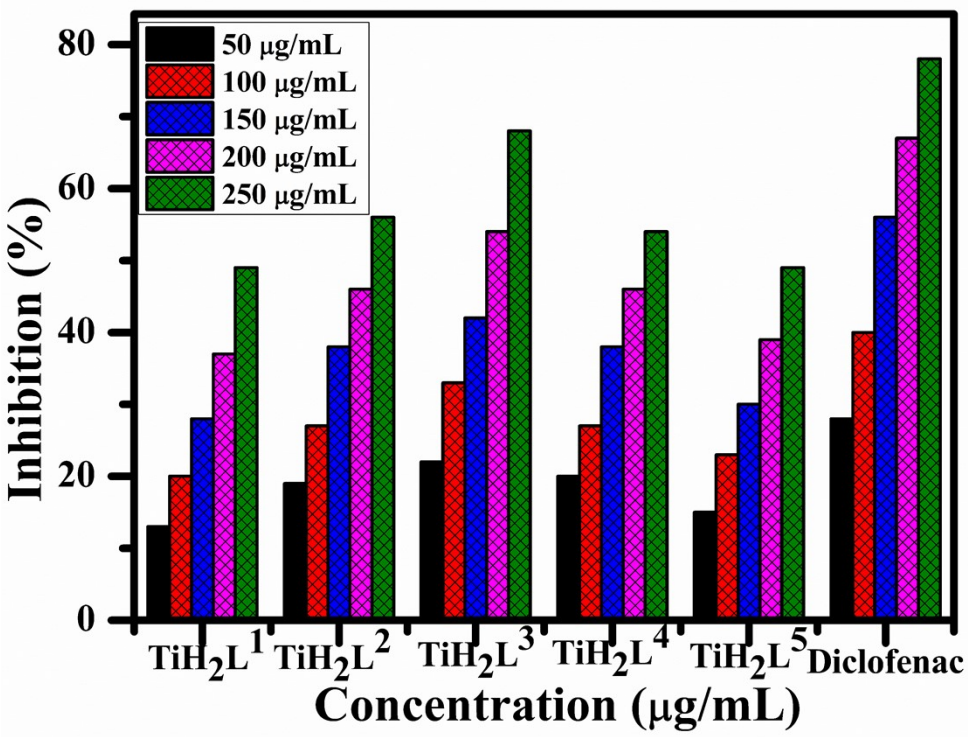

Fig. S33 Anti-inflammatory activity of **TiH_2L^1-TiH_2L^5**

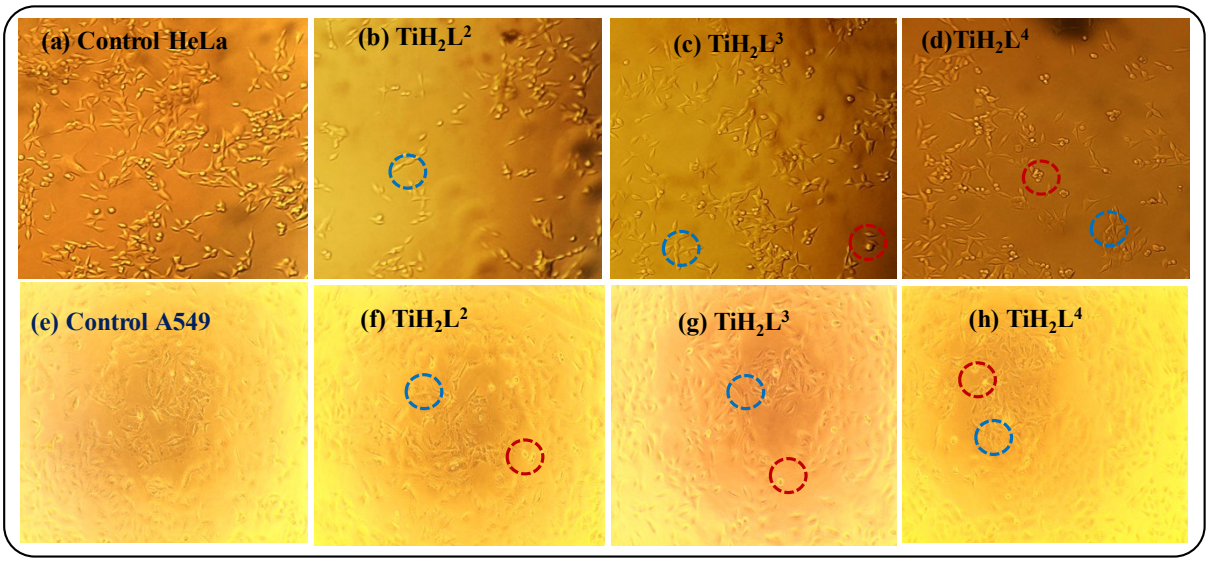

Fig. S34 Microscopic images (a-h) of HeLa and A549 cells treated with titanium(IV) derivatives **(TiH_2L^2-TiH_2L^4)** in 100 µg/mL concentration (dead cells are revealed as red circles and live cells are demonstrated as blue circles)

Table S1 FTIR spectral data (cm^{-1}) of **TiH_2L^1-TiH_2L^5**

Complexes	*v*(C-H)	*v*(C=N)	*v*(C=C)	*v*(N=N)	*v*(C-N)	*v*(C-O)	*v*(C-X)	*v*(Ti-N)	*v*(Ti-O)
TiH_2L^1	3058	1603	1530	1452	1292, 1107	1258, 1027	-	535	493
TiH_2L^2	3071	1602	1532	1467	1294, 1110	1229, 1030	735	537	474
TiH_2L^3	3049	1601	1530	1458	1291, 1113	1256, 1083	737	544	445
TiH_2L^4	3042	1602	1524	1470	1294, 1148	1250, 1018	743	546	457
TiH_2L^5	3061	1603	1520	1458	1293, 1103	1251, 1022	736	533	432

Table S2 Calculated molecular electronic parameters of ligands (H_2L^1-H_2L^5) and titanium(IV) derivatives **(TiH_2L^1-TiH_2L^5)**

S.No	Code	Energy (Kcal/mol)	DM (Debay)	HOMO (eV)	LUMO (eV)	Gap (eV)	χ (eV)	μ (eV)	η (eV)	S (eV)	ω (eV)
1	H_2L^1	-2814653.01	2.31	-5.71	-2.70	-3.01	4.20	-4.20	-1.50	-0.75	-13.29
2	H_2L^2	-2742609.72	3.77	-5.70	-2.70	-3.00	4.20	-4.20	-1.50	-0.75	-13.24
3	H_2L^3	-2742609.40	4.97	-5.72	-2.79	-2.94	4.25	-4.25	-1.47	-0.73	-13.28
4	H_2L^4	-3007380.34	4.81	-5.72	-2.79	-2.93	4.26	-4.26	-1.47	-0.73	-13.27
5	H_2L^5	-2789998.87	10.24	-5.77	-3.24	-2.54	4.50	-4.50	-1.27	-0.63	-12.87
6	TiH_2L^1	-2789998.87	3.48	-5.74	-3.07	-2.67	4.41	-4.41	-1.33	-0.67	-12.95
7	TiH_2L^2	-2789998.87	2.53	-5.75	-3.09	-2.65	4.42	-4.42	-1.33	-0.66	-12.95
8	TiH_2L^3	-2789998.87	1.58	-5.75	-3.15	-2.60	4.45	-4.45	-1.30	-0.65	-12.86
9	TiH_2L^4	-2789998.87	1.75	-5.73	-3.14	-2.60	4.44	-4.44	-1.30	-0.65	-12.77
10	TiH_2L^5	-2789998.87	4.73	-5.78	-3.40	-2.38	4.59	-4.59	-1.19	-0.60	-12.57

*Dipole moment (DM), Energy of HOMO (EH), energy of LUMO (EL), energy band gap (ΔE), electronegativity (χ), global hardness (η), chemical potential (μ), global electrophilicity index (ω) and global softness (S)

Table S3 Optimized bond length (Å) of the Ti(IV) complexes

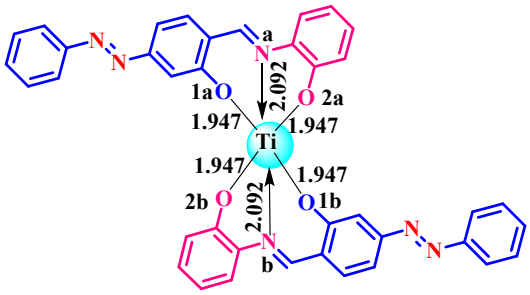

Complex	O_{1a}---Ti	O_{2a}---Ti	N_a---Ti	O_{1b}---Ti	O_{2b}---Ti	N_b---Ti
TiH_2L^1	1.947	1.947	2.092	1.947	1.947	2.092
TiH_2L^2	1.952	1.954	2.071	1.950	1.957	2.069
TiH_2L^3	1.947	1.946	2.088	1.947	1.949	2.087
TiH_2L^4	1.948	1.951	2.087	1.945	1.938	2.093
TiH_2L^5	1.917	1.901	2.148	1.915	1.904	2.143

Table S4 Optimized bond angle (°) of the Ti(IV) derivatives

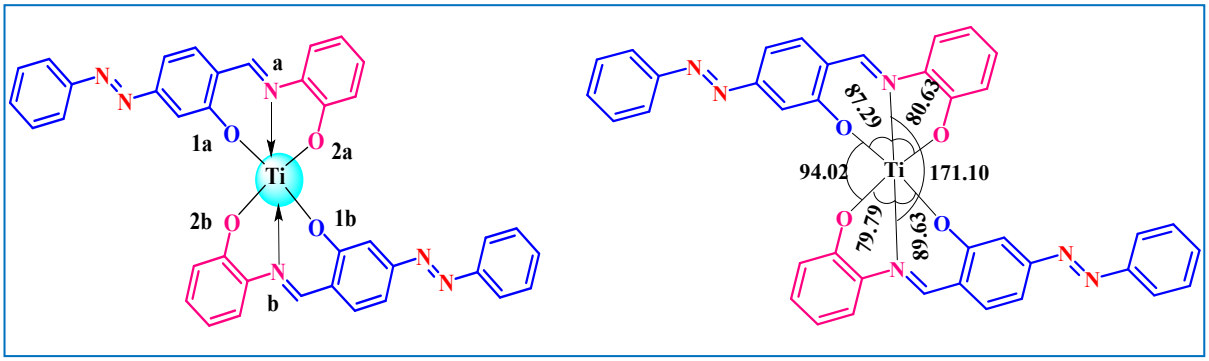

Complexes	O_{1a}--Ti--N_a	O_{2a}--Ti--N_a	O_{1b}--Ti--N_b	O_{2b}--Ti--N_b	N_a--Ti--N_b	O_{1a}--Ti--O_{2b}	O_{2a}--Ti--O_{1b}
TiH_2L^1	87.29544	80.6322	89.60377	79.79954	171.10044	94.02455	87.08391
TiH_2L^2	90.11607	80.39257	87.97321	81.02968	171.75382	94.38754	86.3268
TiH_2L^3	87.14825	79.73369	89.2433	80.38327	171.41851	94.00725	87.12916
TiH_2L^4	89.37351	80.02806	87.61594	80.69729	172.70979	93.83275	86.94033
TiH_2L^5	85.85722	77.54227	85.30993	77.78306	171.11759	95.67048	88.58993

Table S5 Chemical shifts (ppm): protons of the **TiH_2L^3** and CT-DNA bound with **TiH_2L^3** in the system

System	Ha	Hb	Hc	Hd
TiH_2L^3	9.694	7.774-7.849 (multiple splitting peaks)	7.106	6.874
			7.125	6.904
			7.144	6.923
CT-DNA-TiH_2L^3	9.699	7.778-7.853 (multiple splitting peaks)	7.110	6.877
			7.129	6.907
			7.147	6.927

Table S6 Molecular docking studies of titanium(IV) derivatives **(TiH_2L^1-TiH_2L^5)** with DNA and BSA

Ligand	Binding free energy ($\Delta G_{binding}$)$^{\alpha}$	Vdw_hb_desolv energy ($\Delta G_{vdW+hb+desolv}$)	Electrostatic energy (ΔG_{elec})	Total internal energy (ΔG_{total})	Torsional free energy (ΔG_{tor})	Unbound system's energy (ΔG_{unb})
DNA						
TiH_2L^1	-8.68	-9.8	-0.07	-0.42	1.19	-0.42
TiH_2L^2	-8.57	-9.65	-0.11	0.17	1.19	0.17
TiH_2L^3	-9.54	-10.71	-0.02	-0.44	1.19	-0.44
TiH_2L^4	-10.11	-11.27	-0.03	-0.65	1.19	-0.65
TiH_2L^5	-8.11	-11.37	1.47	-0.53	1.79	-0.53
BSA						
TiH_2L^1	-6.26	-7.46	-0.02	-0.47	1.19	-0.47
TiH_2L^2	-5.97	-7.19	0.03	-0.37	1.19	-0.37
TiH_2L^3	-6.95	-8.06	-0.08	-0.34	1.19	-0.34
TiH_2L^4	-7.42	-8.54	-0.07	0.17	1.19	0.17
TiH_2L^5	-5.49	-7.51	0.22	-0.56	1.79	-0.56

Table S7 A glance on cytotoxicity comparison of titanium(IV) derivatives

S.No	Hexacoordinated Titanium(IV) derivatives	Cell lines	IC_{50} Values	Reference
1	Hetero-bis-chelate stabilization of salan (ONNO) and thiosalan (OSSO) with with 2,6-pyridinedicarboxylic acid (dipic) supported titanium(IV)alkoxides	HeLa S3 Hep G2	4.5 ± 0.5 (μM) 3.2 ± 0.6 (μM)	[16]
2	Homoleptic Ti(IV) compounds of dianionic tridentate Schiff base ligands	ovarian carcinoma A2780 colorectal adenocarcinoma HT-29	30 ± 8 (μM) 60 ± 10 (μM)	[17]

3	Salan–titanium(IV) complexes	A2780 A2780CisR	10.3± 0.2; 83 (μM) 7.5±0.2; 88 (μM)	[18]
4	Diamine bis(phenolate) titanium(IV) complexes	HeLa MDA-MB-361 K562	4.4 ± 0.3 (μM) 13.0 ± 1.7 (μM) 5.7 ± 0.3 (μM)	[19]
5	Ti(IV) complexes of hexacoordinate diaminobis(phenolato)-bis(alkoxo) ligands	HeLa colon HT-29 A2780	48 ± 2 (μM) 38 ± 8 (μM) 19 ± 7 (μM)	[20]
6	Titanium(IV) complexes based on [ONON] diaminobis(phenolato) ligands	ovarian A2780 colon HT-29	7.4 ± 1.5 (μM) 26.9 ± 6.2 (μM)	[21]
7	Budotitane based Ti(IV) derivatives	HeLa C6 (glioma) CHO (Chinese hamster ovarian)	10.32 (μM) 20.68 (μM) 48.38 (μM)	[22]
8	**Bioactive O^N^O^ Schiff base appended homoleptic titanium(IV) complexes**	**HeLa** **A549(Lung cancer cell line)**	**14.7 (μg)** **32.9 (μg)** Five new Ti(IV) derivatives have been synthesised and subjected for binding studies with BSA and CT-DNA. Binding interactions are described with Molecular Docking, UV-Vis, FL, CD spectra analysis and geometries of Ti(IV) complexes are well established by DFT study	**Present work**

Experimental procedures

Stability study

The stability of five newly synthesised titanium(IV) **(TiH_2L^1-TiH_2L^5)** complexes were verified in 10% DMSO medium and water medium over time period of 0^{th},24^{th} and 48^{th} hr and aqueous GSH (1mM) medium time period of 0^{th}, 12^{th}, 24^{th} and 48^{th} hr by UV-Visible method.[1,2]

n-Octanol-water partition coefficient (log $P_{o/w}$):

The log $P_{o/w}$ of titanium(IV) derivatives **(TiH_2L^1-TIH_2L^5)** were determined through shake flask method subjecting the previously published procedure.[3,4] On an orbital shaker, known volume of each complexes were suspended in water that had been pre-saturated with n-octanol shaken for 24 hr. Kept aside for the phase separation followed by centrifuged for 10 min at 3000 rpm. The separation of the two layers was followed by a UV-Vis spectroscopic investigation for both water and octanol layer. The OD of the complex in water and octanol has been employed for determining the log $P_{o/w}$ values (partition coefficient).

Conductivity measurement:

The molar conductivity of the titanium(IV) complexes **(TiH_2L^1-TIH_2L^5)** were assessed in DMSO, 10% and GSH medium with the help of conductivity-TDS meter 307 (Systronics, India) instrument and cell constant 1.0 cm^{-2} due to the confirming the interaction of the complexes with DMSO, aqueous DMSO, GSH and Ct-DNA solutions. Concentration for this conductivity experiment we used the complex concentration was 3×10^{-1} M.[5,6]

$$\wedge M = k - 1000/C \quad \ldots\ldots\ldots\ldots\ldots\ldots\ldots\ldots 1$$

Where, *K*= specific conductivity and *C*= concentration of solute.

Viscosity measurement

Viscosity investigation has been carried for to find out the mode of binding interaction of titanium(IV) complexes **(TiH_2L^1-TIH_2L^5)** with CT-DNA using Ostwald's capillary viscometer.[7-9] The average flow time was recorded after each experiment had been conducted in three times. The data was plotted as $(\eta/\eta_0)^{1/3}$ vs [complex]/[DNA], where η and η_0 reveals to viscosity of DNA in the presence and absence of the complexes, respectively.

Molecular docking

The synthesized complexes **TiH_2L^1-TiH_2L^5** were exposed to a molecular docking study using Autodock 4.2, covering the Lamarckian Genetic Algorithm (LGA) to calculate binding affinities of several conformers and AutoDock Tools (ADT) to implement the operation and consequent calculations. The crystallographic structure of DNA with the sequence d(CpGpCpGpApApTpTpCpGpCpG) (PDB ID: 1BNA)[10] and crystallographic structure of BSA (PDB

ID: 4F5S)[11] fetched from the protein data bank with a resolution of 1.90 Å was built using Autodock 4.2 package to establish BSA and DNA-binding properties of **TiH_2L^1-TiH_2L^5**. In order to prevent an undesirable contact with the docked conformers, water molecules were additionally omitted throughout the protein preparation process.

The 3D structures of complexes **TiH_2L^1-TiH_2L^5** derived from DFT optimized geometry were transformed into PDB form through Gauss view. Each atom in both the target and lead compound was fed with Gasteiger charges. Before docking, the binding site was assigned in developing a grid box with spacing of 0.7 Å and 40 × 40 × 40 number of points in x, y and z directions. In the case of BSA, the grid size was considered 40 × 40 × 40 number of points in x, y and z with a spacing of 1 Å encircling all the putative active site residues of BSA (Trp213 and Trp134). The working principle and the output parameters were similar to the above-mentioned DNA docking. Imagining of the docked pose has been done *via* LIGPLOT and PyMol molecular visuals programs.

Anti-inflammatory activities

Anti-inflammatory potential of the synthesized derivatives **TiH_2L^1-TiH_2L^5** were deliberately employed by BSA denaturation technique.[12] The dosages of the drugs and the reference medication *i. e.* diclofenac sodium was taken in varied concentrations such as 50, 100, 150, 200 and 250 µg/mL. The test samples were dissolved in DMSO wherein phosphate buffer and BSA (3 µg/mL) were added as 1 mL each. The final constituents of five test samples were incubated at 37 °C for 15 mins, afterwards, denaturized for 15 minutes at 70 °C on water bath, later cooled and were subjected to measure their absorbance at 660 nm. The identical test solutions were employed for the negative control in absence of medication. Inhibition percentages were computed as the formula provided below (equation7):

$$\text{BSA denatures inhibition by percentage} = 100 \times (A_t - A_c) / A_t \quad \ldots\ldots\ldots\ldots\ldots\ldots\ldots\ldots\ldots\ldots (7)$$

where, A_c and A_t were optical density of control and test solutions, respectively.

Extension of cytotoxicity by MTT assay

Investigation on *in vitro* anti-proliferative activities of **TiH_2L^1-TiH_2L^5** were carried out by employing MTT [{3-(4, 5-dimethylthiazolyl-2)-2, 5-diphenyltetrazolium bromide}] assay.[13,14] The 10,000 cells were placed into 96 well microplates with 100 µL of cell suspensions per well

followed by incubation to promote cell adhesion at 37 ˚C in presence of 5% CO_2, 100% relative humidity and 95% air. Dimethyl sulfoxide solution of each test samples with five varied concentrations were added appropriately into the wells that contain 100 µL of medium containing the cells to acquire the final concentration of the test samples. Further, samples loaded microplate was incubated for 24 hr at 37 ˚C as per aforementioned conditions.

Afterwards, the medium of test wells was evacuated by the addition of 15 µL of MTT (0.5 mg/mL) reagent into all the corresponding wells and these reacting plates were incubated for 4 hr at 37 °C in a CO_2 incubator. Eventually, the media of MTT microplates were discorded and 200 µL of PBS was cast-off to wash the cells. Only living cells were capable of absorbing MTT, consequently, getting transformed into formazan crystals. The MTT with media was removed and the appeared formazan crystals were dissolved in 100 µL of DMSO and the absorbance at 570 nm was measured using a microplate scanner. Three micro wells were kept for all concentrations without addition of titanium(IV) complexes served as the controls. In order to determine the percentage of inhibited cells, equation (8) could be used as mentioned below:

$$\% \text{ Inhibition of cells} = \frac{OD\ of\ test\ samples}{OD\ of\ control\ cells} \times 100 \quad \ldots\ldots\ldots\ldots\ldots\ldots (8)$$

Fluorescent imaging of HeLa cells

After getting appreciable results for complex **TiH_2L^3** from MTT assay on HeLa and A549 cells, that is suitable for cellular uptake study against on HeLa cells (5 x 10^5 cells/ml) was seeded into the 24 well tissue culture plate and was treated with 14.7 µg/ml of test sample in a serum free DMEM medium (Dulbecco's Modified Eagle's Medium). The plate was incubated at 37 ^oC for 24 hr in 5% CO_2 incubator. After incubation, wells are washed thrice with PBS buffer followed by 50 µl of 1 mg/ml acridine orange and ethidium bromide were added into the appropriate wells and mixed gently. Finally, the test sample was centrifuged at 2000 rpm for 5 mins and was transferred into clean glass slide protected with cover glass and was evaluated directly within an hour and surveyed minimum 100 cells by fluorescence microscope.

Cell cycle analysis by employing flow cytometry

A flow cytometry instrument (CytoFLEX, Beckman Coulter, USA) was employed to compute the fraction of cells in every phase of the cell cycle.[15] The HeLa cells (1×10^6 cells/well) were

seeded into 6 well plates followed by incubation for 8 hr before being treated with the optimal doses (IC_{50}) of the drugs **TiH_2L^2** (28.8 µg/mL), **TiH_2L^3** (14.7 µg/mL) and **TiH_2L^4** (31.2 µg/mL). Afterwards, the cells were trypsinized and washed with PBS, consequently, fixed with 70% ethanol and preserved at -20 °C for overnight. The overnight fixation was followed by centrifugation for 10 mins at 4000-5000 rpm. The obtained pellets were suspended in RNase containing PBS with 20 µg/mL of propidium iodide (PI) and incubated for 10 mins in the dark. The above PI stained samples were read at 488 nm in the flow cytometry.

ROS quantification by DCFH-DA staining assay

The cells were seeded in a six-well plate and were treated with the IC_{50} concentrations of each of the compounds **TiH_2L^2** (28.8 µg/mL), **TiH_2L^3** (14.7 µg/mL) and **TiH_2L^4** (31.2 µg/mL). The test wells were trypsinized and washed after the 8 hr incubation. Subsequently, the cells were subjected for 20 µM DCFH-DA (Dichloro-dihydro-fluorescein diacetate) treatment at 37 °C for 30 mins in complete darkness.[1,15] The ROS levels were measured using flow cytometry (CytoFLEX, Beckman Coulter, USA).

Annexin V-APC/PI for apoptosis detection

Annexin V-APC/PI apoptosis detection assay (Elabscience) was used to assess the cell apoptosis. The HeLa cells were treated with IC_{50} doses of corresponding drugs **TiH_2L^2** (28.8 µg/mL), **TiH_2L^3** (14.7 µg/mL) and **TiH_2L^4** (31.2 µg/mL) at 37 °C for 8 hr. As per the procedure of manufacturer, the cells were trypsinized and washed twice with PBS followed by resuspension in 1X Annexin V binding buffer.[1,15] Annexin V antibody labelled with APC and PI were added and incubated at 37 °C for 10 mins. The samples were read in flow cytometer (CytoFLEX, Beckman Coulter, USA), the fluorescence was measured at respective channels - PI (488 nm) and Annexin V (APC 633 nm) to study the apoptosis inducing effect of **TiH_2L^2-TiH_2L^4**.

References

1. N. Roy, U. Sen, Y. Madaan, V. Muthukumar, S. Varddhan, S.K. Sahoo, D. Panda, B. Bose, P. Paira, Mitochondria-targeting click-derived pyridinyltriazolylmethylquinoxaline-based Y-shaped binuclear luminescent ruthenium (II) and iridium (III) complexes as cancer theranostic agents, *Inorg. Chem.*, 2020, **59**, 17689-17711.

2. A. Mondal, U. Sen, N. Roy, V. Muthukumar, S.K. Sahoo, B. Bose, P. Paira, DNA targeting half sandwich Ru (II)-p-cymene-N^ N complexes as cancer cell imaging and terminating agents: Influence of regioisomers in cytotoxicity, Dalton Transactions., 2021, **50**, 979-997.

3. U. Das, S. Shanavas, A.H. Nagendra, B. Kar, N. Roy, S. Vardhan, S.H. Sahoo, D. Panda, B. Bose, P. Paira, Luminescent 11-{Naphthalen-1-yl} dipyrido [3, 2-a: 2′, 3′-c] phenazine-Based Ru (II)/Ir (III)/Re (I) Complexes for HCT-116 Colorectal Cancer Stem Cell Therapy, *ACS Appl. Bio Mater.*, 2023, **6**, 410-424.

4. N. Roy, S. Shanavas, B. Kar, L.Thilak Babu, U. Das, S. Vardhan, S.K. Sahoo, B. Bose, V. Rajagopalan, P. Paira, G2/M-Phase-Inhibitory Mitochondrial-Depolarizing Re (I)/Ru (II)/Ir (III)-2, 2′-Bipyrimidine-Based Heterobimetallic Luminescent Complexes: An Assessment of In Vitro Antiproliferative Activity and Bioimaging for Targeted Therapy toward Human TNBC Cells, ACS omega., 2023, **8**, 12283-12297.

5. S.Nikolić, L. Rangasamy, N. Gligorijević, S. Aranđelović, S. Radulović, G. Gasser, S. Grgurić-Šipka, Synthesis, characterization and biological evaluation of novel Ru (II)–arene complexes containing intercalating ligands, *J. Inorg. Biochem.*, 2016, **160**, 156-165.

6. P. Selvam, S. De, P. Paira, S.K. Kumar, A. Moorthy, A. Ghosh, Y.C. Kuo, S. Banerjee, S.K. Jenifer, In vitro studies on the selective cytotoxic effect of luminescent Ru (II)-p-cymene complexes of imidazo-pyridine and imidazo quinoline ligands, *Dalton Transactions.*, 2022, **51**, 17263-17276.

7. S. Banerjee, I. Pant, I. Khan, P. Prasad, A. Hussain, P. Kondaiah, A.R. Chakravarty, Remarkable enhancement in photocytotoxicity and hydrolytic stability of curcumin on binding to an oxovanadium (IV) moiety, *Dalton Transactions.*, 2015, **44**, 4108-4122.

8. J.H. Shi, J. Chen, J. Wang, Y.Y. Zhu, Binding interaction between sorafenib and calf thymus DNA: spectroscopic methodology, viscosity measurement and molecular docking, *Spectrochim. Acta A Mol.*, 2015, **136**, 443-504.

9. S. De, B. Sarkar, G.R. Jadhav, S.K. Ramasamy, S. Banerjee, A. Moorthy, P. Paira, Experimental and theoretical study on the biomolecular interaction of novel acenaphtho quinoxaline and dipyridophenazine analogues, *ChemistrySelect.*, 2018, **38**, 10593-10602.

10. A. Bujacz, Structures of bovine, equine and leporine serum albumin, Acta Crystallographica Section D: *Biological Crystallography.*, 2012, **68**, 1278-1289.

11. S. Yuan, H.S. Chan, Z. Hu, Using PyMOL as a platform for computational drug design, *Wiley Interdiscip. Rev. Comput. Mol. Sci.*, 2017, **7**, e1298.

12. M. Manimohan, R. Paulpandiyan, S. Pugalmani, M.A. Sithique, Biologically active Co (II), Cu (II), Zn (II) centered water soluble novel isoniazid grafted O-carboxymethyl chitosan Schiff base ligand metal complexes: Synthesis, spectral characterisation and DNA nuclease activity, *Int. J. Biol. Macromol.*, 2020, **163**, 801-816.

13. S. Thanigachalam, M. Pathak, Development of nano titania/polyvinylidene fluoride composite from new titanium (IV) derivative and its investigation on antibacterial, BSA interaction and cytotoxicity, *Mater. Today Commun.*, 2023, **35**, 105774.

14. K. Tummalapalli, C.S. Vasavi, P. Munusami, M. Pathak, M.M. Balamurali, Evaluation of DNA/Protein interactions and cytotoxic studies of copper (II) complexes incorporated with N, N donor ligands and terpyridine ligand, *Int. J. Biol. Macromol.*, 2017, **95**, V1254-1266.

15. S. Sankar, G.K. Muthukaliannan, Combinatorial effect of diclofenac with piperine and D-limonene on inducing apoptosis and cell cycle arrest of breast cancer cells, *Asian Pac. J. Trop. Biomed.*, 2023, **13**, 80-92.

16. M. Grützke, T. Zhao, T.A. Immel, T. Huhn, Heptacoordinate heteroleptic salan (ONNO) and thiosalan (OSSO) titanium (IV) complexes: investigation of stability and cytotoxicity, *Inorganic Chemistry.*, 2015, **54**, 6697-6706.

17. Z. Shpilt, R. Manne, M.A. Rohman, S. Mitra, E.R. Tiekink, T.S. Basu Baul, E.Y. Tshuva, Homoleptic Ti [ONO] 2 type complexes of amino-acid-tethered phenolato Schiff-base ligands: Synthesis, characterization, time-resolved fluorescence spectroscopy, and cytotoxicity against ovarian and colon cancer cells, *Appl. Organomet. Chem.*, 2020, **34**, e5309.

18. C.M. Manna, O. Braitbard, E. Weiss, J. Hochman, E.Y. Tshuva, Cytotoxic Salan–Titanium (IV) Complexes: High Activity Toward a Range of Sensitive and Drug-Resistant Cell Lines, and Mechanistic Insights, *ChemMedChem.*, 2012, **7**, 703-708.

19. S. Barroso, A.M. Coelho, S. Gómez-Ruiz, M.J. Calhorda, Ž. Žižak, G.N. Kaluđerović, A.M. Martins, Synthesis, cytotoxic and hydrolytic studies of titanium complexes anchored by a tripodal diamine bis (phenolate) ligand, *Dalton Trans.*, 2014, **43**, 17422-17433.

20. M. Taha, E.Y. Tshuva, Phenolato Ti (iv) hexacoordinate complexes for anticancer chemotherapy: enhancement of solubility, hydrolytic stability, and cytotoxicity, *Dalton Trans.*, 2023.

21. A. Pedko, E. Rubanovich, E.Y. Tshuva, A. Shurki, Hydrolytically Stable and Cytotoxic [ONO N] 2Ti (IV)-Type Octahedral Complexes, *Inorg. Chem.*, 2022, **61**, 17653-17661.

22. N. Kumar, R. Kaushal, A. Chaudhary, S. Arora, P. Awasthi, Titanium based mixed ligand complexes: Synthesis, spectroscopic and in vitro antiproliferative studies, *Inorg. Nano-Met. Chem.*, 2018, **48**, 467-476.